INVESTIGATING LIPID-PROTEIN INTERACTIONS USING SUPPORTED LIPID BILAYERS

A Dissertation

Presented to the Faculty of the Graduate School

of Cornell University

In Partial Fulfillment of the Requirements for the Degree of

Doctor of Philosophy

by

Mark Jason Richards

February 2016

INVESTIGATING LIPID-PROTEIN INTERACTIONS USING SUPPORTED LIPID BILAYERS

Mark Jason Richards, Ph. D.

Cornell University 2016

Membrane proteins play vital roles in cell function and as such represent the targets of over 60% of pharmaceuticals on the market[1]. Lipid interactions with membrane proteins are a crucial but often overlooked effector of cell physiology. Lipids impart conformational stability and modulation on membrane proteins, which is closely tied to their function. In addition, there is increasing evidence that the cell membrane is heterogeneous with dynamic "raft" domains with different compositions and the dynamics of these domains could regulate membrane protein function via lipid-protein interactions. When studying membrane proteins in cells, these types of lipid-protein interactions are preserved, but decoupling to elucidate specific mechanisms is difficult because of the complexity of the cell system. Other techniques use detergent solubilized membrane proteins to reduce complexity, but lipid interactions are also lost. The proposed bridging technique is the supported lipid bilayer (SLB). It combines a large library of techniques with a simplified, yet sufficient mimic of the properties of the cell membrane; however key functionalities have remained unaddressed.

In this work I discuss development of additional function for the SLB platform in two key areas: 1) generation of patterned supported lipid bilayers that mimic

membrane heterogeneities such as the “lipid raft” to evaluate associated dynamics and 2) the inclusion of membrane proteins in a robust and simplified manner. In Chapter 1, I conduct a thorough literature review of the field. In Chapter 2, I describe a laminar flow patterned two-phase bilayer used to perform an affinity based separation of membrane species. In Chapter 3, I characterize a novel technique for delivery of membrane proteins from cell blebs into a cushioned supported lipid bilayer. In Chapter 4, I detail patterning of two-phase supported lipid bilayers as a mimic for lipid rafts. In Chapter 5, I provide an outlook of how our work has increased the biological relevance of the supported lipid bilayer and has increased its utility for studying a wide range of biological processes.

BIOGRAPHICAL SKETCH

Mark Richards grew up in Harleysville, PA. In 2009, Mark received his B.S. in Chemical Engineering from the University of Delaware with minors in Biochemical Engineering, Math, and Economics. He pursued a Ph. D in the Department of Chemical and Biomolecular Engineering at Cornell University in Susan Daniel's group. He was awarded NSF IGERT fellowship during his time at Cornell. He studied lipid-protein interactions using supported lipid bilayer platforms. In particular, he designed and tested a platform for separating membrane species by phase affinity within a lipid bilayer, developed a new technique for delivering membrane proteins to supported bilayers via cell blebbing and tested bilayer patterning and cushioning strategies in pursuit of improving artificial cell membrane mimics. In his work, he integrated several technologies and techniques including cell culture, fluorescence microscopy, finite element modeling and microfluidic device fabrication at the Cornell Nanofabrication Facility. He has since accepted a position in Upstream Operations at Morphotek in Exton, PA.

I would like to dedicate this paper to my family and friends who continued to support me throughout this process. Without their help, none of this would have been possible.

ACKNOWLEDGMENTS

I would like to thank Susan Daniel for mentoring me through the PhD process. Thanks to Daniel group members for their friendship and collaboration: Deirdre Costello, Donald Lee, Chih-Yun Hsia, Hung-Lun Hsu, Rohit Singh, Lakshmi Nathan, Chun-Ti Chang, and especially Ling Chao who trained me and taught me a lot about how to be an effective graduate student. Without help from this group, I never would have completed what I have. I would like to acknowledge my incredible undergraduate collaborators: Huma Haider and Sijun Yang who both provided a lot of help with experiments and motivation. I would like to thank to my family for the constant support throughout my life. Thanks to my professors at the University of Delaware, particularly my undergraduate research advisor Anne Robinson, whose guidance and assistance with my research aspirations was invaluable, and for recognizing my potential. Thanks to Michelle O'Malley who was an excellent mentor and has consistently provided an example of success in academia. Lastly, I would like to thank my friends in Cornell who kept me grounded throughout my time here: Linxiao Chen, Bryan Rolfe, Wenyu Zhang, Rambert Nahm, Justin Rosch and Rebecca Potash. This work was partially funded by NSF IGERT (DGE-0654112).

TABLE OF CONTENTS

LIST OF FIGURES

LIST OF TABLES

CHAPTER 1

LITERATURE REVIEW – EMERGING TECHNIQUES FOR STUDYING LIPID PROTEIN INTERACTIONS

Note: Portions of this chapter have been published as "A review of traditional and emerging methods to characterize lipid-protein interactions in biological membranes" in Analytical Methods.

1.1 The Cell Membrane and Lipid-Protein Interactions

The cell membrane is a fundamental biological barrier enclosing the cell cytoplasm and nucleus with the purpose of regulating the interaction between the cell and the outside environment. This membrane is comprised of a bilayer of amphipathic lipid molecules and proteins arranged to shield their hydrophobic parts from the aqueous surroundings. The membrane proteins are embedded within the lipid bilayer solvent and take part in many critical functions including transport, signaling and recognition between the cell and its environment. Not surprisingly then, over 60% of drugs on the market target membrane species[1,2]. Improving the understanding of membrane protein structure, function and dynamics is highly desired to allow for the design of more effective drugs and treatment methods[3–8]. It has recently become appreciated that not only is the protein interaction with the drug important for altering its activity or function, but that the level of modulation, or even the final biological outcome, may be coupled to the lipid interactions the protein makes with the surrounding membrane[9,10]. Beyond drug discovery, understanding of such interactions

may prove critical in other biotechnology applications where membrane proteins are key elements, for example in biosensing[11], tissue engineering[12], biofilm formation[13], and so on.

It is difficult to study these species *in vivo* because of complications of isolating individual species behavior within such a complex and interconnected environment. Because of this, much less is known about membrane proteins than more easily isolated soluble proteins[2,8,14]. Only a handful of new membrane protein structures are being solved annually, and even less is known about how they function[5,15]. Expression and purification are major bottlenecks for the isolation and analysis of membrane proteins. Optimizing recombinant protein expression is necessary to attain high concentrations of most membrane proteins. Because of the lack of alternatives, methods used for purification of soluble proteins are used for insoluble membrane proteins. Target proteins are overexpressed in host cells, the cells are lysed, and proteins are separated using a series of chromatographic steps. Because soluble proteins are able to retain their native structures in aqueous solutions, screening of interactions with other soluble proteins or molecules is generally reliable and likely to represent native interactions *in vivo*. Less success has been made with integral membrane proteins because the native cell membrane environment imparts stability and specific interactions to the proteins, and this key interaction is lost when they are removed from the membrane.

Detergents are required to solubilize membrane proteins outside of the membrane[8,16]. The amphiphilic nature of detergents helps shield the hydrophobic domains of the proteins similarly to lipids, but can also result in non-native

conformations and absence of functionally critical lipid-protein interactions. This severely impacts the ability to identify the protein's native structure, functions and interactions. Some success has been found stabilizing the conformations of membrane proteins on a case-by-case basis with careful detergent choice and designer peptide binding[17]. Alternatively, shotgun analysis methods where proteins in both solubilized and membrane embedded form are variably cleaved using specific enzymes have been developed including a comprehensive method to identify proteins, post-translational modifications and membrane protein topology[18]. In this shotgun approach, the pre-digested protein mixtures are run on a liquid chromatography with mass spectrometry system. While these methods can elucidate important information about the form of proteins present in the sample and their topologies, they cannot capture protein-lipid interaction effects. New approaches are needed as we rethink membrane protein study as its own field with unique challenges.

Membrane proteins studies are lagging behind soluble proteins because of their necessary interactions with membrane lipids. These interactions are sometimes seen as an obstacle to overcome, but in fact they should be a main focus. The local interactions and organization of lipids and proteins are believed to regulate membrane protein activity[19]. Removing membrane proteins from the membrane environment often alters their structure, and their function may not be indicative of their native state.

Lipid species interacting with membrane proteins can be classified into two categories: annular lipids and non-annular lipids[9]. Annular lipids form a shell around membrane proteins by binding to their surfaces (Fig. 1.1A), while non-annular lipids

are found buried within protein helices (or protein complex subunits) forming lipid-protein complexes (Fig. 1.1B). The critical differences between annular and non-annular lipids are the binding affinity and their residence time with membrane proteins. Annular lipids exhibit lower affinity to membrane proteins compared to non-annular lipids and possess the motional freedom to exchange with the bulk environment; in contrast, non-annular lipids are more restricted from exchanging with the surrounding lipids and bind directly to specific sites on membrane proteins.

The effects of annular lipids on membrane protein structure and their functions are mainly ruled by the degree of hydrophobic matching between membrane protein core and the surrounding lipid acyl chain and the structure and charge distribution of lipid headgroups and protein amino acid residues located near the lipid-water interface[9].To avoid exposing the hydrophobic domain of membrane proteins to aqueous solution, the hydrophobic thicknesses of lipid bilayers and proteins must match. Mismatching results in the distortion of protein structures, which can influence their functions.

The headgroup region of annular lipids also has important influence on membrane protein conformation and activity. Hydrogen bonding and charge-charge interaction between the specific amino acids of proteins and lipid headgroups can largely affect the structure of the protein. One example of this is the interaction between phosphatidylethanolamine lipid (PE) headgroup interactions with rhodopsin promoting the formation of MII in the rhodopsin photo-activation cycle. Stabilization MII intermediate occurs via hydrogen binding interaction of the exposed Glu-134 amino acid and PE headgroups[20,21].

Lipids exerting higher affinity to specific binding sites on protein transmembrane

domains are referred to as non-annular lipids. These lipids may be integrated within the protein core structure, especially between protein subunits. Due to their high-affinity binding to membrane proteins, non-annular lipids can be resolved in membrane protein crystal structures by high-resolution crystallography, and many examples of non-annular lipid-protein interactions have been reviewed in literature[22,23]. Non-annular lipids serve diverse purposes in modulating protein structure and function on cell membranes. For instance, lipids can act as co-factors for membrane proteins to oligomerize and function, and a typical example is the potassium channel KcsA[24]. Anionic phospholipids, such as phosphatidylglycerols (PGs), were found to bind at the monomer-monomer interface in the KcsA homotetramer. It is believed that the interaction of PGs with the non-annular binding sites of KcsA helps the packing of KcsA structure and supports its conducting state.

Another well-known function of non-annular lipids is their allosteric effect in regulating membrane protein activities. For example, binding between cholesterol and many G-protein-coupled receptor (GPCR) allosteric sites were found to be critical for GPCR biological pathways, such as the full activation of the oxytocin receptor[25] and the ligand binding and G-protein coupling of serotonin$_{1A}$ receptor[26].

Finally, non-annular lipid-protein interactions have been suggested to play a role in targeting proteins to distinct lipid domains. For example, binding between the metabotropic glutamate receptor (a type of GPCR found in *Drosophila melanogaster*) and cholesterol was shown to target the receptor to lipid rafts[27]. In another example, binding of amyloid precursor protein (APP) and cholesterol has been suggested to promote localization of APP in lipid rafts, and the association of APP to lipid rafts is

believed to be essential to the progression of Alzheimer's disease[28].

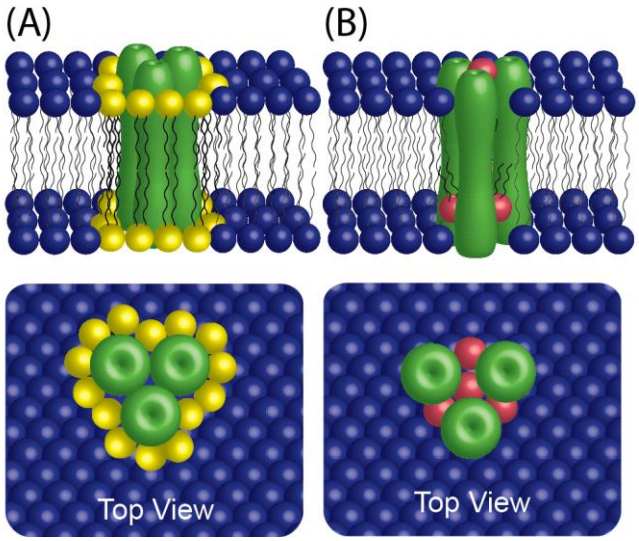

Figure 1.1. Annular vs. Non-Annular lipid protein interaction. (A) Annular lipid arrangement (yellow) around a protein complex (green). (B) Non-annular lipids (pink) arranged within a multi-subunit protein complex. The surrounding lipids (in blue) represent non-raft membranes enriched in phospholipids.

1.2 Lipid Rafts and Membrane Organization

An important manifestation of these interactions is the way lipids and proteins tend to separate into micro-domains through direct association among themselves instead of distributing uniformly as a homogeneous, two-dimensional fluidic environment. Micro-domains compartmentalize distinct kinds of lipids and membrane proteins and are an important paradigm of cell membrane organization. One notable, but still enigmatic, type of micro-domain that results from phase separation is the lipid raft, which is enriched in cholesterol and sphingolipids relative to the surrounding phospholipid-rich membrane[29]. Specific kinds of proteins and glycolipids are enriched in rafts, while others are excluded.

It is hypothesized that the organization of the membrane is a means by which the cell orchestrates membrane function[30–32]. Manipulating the dynamics of these domains

and therefore species partitioning could control when and where species can interact and impact biological function. In addition, the lipid environment itself can attenuate the function of the membrane protein species residing within.

A simplified model of this is on-off regulation where presence in one phase results in active protein while presence in the other phase causes the protein to be inactive (Fig. 1.2). This can be a result of changes in hydrophobic domain length causing changes in membrane protein subdomain tilt, specific lipid interactions or even protein-protein interactions that are more favorable due to local concentration increase in one phase. Examples of these behaviors include the hydrophobic matching based conformational change of the mechanosensitive channel of large conductance (MscL) where a thin non-raft bilayer favors channel opening, but a thicker raft bilayer favors the closed structure[33], or the hydrophobic matching of SNARE protein transmembrane domains in a process mediated by cholesterol which drives their clustering in rafts[34].

The sum of these lipid-protein interactions represents a unique post-translational regulation mechanism with the potential to be wide-reaching in membrane-mediated function. Previous results have shown factors like temperature, ligand induced crosslinking, and changes in the composition of the membrane may control domain dynamics, but additional studies confirming and characterizing this type of lipid-protein interaction are needed[35–37]. Furthermore, correlating these interactions with biological function is even more of a challenge.

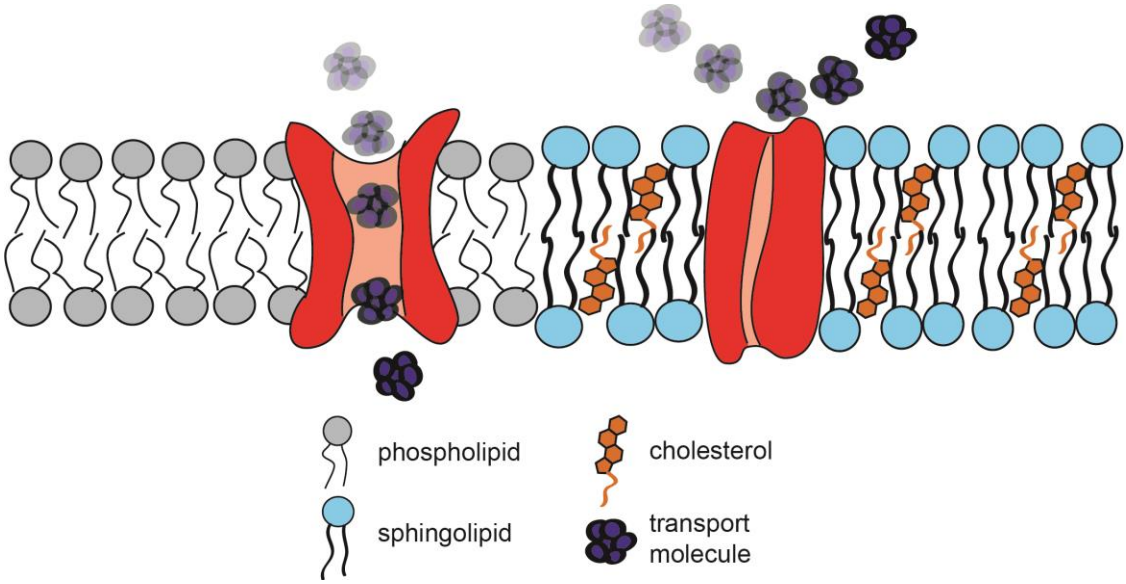

Figure 1.2. Local lipid environment can affect membrane protein activity. In the left side of the membrane, the channel protein is in an "on" state because of interactions with non-raft lipids. Interactions with thicker raft lipids in the right side of the membrane cause a conformation change to match their hydrophobic length. The protein enters an "off" state in the raft membrane and transport is inhibited.

While phase segregation in model membranes was postulated as early as the 1980's[38,39], direct detection of lipid rafts in cell membranes has proven elusive partly because of their small scale and dynamic nature. However, there is a wealth of evidence supporting their existence. Here we provide a brief synopsis, but for a thorough review see Lingwood and Simons[40]. Detergent resistant membrane (DRM) fractionation assays isolate membrane fractions that are enriched in cholesterol, sphingomyelin, and raft-associating species[41]. Surface labeling with antibodies or toxins binding to raft-associated proteins is used to tag raft membrane domains[42]. Single particle tracking methods[43,44] detect changes in protein diffusion, which indicates the presence of more viscous raft domains. Finally, plasma membrane vesicles devoid of cytoskeletal proteins have been shown to readily undergo phase

separation into large, observable raft-like and fluid-like domains[45,46]. In parallel to these techniques, recent advances in spectroscopy[47] and super-resolution imaging[48,49], such as photoactivation localization microscopy (PALM)[50], stochastic optical reconstruction microscopy (STORM)[51], and stimulated emission depletion (STED) fluorescence microscopy[52,53] have revealed dynamic, nanoscale lipid raft assemblies in living cells. Some membrane-bound species show a preference to associate with certain lipid phases in the cell membrane. Glycolipids[54], GPI-linked lipids[55] and certain proteins[56] tend to associate with lipid rafts. Other membrane constituents, a specific example being transferrin receptor, tend to avoid lipid rafts and reside in more disordered phases enriched with phospholipids[57,58]. Studies have shown that co-existent liquid-ordered and liquid-disordered lipid phases can exist in model membrane systems[59–64], but controlling the location of these phases has been a challenge. As the lipid raft hypothesis has gained acceptance, the number of hypotheses for the mediation of cell processes through lipid-protein interactions involving rafts has increased.

Although membrane protein interactions within their local membrane environment are critical to their functions, they are not easy to probe because traditional protein characterization techniques may disrupt the native lipid-protein interaction in the cell or artifactually change the native associations. For example, detergents used in DRM fractionation can coalesce rafts and could kinetically trap non-raft species in them during this process. DRMs are also dependent on choice of detergent as different detergents may cause changes in clustering and fraction compositions[65]. Surface labeling of cells requires antibodies or toxins to bind to specific species, often

crosslinking them and causing artifactual enrichment[64]. An alternative is to label fixed cells, but membrane organization and lipid-protein associations of dead cells are not necessarily indicative of live conditions[66,67]. Isotope labeling methods have some utility[68], but can only be applied to cultured cells, are expensive, and still require isolation methods to identify residents.

Therefore, to expand our current knowledge of how membrane proteins function and are regulated, a variety of techniques including novel membrane platforms are needed to improve characterization of lipid-protein interactions and minimize possible artifacts.

1.3 Cell-Based Techniques to Study Lipid-Protein Interactions and Raft Function

The two primary objectives of raft investigations are often to determine which species are targeted to raft domains and how species are targeted to raft domains. Specific structures of membrane species have been found to dictate their raft-association preferences[69]. For instance, it was found that differences in the structure of glycophosphatidylinositide (GPI) anchors could be correlated to the differences in raft-association of GPI-linked proteins[57]. Diaz-Rohrer et al. further explored this concept[70]. They devised an array of protein constructs based around a single pass protein, trLAT, with variations in transmembrane domain lengths and sequences as well as number of palmitoylation sites. By observing the trafficking behavior of these fluorescent fusion protein constructs in cell membranes and the raft partitioning behavior in model giant unilamellar vesicles, they proposed a unique raft pathway whereby raft-associated proteins are recycled to the plasma membrane. It is important to note that the labeling strategies used in experiments can potentially influence the

interactions between lipids and proteins and the dynamics and stability of membrane domains, so careful controls must be performed to understand and minimize the effects of labels used. For instance, antibody labeling can crosslink species and cause of stabilization of domains[44].

Another objective of raft investigations is to determine how raft environments can affect protein function. Many of these studies use disruption of rafts in live cells to evaluate their influence on protein function, that is, to observe differences in protein function before and after raft disruption. Rafts can be disrupted by either removal of cholesterol using cyclodextrins or using knockouts of sphingolipid biosynthesis enzymes. Depletion of cholesterol by cyclodextrin has been shown to reduce levels of raft marker proteins in detergent resistant membrane fractions. Disruption methods also revealed stimulation of signaling through the tyrosine phosphorylation and Ras-ERK pathways, promoting the idea that raft-association regulates protein activity (particularly LCK) in these cascades[71]. Although cyclodextrins are useful tools to deplete cholesterol, their mechanisms of action are still unclear and may promote raft formation instead of eliminating them[72], may remove cholesterol from raft and non-raft domains at different rates, and, at high enough concentrations, may extract other molecules including phospholipids from the membrane[73].

In another study of cell migration induced through the CXCR4/CXCL12 pathway, sphingomyelin was shown to play an important role. By knocking out sphingomyelin synthases, it was concluded that sphingomyelin acts as a selective regulator of GPCR signaling; low sphingomyelin concentration in rafts leads to an increase in CXCR4 levels in rafts and increased dimerization, both correlating to increased cell

migration[74]. Although the strategy of genetically deleting an individual enzyme targets the lipid-protein interaction directly, it is important to note that there will also be changes in all lipids "downstream" of that enzyme in the pathway, which can also impact other potentially related cellular functions.

A third objective of raft investigations is to characterize the dynamics of biomolecules partitioning into and out of rafts within the membrane plane. Biomolecules move laterally within the lipid bilayer by Brownian diffusion[75]. With the advent of single molecule microscopy techniques to track individual proteins embedded in cell plasma membranes, it has been revealed that protein diffusion is strongly influenced by partitioning into raft domains as well as by interactions with other membrane species, particularly those immobilized by the cytoskeleton. Such studies have highlighted the interplay between cytoskeleton and lipid rafts in guiding cellular control of membrane species distribution[76]. Because of the tight coupling between rafts and the cytoskeleton, separating the impact of these two structures in whole cells is difficult[77,78].

Several models for the complex diffusion of membrane proteins among domains and cytoskeletal corrals have been developed and evaluated using single molecule tracking (SMT) techniques in cells. Kusumi's hop-diffusion compartmentalization model claims that molecular "fences" formed by cytoskeletal elements and bound membrane protein "pickets" help to organize the plasma membrane into patches with free diffusion within a confinement patch, and occasional hops between patches[79,80]. Weigel et al. analyzed Kv2.1 protein tracking, with GFP and quantum dot labeling, to determine the diffusion process is non-random such that certain regions of the

membrane are more likely to be sampled by the membrane protein and proposed a model of a random walk on a fractal[81]. By disrupting actin with depolymerization drugs, they were able to see random diffusion, indicating Kv2.1 binding to actin plays a key role in its diffusional behavior. In another SMT study, Türkcan et al. used a Bayesian inference scheme to characterize hopping events of ε-toxin receptor (labeled with fluorescent nanoparticles) between raft domains, where they found that hopping between raft domains was limited by the proximity of adjacent domains[82]. After destabilization of rafts with sphingomyelinase or cholesterol oxidase, diffusivity of ε-toxin receptor increases and confinement decreases, indicating the influence of rafts on ε-toxin receptor diffusion.

While SMT studies have provided a wealth of new knowledge about protein behavior in cell membranes, it is important to recognize that not all protein clustering and domain formation involves lipid rafts. Other domains can form as a result of protein-protein interactions without typical raft constituents[83,84]. All of this work suggests a complex interplay of lipid-protein and protein-protein driving forces for lateral membrane organization. Decoupling this complexity to conclusively identify and distinguish protein-protein from lipid-protein interactions and characterize their mechanisms of action is an impetus to use reduced models of membranes in model membrane platforms.

1.4 Artificial Bilayer Platforms

Model membrane methods for probing membrane protein activity in lipid environments aim to bridge the approaches of traditional proteomics and cell based assays. Cellular processes are entangled and individual factor effects are difficult to

isolate. This cell complexity is the motivation for the development and use of biomimetic membrane strategies to model and deconstruct cell membrane processes. Model systems are simplified and tunable, helping to visualize organization and dynamics of membrane species and assay activities of individual components, oftentimes using many of the aforementioned microscopy techniques. In the minimal model approach, these systems contain known lipid and protein components and can be used to isolate and assay behavior of individual species. At the other end of the spectrum, incorporation of cell extracts, including cell membrane-derived vesicles (blebs), combines the beneficial techniques for imaging and assaying model membrane systems with the increased complexity and biological relevance of species studied. The two most commonly used model membrane systems that will be reviewed here are vesicles and solid supported lipid bilayers (SLBs) (Table 1). Less common systems, such as nanodiscs, fluorinated surfactants, and amphiphols are reviewed by Popot[85].

1.4.1 Vesicle-Based Model Membrane Studies

Giant unilamellar vesicles (GUVs) and giant plasma membrane vesicles (GPMVs) are the major vesicle-based model membrane systems. A range of biomolecule complexity can be spanned by these systems from simple, few-component lipid GUVs, to reconstituted proteoliposomes[86], to cell-extracted GPMVs[87]. GUVs are reconstituted lipid systems formed from minimal components. These reconstituted vesicle systems have been crucial for the characterization of phase behavior of lipid mixtures and phase segregation of probes and membrane protein components[70,88–93]. GUVs were used to show that cross-linking of GM_1 glycolipids in membranes led to

large-scale membrane phase separation[94], for example.

GPMVs formed from cell plasma membranes contain native lipids and proteins and therefore capture more biological complexity than GUVs. GPMVs generally display a single lipid phase until temperatures are lowered below the critical point where two phases form and protein partitioning occurs[88,95]. These studies reveal that the cell membrane is near a miscibility critical point. Thus perturbations, such as local composition fluctuations, can cause changes in miscibility and may serve as a means to control raft formation and protein partitioning in the cell membrane. Levental et al. showed that GPMVs of various preparations contained a variety of phases with different properties and compositions reflecting complexity of domains that are possible in cells[96].

Vesicle systems are advantageous because they can easily incorporate mobile integral membrane proteins[97,98]. Because of their spherical geometry, vesicles contain an isolated lumen making them great systems for also evaluating function of transport proteins like ion channels[99–101]. Vesicle systems have been used to study protein function in presence of specific lipids and ligands. Two particular studies generated GUVs with a wide variety of lipid compositions to determine which species can alter protein function. In the first study, β-secretase or BACE, a membrane spanning protease, was shown to have its activity most strongly affected by anionic lipids, but also to some extent by glycosphingolipids and cholesterol[102]. The enhancement of activity by classical raft lipids fits the idea that BACE activity is enhanced in rafts where it is able to interact with its substrate, the amyloid precursor protein[103]. In a second study, the activity of placental alkaline phosphatase (PLAP), a GPI-linked

protein, was shown to decrease in the presence of cholesterol and lipid rafts[104]. Since PLAP, like many GPI proteins, is known to be associated with rafts[105], this response follows a repressive regulation of activity in the presence of rafts, as has also been observed for some other GPI proteins[106].

Because vesicles have a fragile, three-dimensional structure, many surface techniques cannot be used and quantitative imaging often requires confocal or other more sophisticated techniques. In these systems, phase separation and protein partitioning occur at the same time, so the kinetics of protein partitioning cannot be monitored easily; usually these systems are used to monitor distributions at equilibrium conditions. However, phase separation in vesicles cannot be spatially controlled, so labels are needed to indicate phase and protein locations.

1.4.2 Supported Lipid Bilayer-Based Model Membrane Studies

Supported lipid bilayers consist of a solid surface onto which a lipid bilayer is adsorbed typically via a vesicle fusion[107] or Langmuir-Blodgett-Schaeffer transfer technique[108]. The supported lipid bilayer (SLB) is attractive because it provides a controlled, planar 2D platform that facilitates use of a vast array of surface science techniques including those which would be of limited use *in vivo*: total internal reflection fluorescence microscopy[109], atomic force microscopy[110], quartz crystal microbalance[111], and surface plasmon resonance[112] while preserving the important interactions between the membrane lipids and proteins.

While SLBs are promising mimics for cell membranes, two challenges are associated with extending their usefulness to studying myriad membrane proteins: 1) incorporating membrane proteins into the SLBs with their native cell membrane lipid

associations, and 2) minimizing interactions between the extramembranous regions of the proteins and the underlying glass support.

The typical method for inserting membrane proteins into supported lipid bilayers is by detergent mediated reconstitution. These methods can be used for both GUVs which are ruptured to form an SLB or directly onto already formed SLBs, but they require careful optimization of conditions for the protein of interest and may cause changes to the protein conformation[113]. However, some creative methods have been proposed that avoid the use of detergents. One example is the use of whole-cell membrane vesicles that are ruptured into bilayers using the rolling motion of a lipid bilayer under shear to catalyze the rupture process in work done by Simonsson[114]. The process used for generating the cell membrane vesicles is a simple extrusion of the host cells, but this may result in unwanted scrambling between leaflets and between various membranes of the cells. In a similar vein, red blood cell membranes called ghost erythrocytes because of their lack of intracellular parts[115], have been used to generate protein-containing supported lipid bilayers by Tanaka et al[116]. Bilayer quality was improved when a cellulose cushion was used, but no effort was made to determine the extent of protein mobility with this technique.

A promising alternative method is delivery of membrane proteins to the supported bilayer platform by cell blebs. Cell blebs are parts of the cell membrane that bud off into a type of proteoliposome as a result of local detachment of the membrane from the actin cystoskeleton[117]. Overproduction of blebs can be triggered by chemical means and then collected from the culture media[88,118]. Expressing membrane proteins directly into mammalian cell blebs circumvents the difficult purification and

reconstitution procedures. The expression levels attainable are high enough to use in bilayer studies since there is no loss from purification and reconstitution steps. Additionally, the mammalian cells have the required glycosylation machinery to correctly glycosylate protein targets. These systems have been used to generate giant plasma membrane vesicles to study directly, but they can also be used to generate SLBs. Native membrane travels with the membrane proteins all the way to the SLB platform, so any crucial interactions will be preserved.

The second drawback to extending supported lipid bilayers to studying membrane proteins are the interactions between the extramembranous regions of the proteins and the underlying glass support. In a typical phosphatidylcholine (PC) SLB there is a small, ~1 nm water gap between the bottom leaflet and the glass surface[119], that cannot accommodate soluble domains of membrane proteins that could extend around 10 nm long[120]. To solve this problem, various bilayer cushioning or tethering strategies have been proposed that extend the distance between the bilayer and the substrate (Fig. 1.3)[121–124]. One particular strategy that is relatively easy to incorporate and shows improved membrane protein mobility is the double cushion strategy (Fig. 1.3d)[125]. The first cushion is created by adsorbing a passivating layer of proteins (typically bovine serum albumin) to the glass support to reduce non-specific binding. The second cushion is composed of polyethylene glycol (PEG) polymer functionalized lipids interspersed in the bilayer[126–128]. The extension length of the polymer cushion can be controlled by selecting the PEG chain length and the concentration in the bilayer[129,130]. The double cushion strategy increased mobility of annexin V to greater than 70%. In particular, it is unclear if the PEG polymers can provide a uniformly cushioned bilayer

that can protect the incorporated membrane proteins or if cushioned and uncushioned domains will form[131]. An additional concern is that at high grafting densities, PEG cushioning can provide a steric barrier preventing access for ligands to the membrane proteins[132,133]. Alternatively, a swollen hydrophilic maleic acid copolymer support was demonstrated to enable mobile fractions of more than 70% for β-amyloid cleaving enzyme[134]. Self-inserting membrane proteins were added to pre-formed cushioned bilayers in these examples.

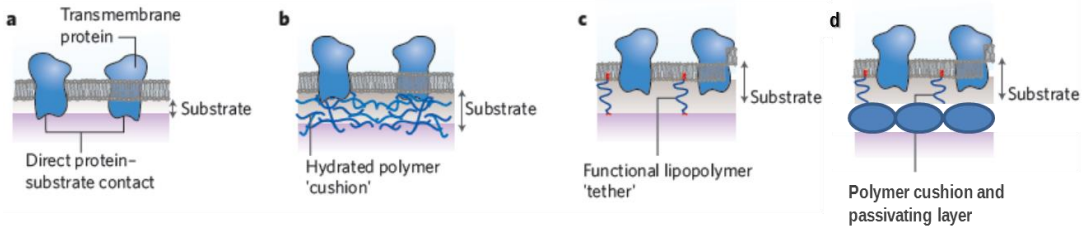

Figure 1.3. SLB cushioning strategies. Incorporation of membrane proteins into supported lipid bilayers has provoked investigation of various strategies to prevent their contact with the solid supports. Figure modified from Sackmann and Tanaka[135].

Unfortunately, although cushioning and tethering techniques show improvement over uncushioned systems, except with self-inserting proteins, many of these strategies still result in less than half of proteins showing any significant mobility, necessitating further development of more generally applicable spacing strategies[123–125,136]. Consequently, application of these cushions to protein assays involving mobile and functional membrane proteins is still in early stages. Because of the limitations described above, most SLB investigations have been restricted to peripheral proteins, small self-inserting proteins, or proteins without domains that extend towards the support.

1.4.2.1 Vesicle Rupture Orientation

Although there has been a strong push towards characterizing supported lipid bilayers to support their use as cell membrane mimics, there are still several key unknowns regarding the widely-used processes of vesicle rupture and bilayer fusion. One of these is the directionality of rupture of vesicles. It would be of great value to know whether this orientation can be predetermined or controlled for the preparation of cytosol side-up or external side-up bilayers for instance. There are four major pathways a vesicle can undergo as it ruptures to form a supported lipid bilayer[137] (Fig. 1.4). Pathway i results in the inner leaflet (white) of the vesicle being in contact with the support in the SLB. Pathways ii and iv form SLBs where the outer vesicle leaflet (grey) contacts the support. Some lipid material is lost to the bulk in pathway iv. Pathway iii forms a mixed bilayer with roughly equal portions of the inner and outer leaflet of the vesicle in contact with the surface.

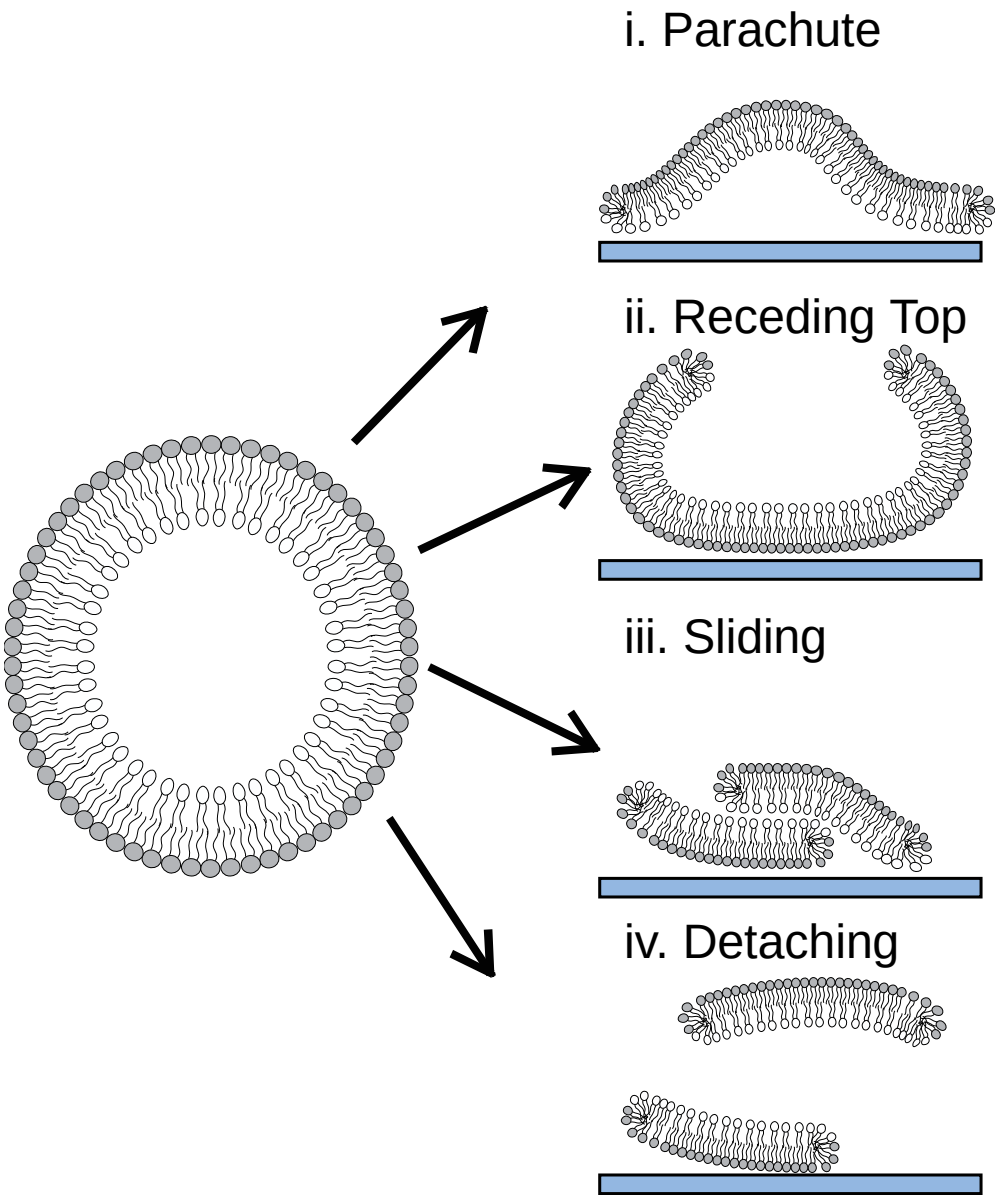

Figure 1.4. Rupture pathways from vesicles to supported lipid bilayers. There are four potential rupture pathways for lipid vesicles. i) The "parachute" mechanism where the outer leaflet of the vesicle (α) becomes the top leaflet of the bilayer. ii) The "receding-top" mechanism where the vesicle unrolls and the inner leaflet (β) becomes the bottom leaflet of the bilayer. iii) The "sliding top" mechanism where the vesicle separates at the high curvature edges and the top bilayer slides off the bottom bilayer giving a mixed membrane. iv) The "detachment" mechanism where a similar behavior to iii occurs, but the upper bilayer drifts away.

The first work done to determine vesicle rupture orientation with membrane proteins was done by Contino et al. in 1994[138]. They reconstituted tissue factor (TF)

into 70% DOPC and 30% DOPS vesicles. Several versions of the vesicles were generated. The initial reconstituted vesicles had a random distribution of inward and outward facing TF molecules. Inward facing TF only vesicles were made by performing a proteolytic digestion of the TF species on the outside. Freeze thaws were used to scramble vesicle orientations after TF to return them to a random distribution and this was confirmed with activity assays on the vesicles. In bilayer assays they saw a reduction to nearly 0% for the digested vesicles and a recovery to about 50% of initial activity with the digested and freeze-thawed vesicles, concluding that the rupture process results in the inner leaflet of vesicles becoming the bottom leaflet of SLBs i.e. mechanism i above. They did not prove that their vesicles had ruptured, however, leaving the possibility that they were simply measuring the in-tact vesicle orientation again.

Jass et al. used AFM to study the rupture process using a carefully designed high cholesterol, DPPG and DPPE containing lipid composition along with DPPC that slowed the process down so that it could be detectable[139]. They sparsely adsorbed 200-400 nm vesicles to the surface, and by scanning the tip sequentially over the same area in a low force tapping mode, they were able to resolve vesicle topography over time. In several cases, visualization of the rupture and bilayer spreading process were captured. In their AFM scans, liposomes with double bilayer thickness spread directionally to form bilayers with single bilayer thickness. The authors concluded that the mechanism was therefore either ii or iii from Fig 1.4. Contact between a spreading bilayer edge and an adsorbed vesicle appeared to trigger fusion of the vesicle which was also observed by others[114]. However, this does not preclude the possibility that the

tapping of the AFM tip could have induced vesicle rupture. Since the tip would contact the upper leaflet, it would be this leaflet that would be destabilized preferentially leading to ii or iii.

Reimhult et al recognized that the work done so far did not sufficiently answer whether bilayer leaflets become scrambled from those of the vesicles that form them[137]. They designed an experiment using their expertise in quartz crystal microbalance (QCM) techniques to try to answer this question. By introducing biotinylated lipids selectively in the outer membrane of vesicles, they could measure neutravidin binding to the bilayers to determine the leaflet orientation. Two side-by-side experiments were used, one where immediately after bilayer formation (~60 s) neutravidin was added and a second where neutravidin was added about 17 hr after bilayer formation to allow for equilibration via lipid flip-flop between leaflets. The results showed that the vesicles ruptured primarily in the inner membrane-up formation following mechanism ii or iv.

Fuhrmans et al. recognized the difficulties experimentalists were having with decrypting the details of the rupture mechanism and designed a coarse-grained model to gain further insight[140]. They determined that both the "parachute" i, and "receding-top" ii, mechanisms were viable under different conditions for interaction strength and range. Lower strength interaction between the bilayer and the substrate would lead to i, while higher interaction strength would lead to ii. They also investigated the effect of bilayer contact with adsorbed vesicles and showed that this mostly followed the "receding-top" mechanism.

Salafsky et al.[141] looked at orientation of photosynthetic reaction centers (RCs)

incorporated into bilayers from reconstituted proteoliposomes. They tested orientation of the RCs in proteoliposomes by looking at bleaching amplitude of $P^+Q_A^-$ recombination kinetics in the presence and absence of cytochrome c which can bind the P-face of the RC and alter the amplitude. In reconstituted proteoliposomes, the orientation of P-face was predominantly outward (95%), confirmed by adding cytochrome c to solution and separately, trapping it within the proteoliposomes. Adding cytochrome c to bilayers with RCs embedded showed a nearly complete loss of bleach amplitude indicating accessibility to the P-face of the RCs. The authors interpreted this as a 90% P-face-up orientation implying vesicle rupture by the "parachute" mechanism (i). They did not explicitly present control samples with inaccessible sites to compare to, so it is possible that cytochrome c could penetrate the bilayer, perhaps through defects, to bind to P-face-down RCs as well.

Human erythrocyte ghost membranes, essentially red blood cells without intracellular parts[115], were used to generate protein-containing supported lipid bilayers by Tanaka et al[116]. It was found that incubation of these ghost membranes directly onto glass supports did not result in rupture or bilayer formation or even much adsorption. Coating the glass surface with a 1.3 nm thick polylysine film resulted in ruptured but segregated patches of bilayer that would not heal together. Using probes for the inside (antibody for transmembrane protein band 3) and outside (peanut agglutinin binding to the glycocalyx) of the ghosts, it was determined that they had ruptured with their insides facing up potentially following the "receding top" or "detachment" mechanism. The authors surmise that the patches did not heal together due to the pinning resulting from strong interactions between the positively charged

polylysine surface and the negatively charged ghost membranes. In another variation, the surface was cushioned using a 10 nm thick cellulose film. In this condition, ghosts ruptured and covered the surface much more completely indicating lateral diffusion of membrane, with the same, inside-up orientation.

1.4.2.2 Supported Lipid Bilayer Patterning

Supported lipid bilayers can be patterned to create arrays of bilayer domains of varied composition or simply separate bilayers into distinct isolated patches. Applications of these techniques include studying membrane compartmentalization during receptor-mediated signaling in mast cells[142], study of T-cell migration[143], screening of drug or protein interactions[144] and measurement of partitioning kinetics of membrane species[145]. Several bilayer patterning techniques exist, each with advantages in certain situations (Fig. 1.5). The four main patterning techniques are polymer mold based stamping or blotting[144,146,147], polymer dry lift-off stenciling[148,149], UV-photopatterning[150] and laminar flow patterning[145,151,152]. Each technique relies on the use of photolithographic processing to create the patterning device with small enough feature sizes to be useful in lipid bilayer studies.

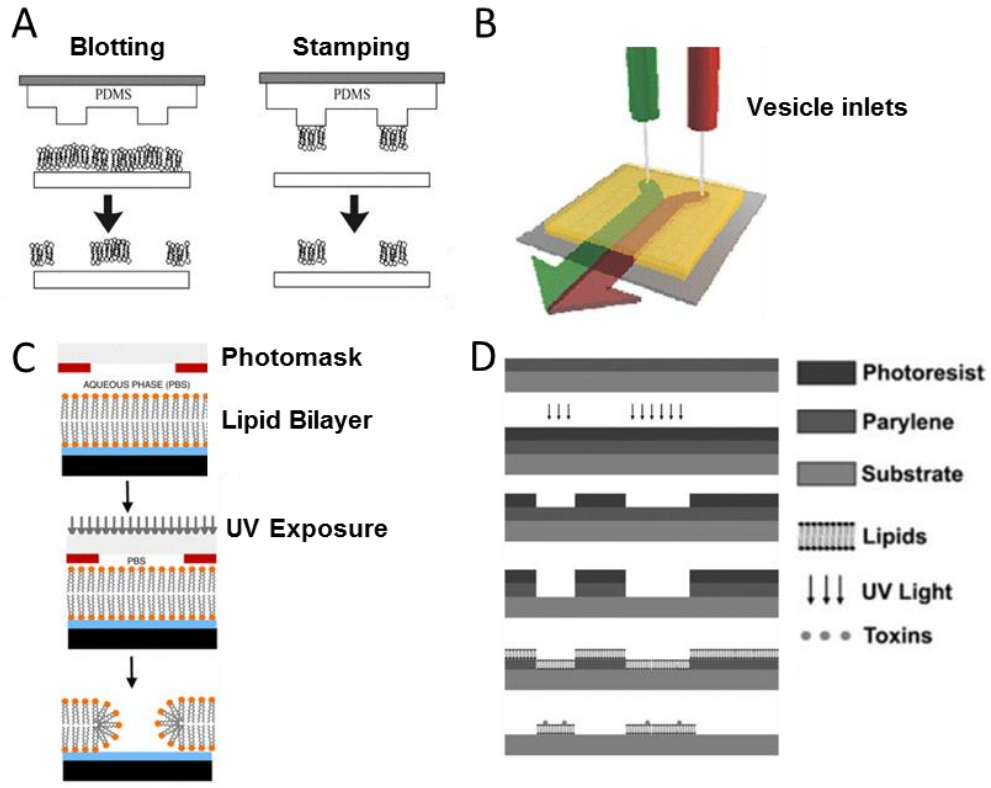

Figure 1.5. Schematic representations of the primary strategies for supported lipid bilayer patterning. Figures reproduced from original works. These types of patterning are: A) polymer blotting and stamping[147], B) laminar flow patterning[152], C) UV-photopatterning[150] and D) polymer lift-off stenciling[149].

The first type of bilayer patterning was patterned grids of photoresist or metals onto SiO_2 using photolithographic techniques[153]. When lipids vesicles are incubated onto these patterned substrates, they readily fuse in the exposed SiO_2, but not on the photoresist or metal barriers. The result is generation of a large array of supported lipid bilayers separated from each other by barriers, which became known as bilayer corrals. A key improvement to bilayer patterning was to simply remove sections of the bilayer using a patterned polymer mold, called microcontact printing[154]. Since the bilayer can only expand a finite amount (~106%)[155], after blotting away a large enough section, a void is created between patches that will remain for at least 1 week.

The inverse of this technique was also demonstrated, where the posts of the stamp are pre-inked with a lipid bilayer and then stamped onto a fresh substrate. It was found that combined with microcontact printing, protein barriers could provide a higher degree of control on the patterned bilayer as well as add in additional functionality while remaining biologically compatibly with the lipid bilayers[146]. Hydrogels can be used as stamping materials to enable easier generation of multiple arrays from a single stamp preparation, increasing statistical relevance, cross-studies of the same bilayer array with different assays, while very efficiently using small amounts of lipids per spot[144].

Another method for patterning is the use of polymer lift-off. A polymer coating is applied to the substrate and patterned using photolithographic techniques. A bilayer is formed into the voids in the polymer (like stenciling) and then the polymer is removed[142]. Polymer lift-off can achieve uniform bilayer patterns down to 1 μm. Another alternative is the use of chemically modified surfaces such as TiO2 surfaces that selectively bind nitrodopamine-mPEG. The PEG domains passivate bilayer formation on those sections of the chip[156].

Two main patterning types exist with a different set of applications in mind. The first and more common type uses patterns where bilayer sections are separated by either voids or protein barriers – we will call this the "bilayer array." The second type employs methods that create voids in the bilayer and then backfills those voids with a second lipid composition. A continuous bilayer that exhibits different compositions and lipid phases in specific locations is formed that remains thermodynamically stable – we will call this the "continuous patterned bilayer."

Bilayer arrays are useful because they facilitate a high number of experiments under the same conditions since they are all on the same chip and as such would be useful in design of biosensors[149]. Generating bilayers with varied receptor density and type of tethering was used to determine binding properties of PEG-linked biotin to streptavidin under shear flow[133]. It has also been used to measure binding kinetics of bacterial toxins[149], look at drug effects on membrane fluidity[144], and present ligands for cell binding in predetermined configurations to investigate cellular processes including mast cell stimulation[142,156].

Continuous patterned bilayers can be used to pattern raft domains into a single continuous non-raft bilayer as a way of mimicking rafts in the cell membrane. Patterning of the underlying support has been used to force raft clustering to predefined regions[157]. It has also been demonstrated that stable patterned DPPC (gel phase) and DLPC (fluid phase) bilayers could be created using blotting or UV photodecomposition and following up with lipid backfilling of the voids[150,158]. This type of pattern can be used to study raft-mediated behavior with lipid compositions more closely aligned to native membranes as demonstrated by Chao & Daniel[145].

They quantified partitioning kinetics of membrane glycolipids using patterned SLBs[145]. The key design point for creating a heterogeneous SLB of pre-determined bilayer phase locations and compositions, is to create two separate lipid solutions already at these precise co-existent compositions rather than one solution that later phase separates on its own at random locations. Using laminar flow to constrain vesicles to specific areas of the platform ensured that via vesicle fusion they would only form bilayers of a distinct lipid phase in a prescribed area. The design generated

two parallel bilayers of co-existent phases that meet along a line interface similar to that shown in Fig. 1.5B. One side contained lipids in the liquid-ordered phase (l_o) (raft-like) and the other contained lipids in the liquid-disordered phase (l_d) and thus eliminated the need for additional components to label the phases. Using a hydrodynamic force provided by the bulk flow in the microchannel, target membrane-bound species to be assayed can be transported in the bilayers. The pre-defined location of stably coexistent phases, in addition to the controllable movement of the target species allowed for control and monitoring of when and where the target molecules approach or leave different lipid phases. Using this approach association and dissociation kinetic parameters for three membrane-bound species, including the glycolipid, GM_1, an important cell signaling molecule and raft domain marker were obtained.

Extensions of this approach that we are currently working on include measuring the partitioning kinetics of other glycolipids; lipid-linked proteins with posttranslational modifications; and transmembrane proteins introduced to the bilayer, enabled by the bleb-SLB approach. We believe this platform will provide insight into how structural factors, membrane compositions, and environmental factors influence dynamic partitioning.

1.5 ACKNOWLEDGEMENTS

Portions of this chapter were published as “A review of traditional and emerging methods to characterize lipid-protein interactions in biological membranes” in Analytical Methods[159]. Mark J. Richards and Chih-Yun Hsia were co-first authors with co-author Susan Daniel. We thank the National Science Foundation (EEC-

0824381, CBET-1149452) for supporting some of the work presented in this chapter. M.J.R. is a fellow in Flexible Electronics for Biological and Life Science Applications. This fellowship is supported by the IGERT Program of the NSF (DGE-0654112) administered by the Nanobiotechnology Center at Cornell. Some of the work presented herein was performed at the Cornell NanoScale Facility, which is supported by the NSF (ECS-0335765).

CHAPTER 2

Two-dimensional Continuous Extraction in Multiphase Lipid Bilayers to Separate, Enrich, and Sort Membrane-bound Species

Note: This chapter was published in its entirety in Analytical Chemistry.

2.1 ABSTRACT

A new method is presented to separate, enrich, and sort membrane-bound biomolecules based on their affinity for different co-existing lipid phases in a supported lipid bilayer using a two-dimensional, continuous extraction procedure. Analogous to classic liquid-liquid phase extraction, we created two distinct lipid phases in our planar membrane system: a liquid-ordered (l_o) phase and a liquid-disordered (l_d) phase arranged in parallel stripes inside a microfluidic device. Membrane-bound biomolecules in an adjacent supported lipid bilayer are convected in plane along the microfluidic channel and brought into contact with a different lipid phase using hydrodynamic force. A mixture of two lipid species, a glycolipid and a phospholipid, with known affinities for the two lipid phases employed here are used to demonstrate continuous extraction of the lipid-microdomain preferring glycolipid to the l_o phase, while the phospholipid remains primarily in the l_d phase. In this demonstration, we characterize the performance of this affinity-based separation device by building models to describe the velocity profile and transport in the two-phase coexistent membrane. We then characterize the impact of residence time on the

extraction yield of each species. This new procedure sorts membrane species based on chemical properties and affinities for specific lipid phases within a membrane environment near physiological conditions, critical for extending this method to the separation of lipid-linked proteins and transmembrane proteins while minimizing denaturation. This platform could facilitate the separation and identification of lipid membrane domain residents, or the characterization of changes in membrane affinity due to post-translational modifications or environmental conditions.

2.2 INTRODUCTION

Membrane proteins and glycolipids are targets for therapeutic development[2], but processing membrane-bound species while maintaining intact structural information, proper orientation, and necessary lipid associations remains a large bottleneck to characterizing and understanding their structure-function behavior[160,161]. The problem stems from the requirement of protecting the hydrophobic regions from water during processing. Many purification strategies use denaturing chemicals or conditions to remove species from the membrane and then use techniques developed mainly for soluble species to isolate them[162,163]. This approach can cause denaturation (in the case of proteins), disrupt orientational order necessary for binding to soluble species, and interrupt critical lipid associations (e.g. lipid microdomains) that are important for function[164,165]. Therefore, additional steps are required to restore the native, active structures and lipid associations. New strategies for separating membrane species in a native-like environment (i.e., a lipid bilayer) near physiological conditions would be attractive alternatives for this class of biomolecules.

A supported lipid bilayer (SLB) platform can protect the hydrophobic regions of membrane species. SLBs are chemically tunable and maintain the mobility of the species residing within them, including lipids[166], glycolipids[167], lipid-linked proteins[168], and even some transmembrane species[123,125,169]. The planar geometry of SLBs facilitates the integration of surface analytical techniques that can be used to monitor lipid-lipid, protein-protein, or lipid-protein interactions, such as fluorescence microscopy[59,170], ellipsometry[171], and atomic force microscopy[60,61,172,173].

Previous studies demonstrate the separation of membrane-bound biomolecules supported lipid bilayers using electrophoresis[166,174–177], bilayer self-spreading[178], or bulk hydrodynamic drag[179,180]. However, these studies used SLBs of homogeneous chemical composition as the separation medium, so the separation was based solely on differences in biomolecule charge and/or mobility through the bilayer medium. None of these strategies separate species based on their affinity for a specific lipid chemistry/environment.

Herein, we describe a planar (2-D) extraction platform that uses a two-phase coexistent SLB to separate membrane species based on their different chemical affinities for chemically-distinct phases in the bilayer. This strategy is suited to this class of biomolecules because of the natural tendency of membrane-bound species to associate with different lipid phases in the cell membrane, such as glycolipids[54], GPI-linked lipids[55] and certain proteins[56]. These species tend to associate with lipid microdomains known as lipid rafts. Other membrane constituents tend to avoid lipid rafts and reside in more disordered phases enriched with phospholipids[57]. We exploit this natural partitioning tendency to carry out a two-dimensional extraction process in

a planar SLB platform. To do so, different phases in the SLB (i.e. membrane heterogeneity) must be constructed and patterned in a useful geometrical shape that facilitates the physical separation and sorting of species. Many studies have shown that co-existent liquid-ordered and liquid-disordered lipid phases can exist in model membrane systems[59–64], but controlling the location of these phases has been a challenge. Recently we described a way to pattern stable phases in an SLB using laminar flow in a microfluidic device for the purpose of measuring partitioning kinetics of membrane-bound species to various lipid phases[145]. These partitioning rates were necessary parameters to measure for the current separation studies we present here. Here, we build upon this platform to perform 2-D extractions in planar membranes, characterize the separation and yield (enrichment) of membrane species to the different lipid phases, and develop a transport model for membrane-bound species in these two-phase bilayers.

2.3 EXPERIMENTAL SECTION

2.3.1 Materials

1-Palmitoyl-2-oleoyl-sn-glycero-3-phosphocholine (POPC), Ovine wool cholesterol (Chol), and 16:0 N-palmitoyl-D-*erythro*-sphingosylphosphorylcholine (PSM) were purchased from Avanti Polar Lipids (Alabaster, AL). N-(4,4-difluoro-5,7-dimethyl-4-bora-3a,4a-diaza-s-indacene-3-propionyl)-1,2-dihexadecanoyl-sn-glycero-3-phosphoethanolamine, triethylammonium salt (head-labeled BODIPY FL DHPE), and Alexa Fluor 594 hydrazide used to label the head group of asialoganglioside-G_{M1} were purchased from Invitrogen (Eugene, OR). Bovine brain asialoganglioside-G_{M1} and all other reagents, unless otherwise specified, were purchased from Sigma (St.

Louis, MO). Glass coverslips (25 mm x 25 mm; No. 1.5) from VWR were used as solid supports for the bilayers. Polydimethylsiloxane (PDMS; Sylgard 184) polymer used to fabricate microfluidic devices was purchased from Robert McKeown Company (Branchburg, NJ).

2.3.2 Fluorescence Microscopy

Images were obtained using an inverted Zeiss Axiovert Observer.Z1 fluorescence microscope equipped with α Plan-Apochromat objectives, a Hamamatsu EM-CCD camera (ImageEM, model C9100-13, Bridgewater, NJ), and X-Cite® 120 microscope light source (Lumen Dynamics Group Inc., Canada). ET GFP filter cube (49002, c106273, Chromatech Inc.) was used to collect the fluorescence emitted from BODIPY fluorophores. ET MCH/TR filter cube (49008, c106274, Chromatech Inc.) was used to collect the fluorescence emitted from Alexa 594 fluorophores.

Zeiss AxioVision software was used to obtain images and the fluorescence intensity data for lipid diffusion and separation analyses. The contrast of an entire image was enhanced in ImageJ (NIH, Bethesda, MD) when necessary.

2.3.3 Preparation of Lipid Vesicles for Formation of Supported Lipid Bilayers

Lipids dissolved in a methanol and chloroform solution were mixed together at the desired compositions and then dried under a vacuum desiccator to remove the solvent. The dried lipid mixture was then reconstituted into multi-lamellar vesicles at a concentration of 2 mg/mL in buffer composed of 5 mM phosphate buffered saline (PBS) with 150 mM NaCl at a pH of 7.4. LUVs were formed by extruding the reconstituted mixture 19 times through a 50 nm Whatman polycarbonate filter in an Avanti Mini-Extruder (Alabaster, AL). The vesicle solutions were diluted to 0.5

mg/mL before use. All vesicles were on the order of 100 nm in diameter after processing as determined by dynamic light scattering measurements (Zetasizer Nano, Malvern Instruments, Worcestershire, UK).

2.3.4 Microfluidic Channel Preparation

The polydimethylsiloxane (PDMS) microfluidic device was made by standard soft-lithography procedures at the Cornell Nanoscale Facility. PDMS prepolymer, along with a curing agent, was cast on the silicon wafer mold and cured at 85^{o}C for 3 hrs, producing a soft flexible material with the channels embedded in negative relief once removed from the mold. The channel inlets and outlets are connected to outside tubing by punching the PDMS mold with 20 gauge needles (610 μm ID). Glass coverslips, which become the fourth wall of the microfluidic channel, were cleaned in piranha solution (70:30 volume ratio of H_2SO_4 to 50% H_2O_2) for 10 min and rinsed thoroughly with distilled water for 20 min. Before use, glass slides and the PDMS mold were rinsed with deionized water, dried under high purity nitrogen air, and then treated with oxygen plasma using a Harrick Plasma Cleaner (Model # PDC-32G, Ithaca, NY) at a pressure of 750 micron on the high setting for 30 seconds. Immediately after plasma cleaning, the glass slide and PDMS mold were pressed together and heated for 10 minutes at 80^{o}C to seal the microfluidic channel device.

2.3.5 Formation of Patterned Supported Lipid Bilayers in a Single Stage Microfluidic Device

In this work, SLBs are formed during laminar flow conditions instead of under stagnant incubation. Laminar flow is advantageous for patterning heterogeneous bilayers in microfluidic channels because particles follow streamlines with minimal

mixing[151]. Thus, lipid vesicles of different compositions can be sent through the channel on different streamlines and upon rupture will form contiguous, parallel bilayers. If the compositions are chosen so that they are phase stable, these bilayer stripes will have stable interfaces. The compositions of the two coexistent phases used in this work were chosen based on a published ternary phase diagram of POPC/PSM/Chol. We plotted a hypothetical tie line in this phase diagram, guided by previous literature[181,182] and chose phase compositions close to the ends of this tie line. Recent work corroborates our selection of compositions for two-phase stability[183]. These compositions are 70/20/10 molar ratio of POPC/PSM/Chol, denoted as l_d phase, and 60/40 molar ratio of PSM/Chol, denoted as l_o phase. We found that we could pattern a composite membrane based on these compositions inside a microfluidic channel using laminar flow (as will be described in detail next) to define regions of specific lipid phases within the channel. Membrane-bound biomolecules are able to move between the phases after patterning.

To form a composite lipid bilayer with these lipid phases and load membrane at specified locations, we used the following procedure illustrated in Fig. 2.1. First, we sent l_o phase vesicles and a buffer stream concurrently through the main microfluidic channel. The buffer flow serves to keep the l_o phase vesicle stream, and thus the supported l_o phase bilayer, confined to one side of the channel. During this step, the system was heated to 65°C (both the device and the lipid mixture), so that the l_o phase lipid mixture was above its phase transition temperature and readily fused to the glass surface to form a bilayer. Afterwards, a 65°C buffer was used to rinse out the excess vesicles and the system was equilibrated to room temperature for 1 hr to allow the l_o

phase membrane to gradually cool down. Next, the vesicles with load mixture (mixture denoted as red and green dots in orange background) were sent through the perpendicular loading channel. The load mixture was composed of the same composition as lipid l_d phase, but also included small amounts of the labeled glycolipid, Alexa 594-G_{M1}, and BODIPY DHPE lipid (approx. 1 mol % of each). At the same time, buffer flow from all other ports was maintained at a slow rate to prevent the load vesicles from entering into the main channel (these streams are omitted in the illustration). The membrane with the load mixture formed only on the glass surface where there was no bilayer under the stream of the load vesicles. Finally, l_d phase vesicles were sent through the main channel (denoted as a pink arrow in the figure) and filled the exposed regions of the glass surface that had not been covered by lipid membranes.

In all of these steps, vesicles were exposed to the glass surface for 5 min under flow and then rinsed with buffer for 20 min. When the load formed, the flow rate of the load vesicle solution in the upstream side channel (50 μm wide and 70 μm high) was 10 μL/min and the overall flow rate of the load vesicle solution and buffers in the downstream side channel (50 μm wide and 70 μm high) was 30 μL/min. When the lipid phases formed, the flow rates of vesicle solutions and rinsing buffers were kept at 20 μL/min in the main channel (100 μm wide and 70 μm high).

To transport the mixed species into the main composite bilayer channel after bilayer formation, aqueous buffer flow was applied in the main channel towards the "Y" branch into the exit ports at a rate of 80 μL/min. The hydrodynamic flow provided a shear force on the membrane biomolecules that served to drag them along

the main channel. Biomolecules were able to partition into either membrane phase across the channel by diffusion and were collected at the end of the channel in the separate ports.

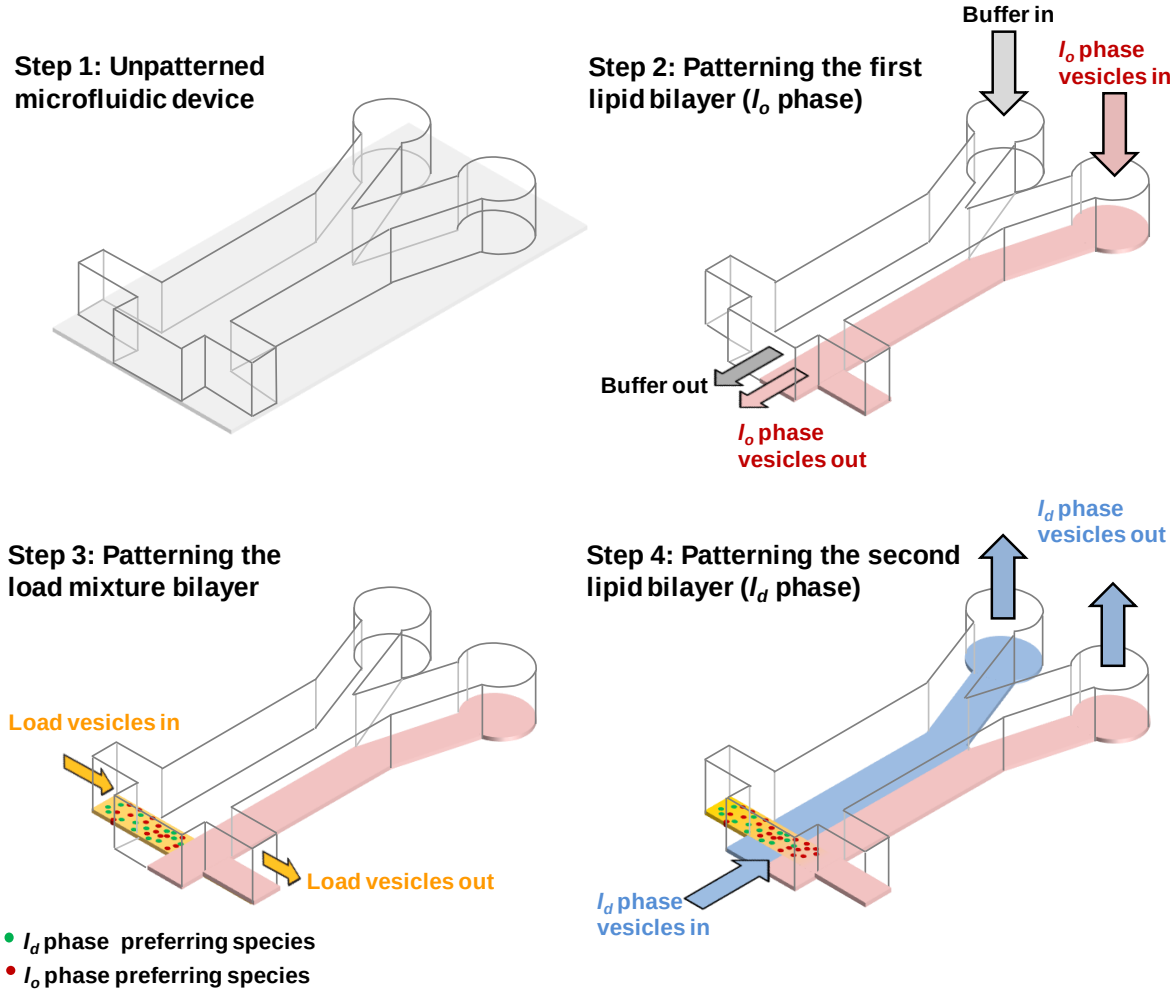

Figure 2.1. A three-dimensional cut-away view illustrating the loading and patterning of bilayers into the microfluidic device via vesicle fusion and laminar flow patterning, as described in the text. The pink color represents lipid l_o phase, the lipid-ordered bilayer; the blue color represents lipid l_d phase, the lipid-disordered bilayer; and the orange color represents the load bilayer that is the same composition as l_d phase, except that it contains the biomolecules to be separated and sorted. Green and red circles represent the biomolecule mixture. The arrows show the direction of the flow and streamlines as the pattern is being formed. Step 1: the blank microfluidic device design consisting of a clear PDMS mold bound to a glass support. The glass support is removed in the subsequent illustrations for clarity. Step 2: patterning lipid l_o phase. During this step the device is warmed to ~ 65°C. Step 3: forming the load bilayer containing the mixture of membrane-bound biomolecules after l_o phase bilayer has been formed. Load only forms where vesicles contact glass, i.e. not where l_o phase bilayer already exists. Buffer flow also enters from the sides to confine the flow to the loading channel, but is omitted here for clarity. Step 4: patterning the l_d phase bilayer after both the load and l_o phase bilayers are formed. Note that while the l_d phase bilayer is forming, some of the l_o phase-preferring species (red here) begin to partition into

the l_o phase bilayer adjacent to the mixture load.

2.3.6 Background Removal and Vignetting Correction

A background subtraction was used to reduce the effect of fluctuations in the light source and to zero the baseline measurement. Background levels measured immediately adjacent to the channel at each time point where subtracted from all intensity measurements. Even after background subtractions, we found that vignetting remained an issue in our system such that our mass balance did not close entirely. Vignetting causes intensities in the center of the image to be slightly higher than at the edges. The main effect of this on our mass balance is to cause the inlet and outlet fluxes to differ depending on where they were located relative to the center of the field of view.

To correct for slight variation in light intensity, we applied a vignetting correction factor *(f)* to scale the outlet intensity to account for slight uneven illumination. We used the mass balance to solve for this factor at various positions, *L*, along the channel then fit the data to a second order polynomial *F(x)* which could then be used to scale the intensity at any position in the channel. We found that less than 10% correction was required to correct for uneven illumination. The vignetting correction was performed for BODIPY DHPE and Alexa 594-GM_1 independently.

2.3.7 Characterization of Diffusion in Supported Lipid Bilayer by Fluorescence Recovery After Photobleaching (FRAP)

To measure the diffusion coefficient of species in the supported bilayer, a 20 μm diameter spot in the supported lipid bilayer was bleached with a 4.7 mW wavelength

tunable Argon/Krypton laser (CVI Melles Griot, Model 643-AP-A01) for 200 ms at the appropriate wavelength for each fluorophore label. The recovery of the fluorescence intensity of the photobleached spot was recorded for 15 minutes. Each image was background subtracted and normalized. The recovery data was fit using a Bessel function following the method of Soumpasis[184]. The diffusion coefficient was then calculated using the following equation: $D = \frac{w^2}{4t_{1/2}}$, where *w* is the width at half-maximum of the Gaussian profile of the focused beam.

2.3.8 Characterization of the Velocity Profile in a Two-Phase Supported Bilayer Using Fluorophore Photobleaching

In order to visualize and determine the velocity profile within the two-phase striped bilayer, a photobleaching technique was performed similar to that described by Jönsson et al[185]. Briefly, the convective motion of the SLB containing fluorescent species was driven by shear force, provided by the flow of buffer through the microfluidic channel. Flow was started prior to the bleaching experiment to ensure a fully-developed flow profile at a rate of 80 μL/min in the main channel. A thin photobleached line was created across the channel width on the SLB under a 20x objective with an Argon-Krypton tunable laser. The photobleached line was generated by quickly moving the stage relative to the focused, stationary laser spot. Images were recorded every 10 seconds post-bleach. The photobleached band moved along the direction of the flow and its shape changed accordingly as shown in Fig. 2.4. The displacement of the photobleached line along with its shape evolution reveals how the target molecules are transported in the SLB and was used to determine a model for the

velocity profile in the two-phase bilayer. In this experiment both phases of the bilayer were doped with 1 mol % BODIPY DHPE so that the entire cross-section of the bilayer could be photobleached with a single laser line and tracked.

2.3.9 Simulation

A convection-diffusion model was constructed using COMSOL Multiphysics to simulate the transport of membrane species in the extraction device. Parameters for the model were obtained from literature or independent experiments, as described in detail in the *Results* section.

2.4 RESULTS AND DISCUSSION

2.4.1 Separating and Sorting Membrane-Bound Species Using Bilayer Extraction

In analogy to classic liquid-liquid extraction, we demonstrate a 2-D continuous extraction in SLBs by separating two lipid species: the glycolipid G_{M1}, and BODIPY DHPE, a phospholipid. These species were chosen because they have known affinities for the particular lipid phases we employ. For these experiments, we chose two stably coexistent lipid membrane phases. The l_d phase is: 70 mol % POPC, 20 mol % PSM, and 10 mol % cholesterol. The l_o phase is: 60 mol % PSM and 40 mol % cholesterol. The geometry of the two phases was patterned to facilitate continuous extraction and biomolecule sorting to different parts of the microfluidic chip following enrichment. The feed bilayer, containing the biomolecule mixture to sort, was chosen to match the l_d phase for maximum stability and compatibility. An illustration of the platform is in Figure 2.2A. Bilayer patterning was carried out using a combination of laminar flow and vesicle fusion techniques as described in the *Experimental* section[145].

After bilayer patterning, an applied hydrodynamic flow of the bulk solution in the microfluidic device provides a shear stress to drive the lipids in the membrane to move[166,179,186]. In this particular system, we characterized independently that the intrinsic mobility of biomolecules in the l_d phase is ~5 times greater than the mobility in the l_o phase using a fluorescence recovery after photobleaching technique[145,184,187]. Thus, most of the convection of biomolecules occurs in the l_d phase. When meeting the l_o phase, a biomolecule has the potential to be extracted depending on its chemical affinity. Figure 2.2B shows fluorescence images of continuous extraction in the patterned SLB platform.

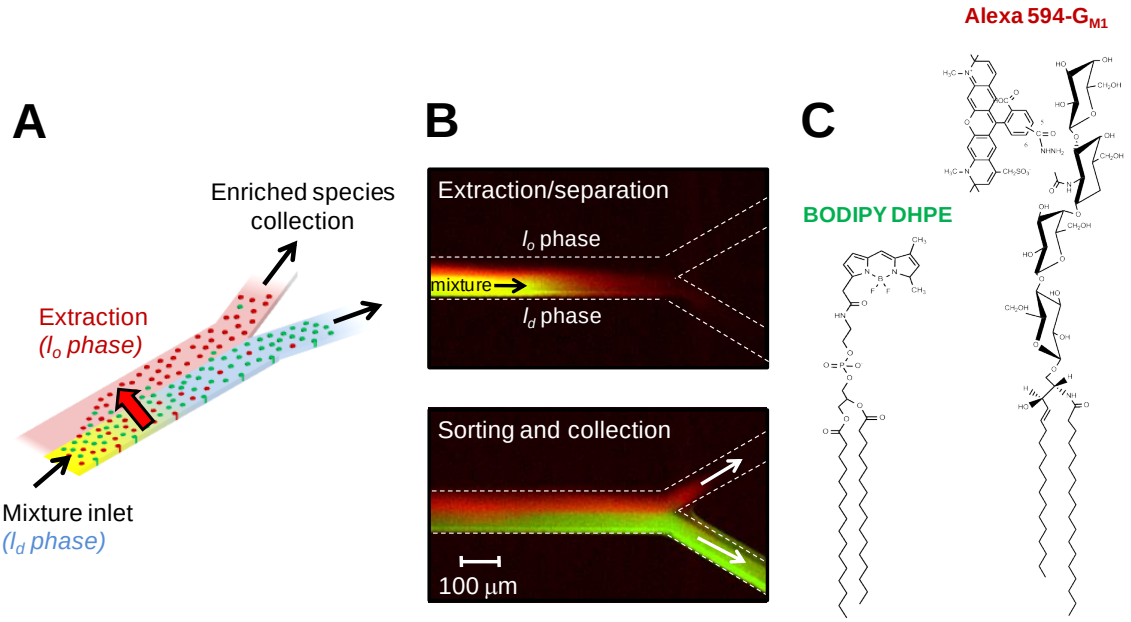

Figure 2.2 (A) A three-dimensional illustration of the two-phase supported lipid bilayer designed to separate and sort membrane biomolecules. The microfluidic device and glass support have been omitted for clarity. Laminar flow in a microfluidic device is used to create parallel stripes of coexistent lipid phases (l_d phase = blue, l_o phase = pink). The interface between the phases is contiguous, allowing membrane-bound molecules to partition into a preferred phase as they are transported down the main channel. The initial mixture is color-coded as red and green dots and is transported in the l_d phase. Red species are extracted into the l_o phase bilayer, causing the l_d phase to become more enriched in green species. (B) In the experiment, the mixture is BODIPY DHPE (green) and Alexa 594-G_{M1} (red) and appears yellow in the upper image. In these top-view images, the l_d phase was patterned in the bottom section, where yellow is dominant, while l_o phase is in the top half (initially devoid of any fluorophore). The species are transported to the right in the l_d phase membrane along the main channel. The red color

ahead of the yellow plug is a small amount of Alexa 594-G_{M1} that moves slightly faster under bulk flow than BODIPY DHPE because it has a larger cross section. In the bottom image, the red Alexa 594-G_{M1} is extracted into the l_o phase, while BODIPY DHPE generally remains in the l_d phase. Separated fractions are split by the "Y" at the end of the channel. (C) The chemical structures of Alexa 594-G_{M1} and BODIPY DHPE.

To demonstrate separation, extraction, and sorting, two fluorescently-labeled membrane biomolecules with differing propensities to partition into the two membrane phases were used. The fluorescent labels make it easy to track the biomolecules' positions in the device and quantify the extraction. We chose the glycolipid, G_{M1}, because it has established membrane partitioning behavior and serves as a typical marker for cell microdomains (lipids rafts). Since the acyl chain label in commercially available fluorescently-labeled G_{M1} disrupts its native preference for ordered lipid phases in cell membranes[54,64], we synthesized a head-labeled version, Alexa 594-G_{M1}[145,170]. We mixed Alexa 594-G_{M1} with another fluorescently-labeled phospholipid, BODIPY DHPE, which generally prefers lipid disordered phases, such as those composed primarily of POPC[145]. The structures of both of these biomolecules are shown in Figure 2.2C.

In a first set of experiments, an approximately equimolar mixture of Alexa 594-G_{M1} (red fluorophore) and BODIPY-DHPE (green fluorophore) was loaded into the device (1 mol% of each in the load bilayer formulation), Figure 2.2B. The mixture is yellow when the red and green false-color images are superimposed on each other (Figure 2.2B, top image). Figure 2.2B, bottom image, is a later snapshot of the continuous extraction, showing the preferential affinity of red Alexa 594-G_{M1} to the l_o phase, and the enrichment of the green BODIPY DHPE in the l_d phase. At the end of the channel a "Y" split directs the fractions to different areas of the chip for collection. A movie of the extraction and sorting process is provided in the *Supporting*

Information available at http://pubs.acs.org. A control experiment without patterning is also shown there.

The exposure times during image acquisition for each channel (red or green) were set such that the starting intensities were nearly the same. The fluorescence intensity for each biomolecule in each phase varied linearly with concentration for the range of concentrations used here[145]. Because of these features, fluorescence intensity can be used to report concentration for these species to quantify the enrichment after the extraction process. To minimize photobleaching, samples were imaged every two minutes instead of continuously. Intensities were normalized to background fluorescence levels and minor corrections for vignetting were made, as described in the *Experimental* section.

2.4.2 Extraction Efficiency – Theory and Analysis

Based on the design of this device, the extraction channel is analogous to a single stage extractor, operating in the 2-D plane of the bilayer. Due to practical kinetic limitations during experimental operation, the real performance of an extractor is often below what is predicted under equilibrium conditions. The real performance is quantified by calculating yield, *Y*, of a particular species in a particular lipid phase. A control volume in the 2-D membrane is shown in Figure 2.3. Initially, the entire control volume is devoid of any fluorescently-labeled species. The yield in phase *i*, $Y_i(t)$, is defined as the amount of species in phase *i* compared to the overall amount entering the control volume:

$$Y_i(t) = \frac{\alpha_{i,out}(t) + N_i(t)}{\alpha_{ld,in}(t) + \alpha_{lo,in}(t)} \qquad \text{(Eq. 2.1)}$$

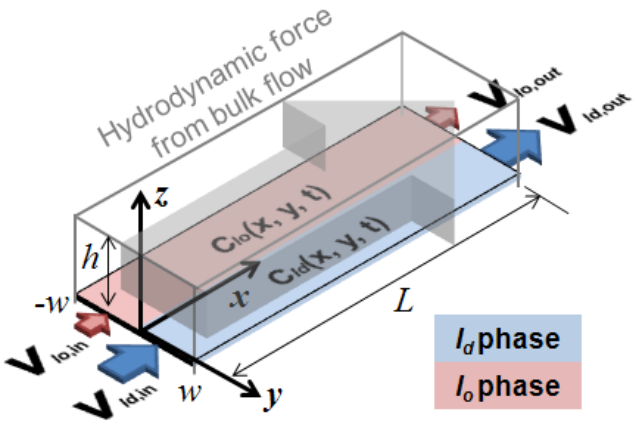

Figure 2.3. 2-D two-phase bilayer control volume in a 3-D view of the microchannel with the parameters used in the data analysis. All parameters are defined in the text. Blue denotes the l_d phase, and pink denotes the l_o phase. The hydrodynamic force from the bulk flow (gray arrow) convects species in the lipid membrane.

Yield in these experiments is a function of time because the initial input (the mixture) is a discrete plug of material and the extracted amount is significantly influenced by the local concentration distribution of the species in the two phases. $\alpha_{i,in}$ and $\alpha_{i,out}$ are the cumulative material that has entered/left the control volume by the reporting time, respectively.

Material accumulation in each phase $N_i(t)$, can be obtained directly by integrating fluorescence from the time-lapse micrographs. Cumulative material entering/exiting a particular phase in the control volume, $\alpha_i(t)$, is defined generally in Eq. 2.2, where $F_i(t)$ is the amount of material entering at $x=0$ or exiting a phase i at $x=L$ in time:

$$\alpha_{i,\,in\,or\,out}(t) = \int_0^t F_{i,\,in\,or\,out}(t)\,dt \qquad \text{(Eq. 2.2)}$$

The equations that describe the amount of the material entering the l_o phase at $x=0$ and exiting at $x=L$ in time are:

$$F_{lo,in}(t) = \int_{y=-w}^{y=0} v(0,y) \cdot C(0,y,t)\, dy \qquad \text{(Eq. 2.3)}$$

$$F_{lo,out}(t) = \int_{y=-w}^{y=0} v(L,y) \cdot C(L,y,t)\, dy \qquad \text{(Eq. 2.4)}$$

where *v(x,y)* is the velocity of a species in the membrane and *w* is the width of the phase cross-section. Under conditions of fully developed bulk flow, the overall velocity profile in the planar membrane is a function of *y* only. The concentration profile across the bilayer can be obtained by measuring fluorescence intensity from experimental images. To calculate the yield, all that remains is to determine the velocity profile in the two-phase membrane.

2.4.3 Characterization of Convection Velocity Profile in a Two-Phase Coexistent Supported Bilayer

In this work, the convection of biomolecules in the supported bilayer is induced by the shear force resulting from bulk buffer flow inside the microchannel. Previous study of homogeneous (single lipid phase) bilayer systems has shown that when sheared in this manner, the upper monolayer of the SLB moves in the direction of the drag while the lower monolayer is approximately stationary[185,188]. These studies suggest that the lipid monolayer can be viewed as a 2-D continuum and the flow velocity can be described by the continuity equation and Navier-Stokes equation for creeping flow in 2-D and assuming fully developed flow and negligible viscous forces and surface pressure gradients.

The velocity profile in a homogeneous bilayer induced by hydrodynamic flow at the bilayer surface within a rectangular channel (Fig. 2.3B) is described by the following set of equations[185,188]:

$$\sigma_{hydro}(y) = -\frac{\Delta p}{\Delta x}\frac{h}{2}\left(1 - \frac{8}{\pi^2}\sum_{k_{odd}}^{\infty}\frac{1}{k^2}\frac{\cosh\left(\frac{k\pi y}{h}\right)}{\cosh\left(\frac{k\pi w}{h}\right)}\right) \quad \text{(Eq. 2.5)}$$

$$v(y) = \frac{\sigma_{hydro}(y)}{b}e_x \quad \text{(Eq. 2.6)}$$

where $\sigma_{hydro}(y)$ is the shear force from hydrodynamic bulk fluid flow; $\Delta p/\Delta x$ is the pressure drop over length of the channel; y is the position across the channel, perpendicular to the flow direction; h is the channel height; $2w$ is the width of channel; $v(y)$ is the velocity; b is the intermonolayer friction factor; and e_x is the unit vector in the x direction. Note here that the buffer flow is assumed to be fully developed and constant and that viscous forces and surface pressure gradients are negligible compared to the hydrodynamic force[188].

We build upon this work to describe the motion of biomolecules in a two-phase heterogeneous bilayer arranged in two stripes parallel with the bulk hydrodynamic flow. We have experimentally observed that there are three regions with distinct membrane compositions: a l_o phase region, a l_d phase region, and an interfacial transition region in-between[145]. Species present in these different bilayer environments possess different mobilities, and therefore velocities, when subjected to a shear force. The overall velocity profile in this system is approximated as a piece-wise function of the velocity profile in each phase and interfacial region:

$$v(y) = \begin{cases} \dfrac{\sigma_{hydro}(y)}{b_{lo}} e_x & \text{when } y < y_{Tlo} \text{ in the } l_o \text{ phase} \quad \text{(Eq. 2.7 a)} \\ \dfrac{\sigma_{hydro}(y)}{b_{trans}} e_x & \text{when } y_{Tlo} < y < y_{Tld} \text{ in the transition zone} \quad \text{(Eq. 2.7 b)} \\ \dfrac{\sigma_{hydro}(y)}{b_{ld}} e_x = \dfrac{5\sigma_{hydro}(y)}{b_{lo}} e_x & \text{when } y > y_{Tld} \text{ in } l_d \text{ phase} \quad \text{(Eq. 2.7 c)} \end{cases}$$

where y_{Tlo}, y_{Tld} are the locations of the boundaries of the transition zone between the l_o side and l_d side, respectively. b_{lo} = friction factor in the l_o phase, b_{trans} = friction factor in the transition zone between phases, and b_{ld} = friction factor in the l_d phase. The ratio for friction factor in l_o to l_d was ~5 for both BODIPY DHPE and Alexa 594-G_{M1} determined via a photobleaching technique. This ratio is substituted into Eq. 2.7c to reduce the number of parameters.

b_{trans} is difficult to define because the exact structure of the interfacial zone is unknown. However, since this region is small compared to the rest of the channel, we make the approximation that the velocity (and therefore b) varies linearly in this region. Thus, the velocity in this region can be rewritten to eliminate b_{trans} in Eq. 2.7 b as:

$$v(y) = \sigma_{hydro}\left(\frac{1}{b_{lo}} + \frac{y - y_{Tlo}}{y_{Tld} - y_{Tlo}}\left(\frac{1}{b_{ld}} - \frac{1}{b_{lo}}\right)\right)e_x = \sigma_{hydro}\left(\frac{1}{b_{lo}} + \frac{y - y_{Tlo}}{y_{Tld} - y_{Tlo}}\left(\frac{4}{b_{lo}}\right)\right)e_x \quad \text{when } y_{Tlo} < y < y_{Tld}$$

(Eq. 2.8)

The general velocity profile shape was visualized (Fig. 2.4A, inset) using a photobleaching technique. The general shape is captured by our piece-wise model, so b_{lo} is the only parameter remaining to obtain the $v(y)$.

Note that the photobleaching technique cannot be used directly to obtain b_{lo} in each extraction run because fluorescence intensity is being tracked as a proxy for concentration. Instead, an independent mass balance is used to determine the value of b_{lo} that corresponds to the experimental conditions of a particular run. To illustrate the mass balance process, we present the result for one experiment using the longest channel length, 710 μm, at 80 μl/min bulk flow rate (Fig. 2.3). This mass balance procedure is repeated for each experiment to obtain the best fit parameter for that experiment. The mass balance on the control volume is:

$$Accumulation(t) = \int_0^t \int_{-w}^{+w} \left[C(0,y,t)\cdot v(y)\right]_{in} - \left[C(L,y,t)\cdot v(y)\right]_{out} dy\, dt \quad \text{(Eq. 2.9)}$$

Accumulation (LHS side of Eq. 2.9) can be obtained directly from time-lapse fluorescence micrographs and plotted as a function of time, as shown for Alexa 594-G_{M1} in Fig. 2.4C (solid line). For the RHS of Eq. 2.9, the concentrations, $C(0,y,t)$ and $C(L,y,t)$, are obtained directly from the fluorescence micrographs at the inlet and outlet locations. At this point, the magnitude of $v(y)$ for the RHS of Eq. 2.9 is unknown, but the shape of the profile has been experimentally verified, as described above, and is given by Eq. 2.7. Because the flow is steady, $v(y)$ does not vary with x, so the values at the inlet and outlet on a particular streamline are the same, i.e., $v(y)_{in} = v(y)_{out}$. b_{lo} is determined by minimizing the difference between the LHS and RHS of Eq. 2.9 (solid vs. dashed lines, Fig. 2.4C). For Alexa 594-G_{M1} for this particular run, $b_{lo} = 3.0 \times 10^8$ Pa·s/m. The red line in Fig. 2.4B is the corresponding velocity profile for Alexa 594-G_{M1}. The same procedure is followed for BODIPY DHPE. The values for intermonolayer friction coefficients (b_i's) averaged over several experiments are shown in Table 2.1 and correspond well to values found in literature for similar bilayer

phases[180,189].

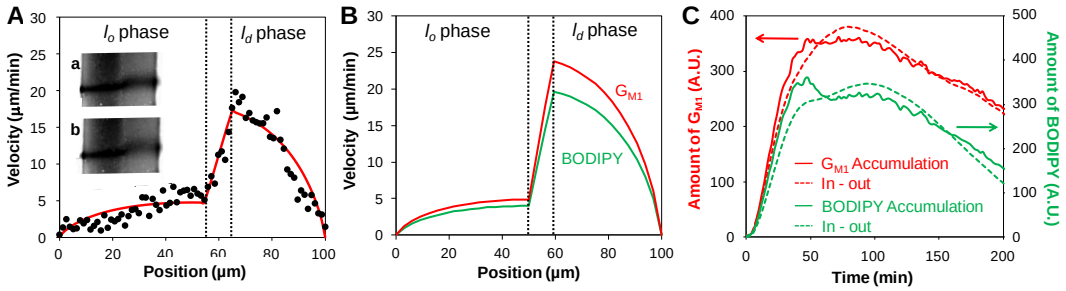

Figure 2.4. Velocity profile and mass balance. (A) Velocity profile obtained by photobleaching experiments (inset) to verify the shape of the profile and our model. Black data points are the velocities as a function of position across the channel, derived from the photobleached images, (a) and (b), during 80 μl/min buffer flow rate. The red line is the best fit of the data by our model, equation 5. (B) Velocity profiles for Alexa 594-G_{M1} (solid red) and BODIPY DHPE (dashed green) determined for a particular extraction experiment using the 710 μm extraction channel. The interface region between each phase is defined by the black dashed lines. (C) The accumulation of species in the control volume (LHS Eq. 7) versus the difference between the inlet and outlet material flux for the control volume (RHS Eq. 2.7) in a representative run at 80 μl/min bulk flow rate for Alexa 594-G_{M1} (red), and BODIPY DHPE (green). These curves have been purposely offset to by an arbitrary factor to separate the data. Velocity for each species was determined independently by minimizing the least squares error between the LHS and RHS.

Table 2.1. Average values determined for *b* based on four experiments.

Intermonolayer friction coefficient, *b* [Pa·s/m]	**BODIPY DHPE**	**Alexa 594-G_{M1}**
l_o phase	$3.6 \pm 1.1 \times 10^8$	$2.8 \pm 0.8 \times 10^8$
l_d phase	$7.3 \pm 2.1 \times 10^7$	$5.6 \pm 1.7 \times 10^7$

2.4.4 Extraction Performance

Once the velocity profile for an experimental run has been obtained, the yield of species can be calculated from Eq. 2.1. To quantify the enrichment of species in each phase, we measured the accumulation (yield) of both G_{M1} and BODIPY DHPE in the l_o phase as a function of the average residence time of a species in the device. The residence time, τ, is defined as the ratio of the channel length, L, to the average velocity of a species, $\hat{v}_{ld}$, in the l_d phase: $\tau = L/\hat{v}_{ld}$.

The residence time can be increased by increasing the length of the control volume or reducing the bulk flow rate. Here, we fix the bulk flow rate at 80 μl/min and varied the control volume lengths: 89, 355, and 710 μm. Each experiment is performed using the same channel geometry, bilayer compositions, and patterning, and a 50:50 starting mixture. % yield obtained from the experimental results for different residence times are shown in Fig. 2.5. For the longest residence time, ~ 34% of the entering Alexa 594-G_{M1} is extracted into l_o phase during 200 minutes, while ~19% of the BODIPY DHPE is extracted.

Species	L (μm)	τ (min)	Yield in l_o phase (%)
Alexa – G_{M1}	89	4.7	26 ± 5
	355	19	28 ± 1
	710	37	34 ± 2
BODIPY DHPE	89	6.2	10 ± 4
	355	25	13 ± 3
	710	50	19 ± 3

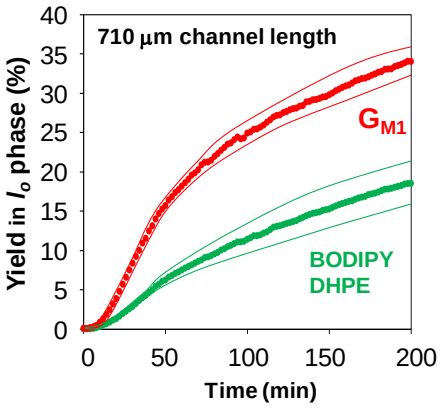

Figure 2.5. (Left) Yield of species to the l_o phase at various residence times, τ. The buffer flow rate was constant at 80 μl/min, but the length of the channel, L, was varied. These yields correspond to total experimental time, t = 200 min of collection. (Right) The accumulated yield of species in the l_o phase normalized by the total amount that has entered the control volume for L = 710 μm. These data are averaged over 4 experiments at the same conditions. The thin lines bounding the data points are the standard deviation of the data.

The shape of the yield curve is influenced by the transport properties the biomolecule. If operated at equilibrium conditions, the extraction yields to the l_o phase are 66% and 38% for Alexa 594-G_{M1} and BODIPY DHPE, respectively, based on previously measured equilibrium partition coefficients of 1.96 and 0.6 from Chao & Daniel[145]. Thus, even at the longest channel length investigated, equilibrium is not

reached. Optimization of the channel dimensions, patterning, lipid phase selection, and process conditions can be carried out to approach equilibrium. One possibility is to lengthen the channel more, but this is only practical to a limit, beyond which diffusion becomes significant during laminar flow patterning and results in a less defined interface between lipid phases. Alternatively, decreasing the flow rate could allow partitioning to approach equilibrium. We found that halving the bulk flow rate increased the yield of G_{M1} to the lipid-ordered phase to ~ 40% at t = 200 min for L = 710 μm. The tradeoff here is that the extraction takes longer.

2.4.5 Verification of mass balance analysis using convection-diffusion model of species transport

To independently verify $v(y)$ and the intermonolayer friction factors (b_i's), we modeled the convection-diffusion for each species using COMSOL to simulate the extraction process. Parameter inputs were diffusivity, partitioning rates, and the b_i's (calculated as described above) to obtain the temporal concentration profiles in the control volume.

A simple model of the extraction channel was developed which used experimental concentration data and measured quantities to predict the species distribution during an extraction run (Fig. 2.6).

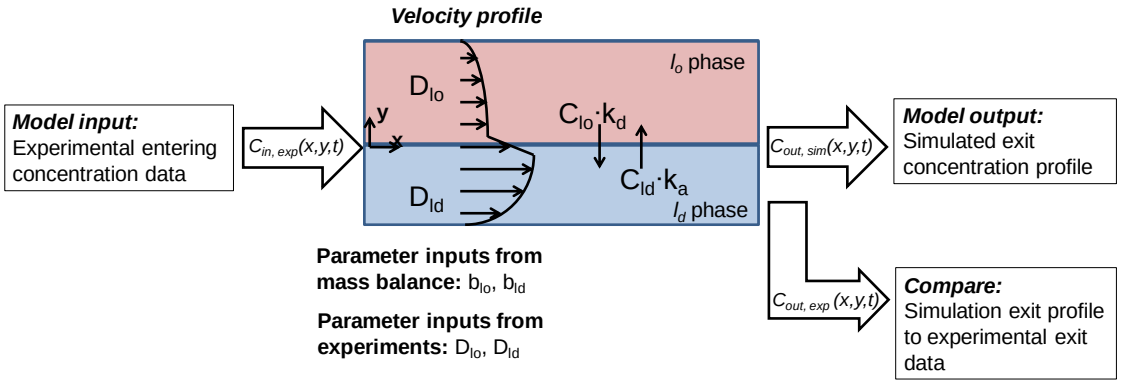

Figure 2.6. Strategy for comparing experimental data to simulated concentration profiles from the COMSOL model of convection-diffusion.

The model governing equation comes from the convection-diffusion process with an imposed velocity profile in the x-direction, given by the following equation:

$$\frac{\partial \mathrm{c}(\mathrm{x},\mathrm{y},\mathrm{t})}{\partial t} = \nabla(D(y)\nabla c(x,y,t)) - \nabla(\vec{v}(y)c(x,y,t)) \qquad \text{(Eq. 2.10)}$$

where c is the concentration of the species, D is the diffusion coefficient of a species, and v is the velocity of the species. The diffusivity of each species in each phase is experimentally measured and is dictated by the properties of the lipid environment. We used fluorescence recovery after photobleaching to determine diffusion coefficients of each species in separate experiments (as described above). These values are reported in Table 2.2.

Table 2.2. Diffusion coefficient values used in Eq. 2.14 in the COMSOL simulation.

Lipid environment	**BODIPY DHPE**	**G_{M1}**
Liquid-disordered phase	0.63 μm^2/s	0.70 μm^2/s
Liquid-ordered phase	0.13 μm^2/s	0.14 μm^2/s

The velocity profile assumed here is that given by Eq. 7. Note that the

experimentally measured inlet concentrations from raw fluorescence intensity values are the inputs to the COMSOL model. The boundary condition at the interface between phases is a flux corresponding to the partitioning kinetics of the system:

$$\frac{dN_{lo}(x,t)}{dt} = k_a c_{ld}(x,t) - k_d c_{lo}(x,t) \qquad \text{(Eq. 2.11)}$$

In this equation, N is the accumulation in the liquid-ordered phase, c represents concentration at the interface in either the l_d or l_o phases, and k_a and k_d represent the association and dissociation rate constants for the l_o phase, respectively.

The model was evaluated by comparing predicted outlet concentration profiles with experimentally measured profiles. Figure 2.7 shows comparisons of predicted to measured profiles for both G_{M1} (red) and BODIPY DHPE at the three different channel lengths studied. The parameters used in these cases were measured diffusivities and partitioning coefficients and calculated intermonolayer friction factors. It was found that these parameters resulted in close matches to experimental data, especially for the shorter channel lengths. Increasing the friction factor would lead to a later eluting plug and decreasing leads to an earlier eluting plug causing significant mismatch in the profiles.

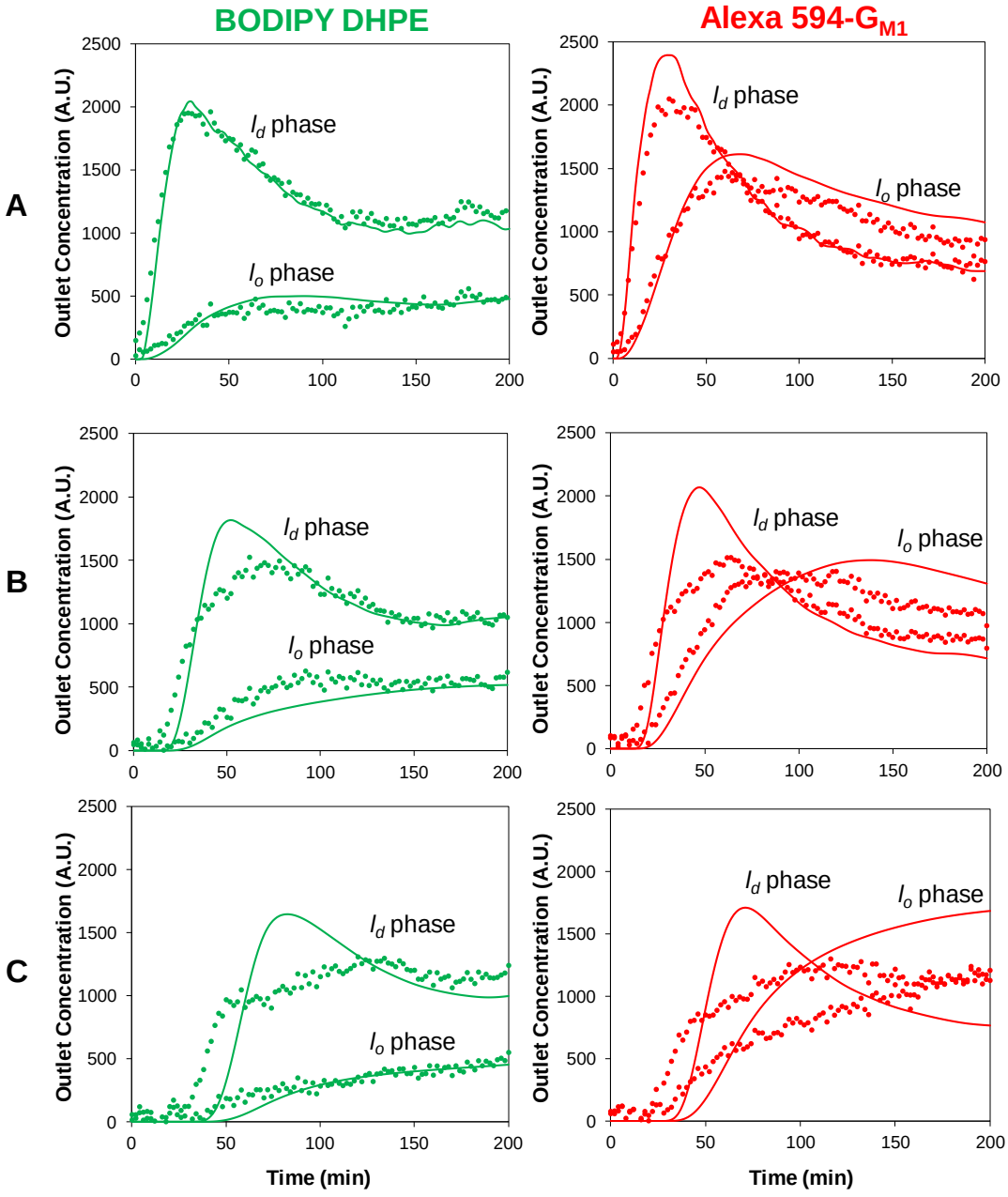

Figure 2.7. Comparison of outlet concentrations in each lipid phase from a representative experiment (points) to model predictions (solid lines) for various channel lengths. (A) 89 μm; (B) 355 μm; (C) 710 μm. Data are separated into average l_o and l_d phase concentrations in the control volume for BODIPY DHPE (green, left side) and Alexa 594-G_{M1} (red, right side).

There are some differences between the predicted concentration profiles and the experimentally measured profiles that we attribute to complexities not accounted for in

this model. We believe one source could be patterning and bilayer imperfections. Our model assumes that the geometry of the bilayer phases is two rectangular regions, but imperfections in the patterning could lead to varied extractor geometries. Additionally, minor bilayer imperfections in the extractor contribute to a dispersive effect in part by immobilization of species in bilayer defects. The cumulative effect of these defects could lead to deviations between the model predictions and the fluorescence data over long channel lengths. Dispersion differences are apparent by the change in the shape of the experimental data compared to the simulation curve as the channel length increases. Notice that the peak position for the experimental data and simulation generally remain registered, which is most obvious in the l_d phase data, but as the channel length increases, the width of the experimental peak grows larger relative to the simulation. In addition, we have made the simplifying assumption in our model that the interface region is infinitesimally small. Perhaps modeling the interface region as having a finite width with mixed phase properties could also improve the accuracy of the simulation.

The b_i's determined by mass balance and used in the simulation predicted concentration profiles that closely matched experimental profiles (Fig. 7), especially for shorter channel lengths. Other values shifted the elution time of the plug forward or backward because b directly impacts the velocity of the species in the bilayer. The shape of the velocity profile is also critical to accurate modeling of the extraction. Inputting, for example, a uniform (average) velocity in each lipid phase across the channel (a step function velocity profile) with constant averaged b_i's was unable to capture the experimental concentration profiles.

When simulating the extraction for longer channel lengths, deviations grew between the experimental output concentration profiles and the model predictions (Fig 2.7). However, these deviations appear to have only a small effect on the predicted yield curve of an extracted species to the l_o phase up to the time of collection at t = 200 min as shown in Fig. 2.8.

Deviations between experimental results and simulation may result if the experimental velocity profile is not fully developed. We confirmed via photobleaching experiments that the flow is fully developed. Another explanation is that additional experimental dispersive effects that are not accounted for in the model become compounded as the channel lengthens. These effects may include patterning defects that disrupt the flow slightly and/or result in immobilization of biomolecules. These effects may accumulate as the length of channel increases. Nonetheless, our basic simulation reasonably predicts the extraction in this device, verifying that the parameters used in the model are acceptable. This model can be used to predict the enrichment of other biomolecules in this and other two-phase systems, or in optimizing the design of extraction devices.

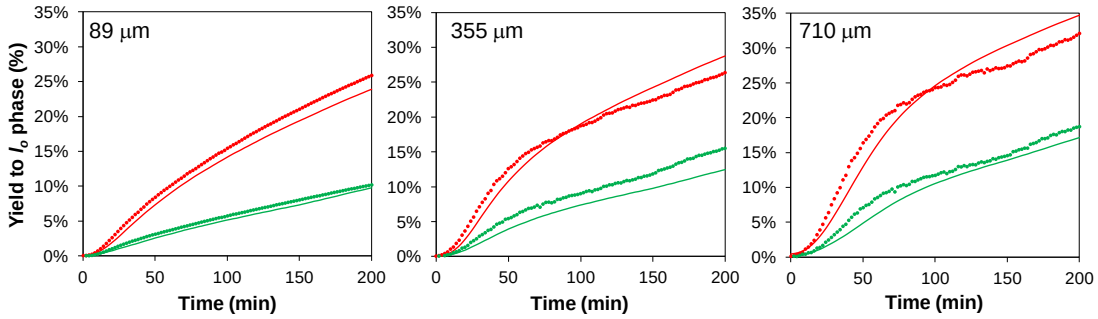

Figure 2.8. Comparison of yield of each species to the l_o phase for various channel lengths, as determined by experiment (points) and the model (lines) for Alexa 594-G_{M1} (red) and BODIPY DHPE (green).

2.4.6 Control Experiment Conducted in Single Phase Bilayer

The following control experiment shows that the observed enrichment of species along the axial length of the channel is not an artifact of the experiment. Here we conduct the experiment in exactly the same manner as described previously, except that instead of patterning with a two-phase bilayer of parallel phase zones down the axial length of the channel, we pattern the channel with a bilayer of only one composition (l_d phase). In Fig. 2.9, l_d phase has been patterned in the channel and illustrates that enrichment is not observed in the absence of a two-phase patterned bilayer. A similar result is obtained when only l_o phase bilayer is used as a homogenous bilayer phase in the channel.

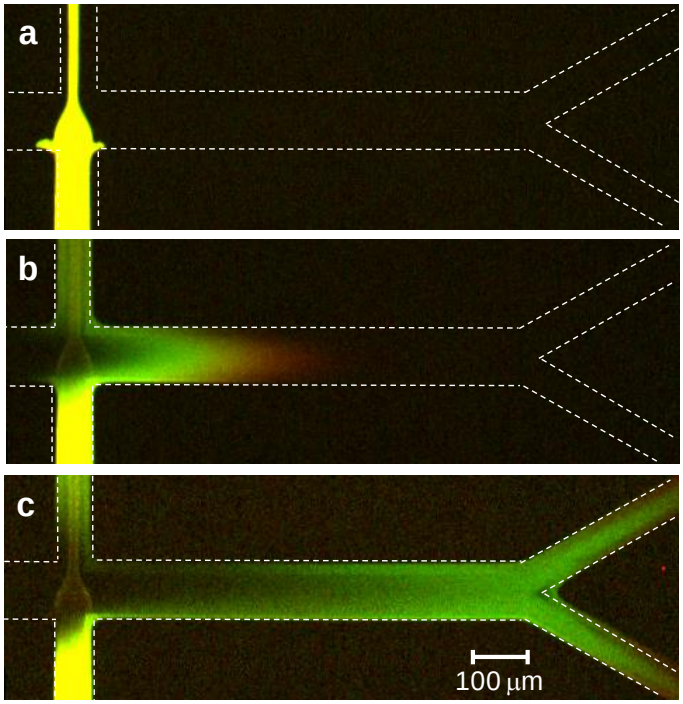

Figure 2.9. Control experiment of separation channel composed of only one phase. In this case only l_d phase composition is used to pattern the microchannel with a bilayer. In (a) the load consists of a mixture of Alexa 594-G_{M1} (red) and BODIPY DHPE (green). The dashed lines are superimposed on the image to outline the microchannel. (b) The load channel is transported down the main microchannel by hydrodynamic flow and no partitioning across the channel is observed. (c) In the absence of the two-phase bilayer, equal portions of the initial load are split equally at the "Y", resulting in no separation, sorting, or concentration of species from the initial load amount.

2.5 CONCLUSIONS

The SLB extractor platform described herein can spatially separate, enrich, and sort membrane-bound species based on their affinity for a specific lipid phase. We created two coexistent lipid phases, in analogy to classic liquid-liquid extraction, but operating in a flat plane of the supported bilayer. We demonstrate that G_{M1}, a typical lipid microdomain marker. can be extracted to an ordered lipid phase and become enriched, relative to non-raft species. This new platform does not require detergent, secondary antibody labeling methods, or electric fields often used in other strategies to

identify lipid microdomain residents. Additionally, since the phase locations can be patterned to direct the species to a collection area, characterization tools, such as mass spectroscopy and surface plasmon resonance, could be also integrated at the outlet of this platform to identify unknown species or combined with other downstream analytical assays.

The approach described here is currently being extended to separate and sort lipids and proteins with posttranslational modifications, such as the addition of GPI anchors, sterols, and single saturated or unsaturated fatty acids. The platform is compatible with species derived from cell membranes and creating supported bilayers from sections of cell membrane has recently become possible[114,190], including a new technique developed by us[191]. In the future, this platform could be extended to separating and sorting transmembrane species by integrating an appropriate cushion beneath the bilayer to minimize protein-support interactions[190]. Finally, this platform may be useful not just for separating and facilitating the identification of membrane domain residents, but for characterizing how post-translational modifications, interactions with soluble species, or environmental conditions shift the affinity of species to a particular lipid phase[69,192].

2.6 ACKNOWLEDGMENT

This chapter was published in its entirety in Analytical Chemistry[193]. Mark J. Richards and Ling Chao were co-first authors on this paper with co-authors Chih-Yun Hsia and Susan Daniel. We thank the National Science Foundation (EEC-0824381, CBET-1149452) and an Innovation Grant from the Institute for Biotechnology and Life Science Technologies at Cornell University for support. M.J.R. is a fellow in

Flexible Electronics for Biological and Life Science Applications. This fellowship is supported by the IGERT Program of the NSF (DGE-0654112) administered by the Nanobiotechnology Center at Cornell. This work was performed in part at the Cornell NanoScale Facility, which is supported by the NSF (ECS-0335765).

CHAPTER 3

MEMBRANE PROTEIN MOBILITY AND ORIENTATION PRESERVED IN SUPPORTED BILAYERS CREATED DIRECTLY FROM CELL PLASMA MEMBRANE BLEBS

Note: A manuscript derived from this chapter is in review in Langmuir

3.1 ABSTRACT

Membrane protein interactions with lipids are crucial for their native biological behavior, yet traditional characterization methods are often carried out on purified protein in the absence of lipids. We present a simple method to transfer membrane proteins expressed in mammalian cells to an assay-friendly, cushioned, supported lipid bilayer platform using cell blebs as an intermediate. Cell blebs, expressing either GPI-linked yellow fluorescent proteins or neon-green fused transmembrane P2X2 receptors, were induced to rupture on glass surfaces using PEGylated lipid vesicles, which resulted in planar supported membranes with over 50% mobility for multi-pass transmembrane proteins and over 90% for GPI-linked proteins. Fluorescent proteins were tracked, and their diffusion in supported bilayers characterized, using single molecule tracking and moment scaling spectrum (MSS) analysis. Diffusion was characterized for individual proteins as either free or confined, revealing details of the local lipid membrane heterogeneity surrounding the protein. A particularly useful result of our bilayer formation process is the protein orientation in the supported

planar bilayer. For both the GPI-linked and transmembrane proteins used here, an enzymatic assay revealed that protein orientation in the planar bilayer results in the extracellular domains facing towards the bulk, and that the dominant mode of bleb rupture is via the "parachute" mechanism. Mobility, orientation, and preservation of the native lipid environment of the proteins using cell blebs offers advantages over proteoliposome reconstitution or disrupted cell membrane preparations, which necessarily result in significant scrambling of protein orientation and typically immobilized membrane proteins in SLBs. The bleb-based bilayer platform presented here is an important step towards integrating membrane proteomic studies on chip, especially for future studies aimed at understanding fundamental effects of lipid interactions on protein activity and the roles of membrane proteins in disease pathways.

3.2 INTRODUCTION

Understanding the functions of membrane proteins is important for combating disease and designing therapeutics, but they are a complicated and challenging class of biomolecules to study, as reviewed in a recent publication[159]. Cell-based studies of membrane proteins have provided valuable information because all native interactions are captured, but system complexity makes it difficult to isolate individual factor effects quantitatively. An alternative is to extract the proteins from the cell membrane and assay their behavior in an aqueous environment, but this often alters membrane protein structure and function from that of the native state[113]. Furthermore, the local interactions and organization of lipids and proteins are believed to regulate membrane protein activity[36,194] and thus are a crucial component of their study. With this in mind, new techniques bridging whole-cell complexity and membrane interactions with quantitative and flexible *in vitro* methods are desired.

Model membrane studies which utilize an artificial lipid bilayer have provided a framework for retaining critical membrane interactions among constituents while enabling the use of a wide variety of experimental techniques for characterization[108,125,145,193,113,195]. The supported lipid bilayer (SLB) platform provides a chemically tunable, planar geometry that is compatible with a vast array of surface characterization tools, such as total internal reflection fluorescence (TIRF) microscopy[109], atomic force microscopy (AFM)[110], quartz crystal microbalance (QCM)[111], and surface plasmon resonance (SPR)[112], among many others. While significant work has been carried out using SLBs, their full potential has yet to be reached because of the challenges associated with integration of membrane proteins.

Several significant challenges remain for incorporating membrane proteins into SLBs, namely maintaining their fluidity, orientation, and function. The most significant bottleneck is the method in which membrane proteins are introduced into the SLB. To sidestep these issues, some studies use peripheral or self-inserting membrane proteins which can be introduced in solution after a bilayer has been formed and insert themselves in the membrane[123,125,196]. This limits the scope of the platform to a very small subclass of proteins. A prevalent alternative is to use a membrane disruption and proteoliposome reconstitution procedure often with the use of detergents[186,197,198,136]. Here, proteins are solubilized from the membrane with detergent, isolated from the cell debris, then reformed into proteoliposomes. Not only do these methods involve tedious optimization of detergents, lipids, and conditions for each protein, but the process can also alter the protein orientation and structure[5,199–201]. A recent publication used sonication of cell-membrane vesicles to merge them with PEG-containing vesicles before forming a supported lipid bilayer[202]. This approach apparently assists in the formation of a planar bilayer, and an improvement in membrane protein mobility in this platform is achieved; however, the sonication process causes a scrambling of the leaflets, so membrane orientation is no longer preserved.

We have developed a general method for the delivery of membrane proteins to the supported bilayer platform via cell blebs, which results in oriented, mobile proteins in the SLB. Cell blebs are sections of the cell membrane that bud off into a type of proteoliposome as a result of local detachment of the membrane from the actin cystoskeleton[117]. Overproduction of blebs is typically triggered by chemical means,

and afterwards the blebs are collected from the culture media[88,118]. However, under specific conditions certain cell types bleb naturally without chemical induction. Expressing membrane proteins directly in mammalian cells and collecting the cell blebs circumvents the difficult purification and reconstitution procedures. Importantly, native membrane travels with the membrane proteins all the way to the SLB platform, so any crucial lipid interactions can be preserved. Finally, the use of mammalian hosts ensures proper folding and post-translational modifications such as glycosylation and S-acylation. In previous work, we demonstrated that membrane proteins can be delivered to a supported lipid bilayer using this blebbing technique and remain functional as viral receptors[191,203]; however, these receptors were not mobile, which can reduce the efficacy of multivalent binding interactions. In general, protein mobility is important because membrane proteins need to be able to diffuse laterally to properly interact with co-factor species to function as they do within the cell plasma membrane. Thus, for this platform to be most useful, gaining protein mobility while preserving proper orientation is paramount.

The major hurdle with this system, and SLBs in general, is protein immobility caused by interactions between the extramembranous regions of the proteins and the underlying glass support. In a typical SLB there is a small, ~1 nm water gap[119], that cannot accommodate extracellular or cytosolic domains of membrane proteins that could extend around 10 nm from the membrane[120]. In this work, we overcome protein immobility by step-wise mixing of cell blebs with polyethylene glycol (PEG) containing vesicles to generate a cushioned bleb bilayer which increases the distance between the bilayer and glass surface[125]. Our design goal was a platform that would be

general and applicable to a wide variety of types of membrane proteins. To this end, we tested a peripheral glycophosphatidylinositol (GPI-linked) protein and a multi-pass transmembrane protein (MPTMP) (Fig. 3.1). The GPI-linked yellow fluorescent protein (GPI-YFP) was our representative GPI protein for this study. GPI proteins are linked to the extracellular leaflet of the plasma membrane via a lipid anchor instead of a transmembrane peptide and are involved in a variety of cellular processes including signaling, enzymatic catalysis, and cell adhesion[204]. They are typically sorted to raft microdomains[41] and some are used as targets for anti-cancer therapeutics because of their overexpression in tumors[205]. For a MPTMP, we examined the P2X2 receptor fused to a neon green fluorescent protein, referred to here as P2X2-Neon. The P2X receptors are ATP-gated ion channels that are found in almost all mammalian cells and play important roles in inflammation, sensation of pain and taste, and control of vascular tone[206]. Each P2X2 receptor harbors two transmembrane helices and assembles into a functional trimer (thus total six transmembrane helices) in the plasma membrane[207]. Individual membrane proteins were tracked and their motions were analyzed to distinguish diffusion modes in the cushioned bleb-based bilayer system. We characterized the orientation of membrane proteins in the bleb bilayer and determined that the rupture process for both types of proteins results in predominantly outward facing membrane proteins, implying a “parachute”-type mechanism of bleb rupture, similar to a mechanism proposed in the literature[137,140]. Finally, we compare bleb bilayers created using chemically induced and native blebbing and found that at low levels, chemical induction does not hinder protein mobility in bleb bilayers. These supported bleb bilayers containing mobile, oriented proteins preserved with lipids

from the plasma membrane are a critical intermediate platform that bridges whole cell to *in vitro* systems and will play a key role in novel membrane proteomic and lipidomic studies in the future.

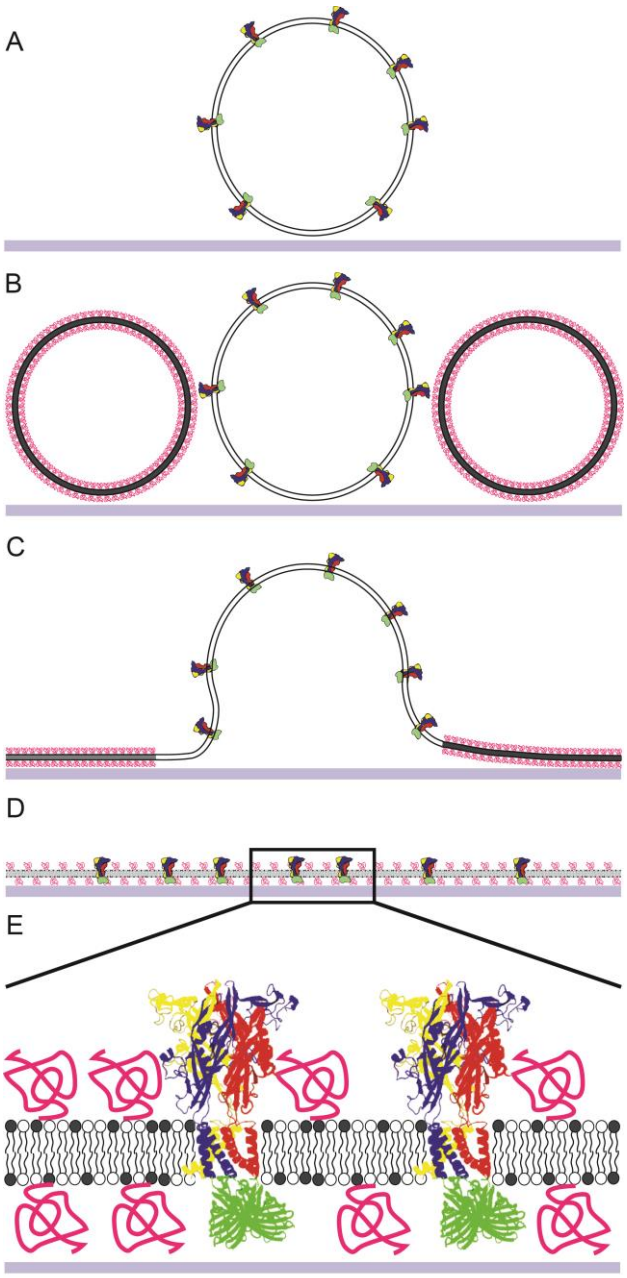

Figure 3.1. Depiction of the proposed PEGylated bleb bilayer formation process demonstrated for P2X2-Neon membrane protein delivery (based on P2X4 structure solved by Kawate et al.[208]). Blebs (depicted by white lipids) are first adsorbed to the glass slide (A) and PEGylated lipid vesicles (depicted by black lipids with magenta polymer coils) are then added (B). (C) As the lipid vesicles rupture, they induce rupturing of neighboring blebs. The dominant rupture mechanism appears to be a "parachuting"

mode where the inner leaflet of the bleb becomes the lower leaflet of the bilayer as determined from enzymatic accessibility assay results. We note here that some versions of this proposed parachute mechanism found in the literature include a small patch of inverted bilayer where the vesicle initially adsorbs to the surface. (D) Bilayer constituents are free to diffuse in the resulting cushioned bleb bilayer. (E) A magnified view of the bleb bilayer shows the relative scale of the P2X2-Neon membrane protein.

3.3 METHODS

3.3.1 Cells and plasmids

HeLa cells were maintained in RPMI 1640 medium (CellGro) supplemented with 10% fetal bovine serum (GIBCO), 100 U/mL penicillin (CellGro), 10 μg/mL streptomycin (CellGro), 2 g/L sodium bicarbonate (Sigma), and 1% HEPES buffer (CellGro) in a 37°C, 5% CO2 incubator (ESCO). The pYFP-GPI-N1 plasmid, a generous gift from the Baird/Howlawka research group at Cornell University, was used in transfection to produce a glycophosphatidylinositol (GPI) anchored yellow fluorescent (YFP) protein. The pINR3-Neon-THR-P2X2 plasmid was generated by inserting the full length mouse P2X2 receptor (GI: 258679504) followed by a thrombin cleavage site (Gly-Leu-Val-Pro-Arg-Gly) between BamHI and XhoI in pINR3 vector using a standard molecular biology technique. The pINR3 vector was modified from the pIRES-EGFP RK6 vector (provided by M. Mayer, National Institutes of Health, Bethesda, MD) such that the Neon Green fluorescent protein can be expressed as a fusion protein while mRuby2 fluorescent protein is expressed using an internal ribosome entry site. All DNA constructs were verified by sequencing.

3.3.2 Cell membrane bleb preparation

Cell blebbing was performed using two different methods: serum starving of HeLa cells and via chemical induction. For both methods, 6 mL of cells were seeded

at a density of 1.5 x 10^5 cells/mL in a 10 cm culture dish (Corning). Transfections were performed using 2 µL TurboFect (Thermoscientific) and 6 µg of DNA in each culture dish and according to manufacturer instructions and incubated for 24 hrs. In the serum starving protocol, HeLa cells were washed with serum-free RPMI media and then incubated with 4 mL of serum-free RPMI media for 4-6 hrs before collection of the bleb containing supernatant. The chemical induction protocol has been described previously[191]. Briefly, after 24 h cells were washed with a buffer containing 2 mM $CaCl_2$ (J.T. Baker), 10 mM HEPES, 150 mM NaCl (BDH) at pH 7.4. Subsequently, 4 mL of a second buffer containing the same base components but additionally either 25 mM formaldehyde (Sigma) and 2 mM dithiothreitol (Sigma) or 500 mM formaldehyde and 40 mM dithiothreitol to induce blebbing. Blebs were collected from the supernatant and stored at 4 °C for up to one week before use, although it was determined that they were stable for up to one month.

3.3.3 Liposome preparation

1-oleoyl-2-palmitoyl-sn-glycero-3-phosphocholine (POPC) and 0.5% (mol/mol) 1,2-dipalmitoyl-sn-glycero-3-phosphoethanolamine-N-[methoxy(polyethylene glycol)-5000] (PEG5000-PE) were used to formulate fusogenic liposomes. These materials were purchased from Avanti Polar Lipids (Alabaster, AL). Liposomes were prepared by dissolving components in chloroform (Sigma), mixing in appropriate ratios, and drying under a stream of nitrogen. Two formulations were used in this work, the first was purely POPC, the second, referred to as POPC-PEG5k, consists of 99.5% (mol/mol) POPC and 0.5% PEG5000-PE. In a lipid bilayer at this composition, the PEG5k polymer should be at the mushroom-to-brush transition state[209].

Subsequently, lipid films were desiccated under vacuum for 3 hr to remove trace solvent. Phosphate buffered saline (PBS) composed of 5 mM NaH_2PO_4, 5 mM Na_2HPO_4, 150 mM NaCl at pH 7.4 was added to a lipid concentration of 2 mg/mL and lipids were frozen. After thaw, liposomes were sonicated using a VWR B2500A-DTH bath sonicator for at least 60 minutes prior to use. Liposomes were stored at 4°C until use.

3.3.4 Bleb bilayer formation for fluorescence microscopy

Glass slides (25 x 25 mm No. 1.5, VWR) were cleaned with piranha solution (mixture of 70% (v/v) H_2SO_4 (BDH) and 30% (v/v) H_2O_2 (Sigma 50 wt. %) for 10 min then rinsed for 20 min under 18.2 MΩ-cm water (ELGA Purelab Ultra, Woodridge, IL). Polydimethyl siloxane (PDMS) wells (5 mm diameter, 3 mm thick) were affixed to the clean, dry slides. 70 μL of bleb solutions at approximately 4 x 10^8 blebs/mL were incubated for 10 min in the wells (see Supporting Information). Afterwards, the well was rinsed vigorously with PBS buffer to remove excess, unadsorbed material. Bleb bilayer formation was induced by adding 70 μL of rupture liposomes at 0.5 mg/mL into the well and incubating for 30 min before rinsing again with PBS buffer. In a subset of experiments to verify rupturing of blebs, octadecyl rhodamine (R18, Molecular Probes), a membrane-intercalating fluorophore, was doped into blebs, and unincorporated probe was removed using a G25 spin column (GE Healthcare, Buckinghamshire, UK) prior to bleb incubation on a glass slide. An inverted Zeiss Axio Observer.Z1 microscope with α Plan-Apochromat objectives, a Hamamatsu EM-CCD camera (ImageEM, model C9100-13, Bridgewater, NJ), and X-Cite® 120 microscope light source (Lumen Dynamics Group Inc., Canada) were used to visualize

the bleb rupturing process. An ET MCH/TR filter cube (49008, c106274, Chromatech Inc.) was used to collect the fluorescence emitted from the R18 fluorophores. A 20 μm diameter spot in the supported lipid bilayer was bleached with a 4.7 mW 488 nm krypton/argon laser for 400 ms. The recovery of the intensity of the photobleached spot was recorded for 15 min at regular intervals. The fluorescence intensity of the bleached spot was determined after background subtraction and normalization for each image. The recovery data was fit using a Bessel function following the method of Soumpasis[184]. The diffusion coefficient is then calculated using the following equation: $D = w^2 / 4t_{1/2}$, where w is the full width at half-maximum of the Gaussian profile of the focused beam.

3.3.5 Quartz crystal microbalance with dissipation monitoring (QCM-D)

QCM-D was used to verify bleb bilayer formation. All experiments were measured on QCM-D crystals made of silicon dioxide (QSX303, Q-Sense, Sweden) using a Q-Sense E1 (Q-Sense, Sweden) instrument. Solutions were pumped into the chamber by peristaltic pump (Ismatec Reglo Digital M2-2/12, Q-Sense, Sweden).

This technique measures changes of resonance frequency (Δf) and energy dissipation (ΔD) of an oscillating piezoelectric quartz crystal, which is driven by an applied AC voltage. In this paper, we focus on the third overtone (15 MHz), which captures the bleb bilayer formation process. The shift of resonance frequency (Δf) reflects the change of adsorbed mass on the quartz crystal sensor. Simultaneously, shifts of energy dissipation (ΔD) were measured, which characterize the viscoelastic properties of the adhered layer to the crystal surface.

Before measurements, crystals were cleaned with 18.2 MΩ-cm water and ethanol, and dried with nitrogen gas. Crystals were then plasma cleaned in UV-Ozone Procleaner (Bioforce) for 10 minutes to remove any organic contamination. PBS buffer was pumped into the system at a flow rate of 100 µL/min for 5 min. Thereafter, 500 µL blebs solutions were sent into the flow chamber at 100 µL/min. The solutions were circulated in the system until desired values of Δf and ΔD were reached indicating surface coverage of adsorbed blebs. Then the system was rinsed with PBS buffer for 10 minutes to wash out excess blebs. 300 µL of 99.5 mol% POPC, 0.5 mol% PEG 5000-PE liposome solution was then pumped into the flow chamber at 100 µL/min until Δf and ΔD reached steady state. PBS buffer was then sent through the system to wash the bilayer to achieve stabilized final frequency and dissipation shifts.

3.3.6 Tracking the motions of individual membrane proteins

Bleb bilayers were imaged using total internal reflection fluorescence microscopy (TIRFM) on an inverted Zeiss Axio Observer.Z1 microscope with an α Plan-Apochromat 100x oil immersion objective. Samples were excited using a solid-state laser at 488 nm excitation wavelength. A Laser TIRF 3 slider (Carl Zeiss, Inc.) was used to control the incidence angle at ~ 69° ensuring total internal reflection and generating an evanescent wave around 100 nm thick. The laser light was filtered by a Semrock LF488-B-ZHE filter cube and sent to an electron multiplying CCD camera (Hamamatsu ImageEM C9100-13, Bridgewater, NJ).

Acquired images were analyzed using MATLAB (Mathworks) and ImageJ (NIH). A custom detection method was used to achieve high sensitivity to enable accurate tracking. This method determined particle locations based on pixel clusters that meet

an intensity cutoff. Full sample trajectories were found and calculated using in-house scripts based primarily on the "Diffusing-Spots" tracking methods described by Smith[210]. Briefly, linking of trajectories was performed by finding maximizing value of $w_t = w_i f_i + w_{\Delta i} f_{\Delta i} + w_d f_d$ (Eq. 2.1) among all candidate particles in each frame[210]. Weighting values used were: w_i = 0.05 , $w_{\Delta i}$ = 0.05 , w_d = 0.9. Equations for each criterion are given as:

$$f_i = e^{\left(\frac{I-\langle I\rangle}{\langle I\rangle - I_{bg}}\right)}$$

$$f_{\Delta i} = e^{\left(\frac{-\Delta I^2}{2\sigma_{\Delta I}^2}\right)}$$

$$f_d = e^{\left(\frac{-d^2}{2\sigma_d^2}\right)} \qquad \text{(Eq. 2.2)}$$

In these equations, I represents the intensity of the particle, I_{bg} is the background intensity averaged over all frames, ΔI is the change in intensity from the previous frame and d is the displacement from the previous frame. Particle candidates are only accepted into trajectories if they have $w_t > 0.7$.

The algorithm we used includes criteria for removing immobile particles, rapidly diffusing particles, and overlapping particles for which particle identity is lost from the final diffusivity analysis. Only particle trajectories that last for at least 20 frames were used in the analysis to minimize noise. Parameters of the model were adjusted to achieve the best possible tracking fidelity. To verify accuracy of the methods, some individual trajectories were semi-manually tracked with computer assistance for comparison using the open-source SpeckleTrackerJ plugin for ImageJ.

A variety of methods for bilayer single particle tracking (SPT) analysis have been described previously in the literature[75,211–214]. In this paper, reported diffusion coefficients are the initial diffusion determined from the slope of the mean squared displacement vs. time lag plot (Eq. 2.3) up to $2\delta t$ giving a "homogeneous" diffusion coefficient, that is not influenced by the heterogeneity of the bilayer and resultant changes in diffusion mode[215,216]. These are referred to elsewhere as D_0 or $D_{1\text{-}3}$ and are represented as the diffusion of a particle independent of the diffusion mode.

$$MSD = 4D\delta t \qquad \text{(Eq. 2.3)}$$

To then objectively characterize the heterogeneity of the bilayer and quantify its diffusion mode, we used moment scaling spectrum (MSS) analysis, as it is appropriate for the type of anomalous diffusion observed in this system[214,217].

Moment scaling spectrum analysis is performed on each trajectory j individually. Let M be the length of the trajectory, n be the frame number, Δn be the frame step displacement (in this paper, we limited Δn to $M/4$ to limit error[217]), x be the position of the particle, p be the moment order, and $\|\cdot\|_2$ be the Euclidean norm. First, the displacement moments μ are calculated as

$$\mu_p = \frac{1}{M_j - \Delta n} \sum_{n=0}^{M_j - \Delta n - 1} \left\| x_j(n + \Delta n) - x_j(n) \right\|_2^p \qquad \text{(Eq. 2.4)}$$

for p values from 1 through 6. Each moment follows a power law where $\mu_p \propto \delta t^{\gamma(p)}$. The exponential factors, $\gamma(p)$, are determined by a linear regression through $\log(\mu_p)$ vs. $\log(\delta t)$. If the diffusion process is strongly self-similar, the moment scaling spectrum, i.e. $\gamma(p)$ vs. p, will be linear with a slope defined as β which quantifies the

type of diffusion. Species with β values near 0.5 are exhibiting normal diffusion, $0.5 < \beta < 1$ are superdiffusive and $0 < \beta < 0.5$ are subdiffusive.

3.3.7 Enzyme accessibility assays for the determination of protein orientation in cell blebs and in planar supported bilayers

Enzyme (either 300 U/mL of Thrombin (Sigma) for probing accessibility to the N-terminal Neon domain of P2X2-Neon or 100 μg/mL of Proteinase K (Ambion) for probing accessibility to the YFP domain of the GPI-YFP protein) was added to 100 μL samples of either adsorbed blebs or bleb bilayers on the glass slides. Images of several regions of the surface were recorded at 10 min intervals to capture the enzymatic action. As the enzyme cleaved the protein, the fluorescent fusion protein domains were no longer attached and could diffuse out of the evanescent field resulting in a loss of fluorescence at the surface of the bilayer or bleb. Particles were counted and a percent change compared to control samples without enzyme was calculated. From this information, we can infer the orientation of proteins in the bilayer and blebs by their susceptibility to enzymatic cleavage, as will be described extensively in the *Results and Discussion* section.

3.4 RESULTS AND DISCUSSION

3.4.1 Verification of bleb rupture into planar bilayers

Harvested blebs were directly incubated on glass substrates. Blebs generally did not spontaneously rupture to form supported bilayers on their own, but required addition of fusogenic lipid vesicles, as verified using quartz crystal microbalance (QCM) measurements and by direct observation of fluorescent species diffusing from ruptured blebs. QCM with dissipation detects bleb rupture as a change in frequency

and dissipation from the initial adsorbed bleb state to that of the final bleb bilayer. In Figure 3.2A we compared the formation of a bilayer formed from only fusogenic POPC-PEG5k vesicles (left) with that formed from blebs and fusogenic vesicles (right). In both cases, it is the fusogenic lipid vesicles that cause rupture and bilayer formation as evidenced by an increase in frequency and simultaneous decrease in dissipation. As vesicles rupture they expel their luminal water to become less massive and more rigid[111]. In the bleb bilayer case, the rupture step happens on a much longer time-scale of around 30 min compared with 1 min for fusogenic vesicles on their own. From the QCM data, the rupture process of lipid vesicles appears to initiate the much more stable blebs to rupture. The final frequency of the POPC-PEG5k bilayer is -33 Hz (matching well to Kaufmann's results[126]), while that of the bleb bilayer is -50 Hz, aligning with the expectation that the bleb bilayer is more massive due to the additional protein content in the bilayer.

A possible alternative interpretation is that some blebs desorb from the surface during bilayer formation, and the mass increase over the POPC-PEG5k bilayer is due to residual adsorbed unruptured blebs. However, we see that there is a slower increase in frequency during bleb bilayer formation which we attribute to bleb rupture (Fig. 3.2A). Since QCM-D is carried out on a SiO_2 coated substrate, we believe the behavior is similar to our imaging experiments with glass coverslip substrates (described below), although the surface is not identical.

While it is possible that some blebs never rupture, we confirm that most blebs do rupture and deliver protein to the SLB using two direct visualization methods. First, we label blebs with membrane-intercalating fluorescent probes prior to rupture to

visualize the rupture process in real time, and second, we track fluorescently-labeled membrane proteins that are released into the SLB upon bleb rupture. Both of these experiments confirm the formation of contiguous planar bilayers from the ruptured cell blebs. The membrane-intercalating probe experiment is described next, while discussion of the protein tracking experiments is described later in the *Results* section.

To observe and verify cell bleb rupture and planar bilayer formation as it occurs, a membrane-intercalating probe, octadecyl rhodamine B (R18), was incubated with intact blebs for 30 mins. Excess, free R18 was removed from the bleb solution using a G25 spin-column. The R18 incorporated into the bleb membranes is a reporter for lipid mobility, and its spreading is indicative of bleb rupture. In the first step, labeled blebs were incubated with the glass support. A laser was focused to a ~ 20 μm diameter spot on the surface of adsorbed blebs and used to bleach the R18 molecules. No recovery of fluorescence was observed from the adsorbed blebs, indicating that a planar bilayer had not yet formed. Next, unlabeled fusogenic lipid vesicles, either POPC-PEG5k or POPC, were added.

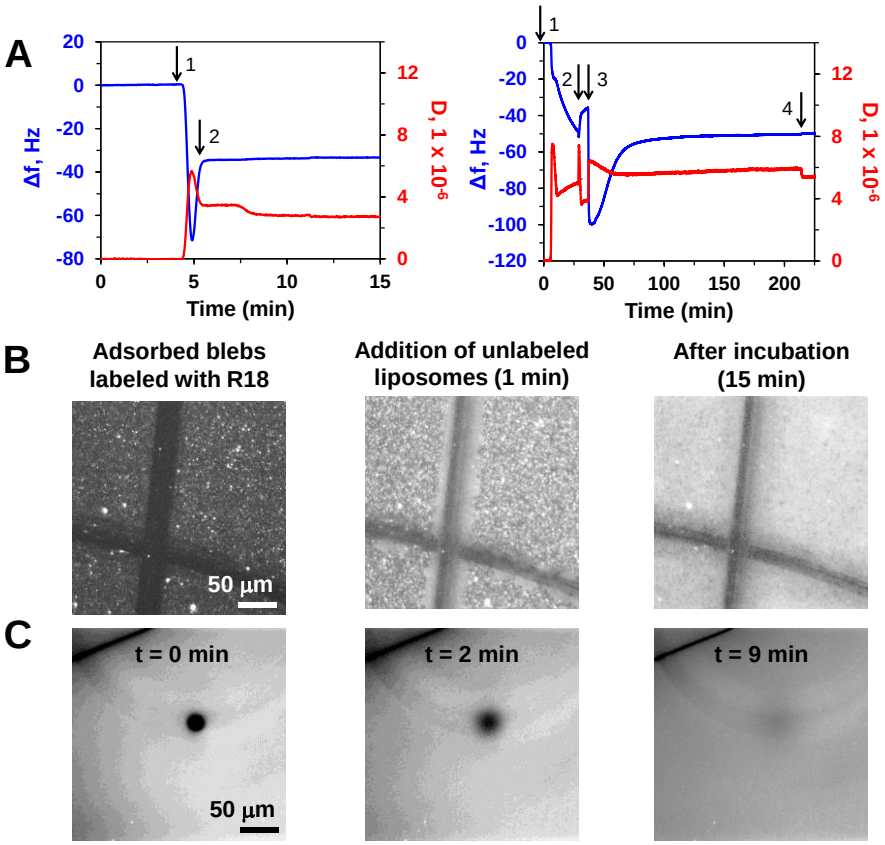

Figure 3.2. Characterization of bleb rupture process. A) Left, a QCMD frequency and dissipation trace for POPC-PEG lipid vesicle adsorption and lipid bilayer formation. Vesicles are added (step 1) and bilayer forms quickly as seen by the sharp increase in frequency and decrease in dissipation. After bilayer formation (step 2), excess vesicles are rinsed away with buffer. On the right, the trace is shown for HeLa bleb rupture. Initially, blebs were injected into the system (step 1) and allowed to incubate for ~30 minutes before being rinsed (step 2). During rinsing the frequency decreased, indicating loosely associated blebs were rinsed away. Fusogenic liposomes were then added (step 3) resulting in a rupturing process to form a bleb bilayer and excess vesicles were rinsed away (step 4). B) Fluorescent images of bleb bilayer formation process. Initially R18 signal in blebs was isolated to adsorbed bleb positions and the dark cross is a mechanical scratch made to verify focus throughout the experiment. When fusogenic vesicles were added, they triggered rupture of adsorbed blebs into bleb bilayer. During this process, the R18 was able to diffuse laterally and spread out within the bilayer. C) The bilayer is allowed at least 30 minutes to complete formation and excess vesicles are rinsed away with buffer. R18 signal from the bleb bilayer is bleached with a laser and recovery is observed. The resulting FRAP diffusivity is 0.3 $\mu m^2/s$.

For both cases, the blebs began to rupture and form a bilayer within minutes. SLB formation was indicated by spreading of the R18 dye from the original punctate spots of the intact blebs to a fully fluorescent surface (Figure 2B). After laser-bleaching this

surface with 20 μm diameter spot in the bilayer from a 4.7 mW wavelength tunable Argon/Krypton laser (CVI Melles Griot, Model 643-AP-A01) for 200 ms, recovery of fluorescence was observed for 9 minutes (Figure 2C). The recovery data was fit using a Bessel function following the method of Soumpasis[184]. The diffusion coefficient, *D*, was then calculated using the equation: $D = \frac{w^2}{4t_{1/2}}$, where *w* is the width at half-maximum of the Gaussian profile of the focused beam and $t_{1/2}$ is the recovery half-time. A sample recovery curve is shown in Figure 3.3.

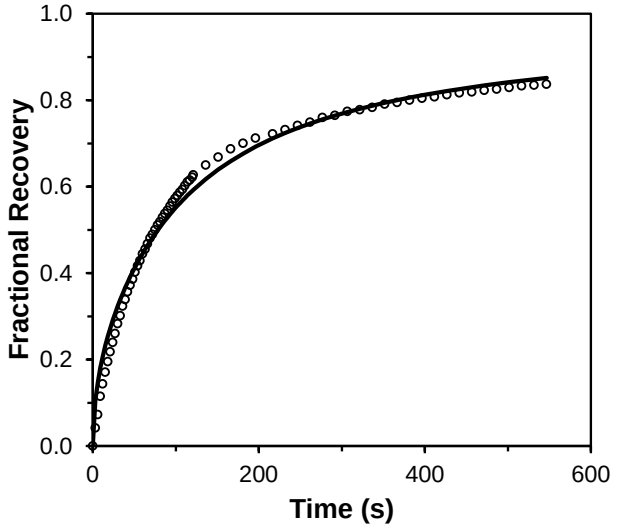

Figure 3.3. Example FRAP of R18 molecules in bleb bilayer (blebs + POPC-PEG5k). A small circle of R18 molecules was bleached with a laser at 0 s. The fluorescence intensity recovers over time as the R18 molecules diffuse freely in the bilayer indicating that the blebs have fused into the SLB. Fitting of experimental data (diamonds) based on Soumpasis' equation is shown by the solid line. D = 0.3 $\mu m^2/s$.

Diffusivity of R18 molecules was 0.30 ± 0.03 $\mu m^2/s$ in the bleb bilayers. The mobile fraction of R18 was found to be 0.95 ± 0.07. Because almost all of the R18 initially present in blebs is mobile, and recovery is nearly complete, we can infer that almost all blebs must be rupturing. We found no difference in R18 diffusion when

using POPC rupture vesicles without PEG, so the polymer does not appear to affect the R18 diffusion.

3.4.2 Membrane protein integration into SLBs via blebs

HeLa cells expressing P2X2-Neon or GPI-YFP were observed using brightfield and fluorescence microscopy and determined to be at adequate densities and expressing adequate levels of target protein (Figure 3.4).

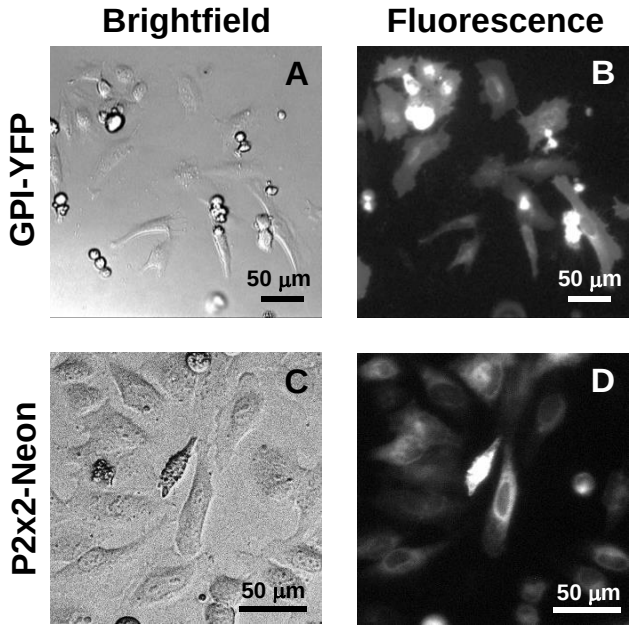

Figure 3.4. Expression of GPI-YFP (A,B) and P2X2-Neon (C,D) in HeLa cells in 10 cm dishes. Brightfield contrast images and corresponding fluorescent images of HeLa cells are shown.

Blebs derived from these cells were incubated on glass coverslips and observed using 100x TIRF microscopy. Bleb density and protein concentration in the bleb bilayer can be controlled by dilution of blebs in a consistent manner since we found batch-to-batch variability of bleb yields to be low (see later section on QCM batch variability). After adsorption of blebs and subsequent addition of fusogenic,

PEGylated vesicles, it was possible to watch bilayer formation through the radial spreading of species originating from the blebs into the surrounding SLB (see videos V1 and V2 in Supporting Information).

Sufficient time (at least 30 minutes) was given to allow for complete bilayer formation prior to rinsing any loosely associated blebs or lipid vesicles and quantitatively tracking membrane species within the bilayer. An image series was taken at various positions for each bleb SLB. Acquisition settings were chosen to maximize signal while minimizing photobleaching. For these samples an exposure time of 50 ms was used with a laser power of 0.6 mW. A sample tracking analysis for GPI-YFP and P2X2-Neon is shown in Figure 3.5.

Trajectories were mapped following a cost-minimizing function that used the particle locations and intensities to optimize linking across the sample for the duration of the image series (Fig 3.5 A,B,E,F). The trajectory data was analyzed using the slope of the mean squared displacement (MSD) to determine diffusivity, D, and the moment scaling spectrum (MSS) analysis pioneered by Ferrari[214] to quantify the mobility via a parameter, β. Initially, moments of displacement are determined for each trajectory and the slope of the plot of moment scaling factors, β, describes the type of motion for the trajectory (Fig. 3.5 D,H). Diffusion modes can be grouped as follows: $\beta < 0.4$ as confined diffusion, $0.4 \leq \beta \leq 0.6$ as quasi-free diffusion and $\beta > 0.6$ as convective diffusion. Particles that are confined to an area smaller than the maximum observed displacement for immobile fluorescent beads in our system are considered immobile[211]. The single particle analysis is useful when there is not enough fluorescent material to carry out ensemble diffusion measurements and provides an

additional level of detail for individual proteins, important when tracking in heterogeneous environments and probing the local nature of the membrane.

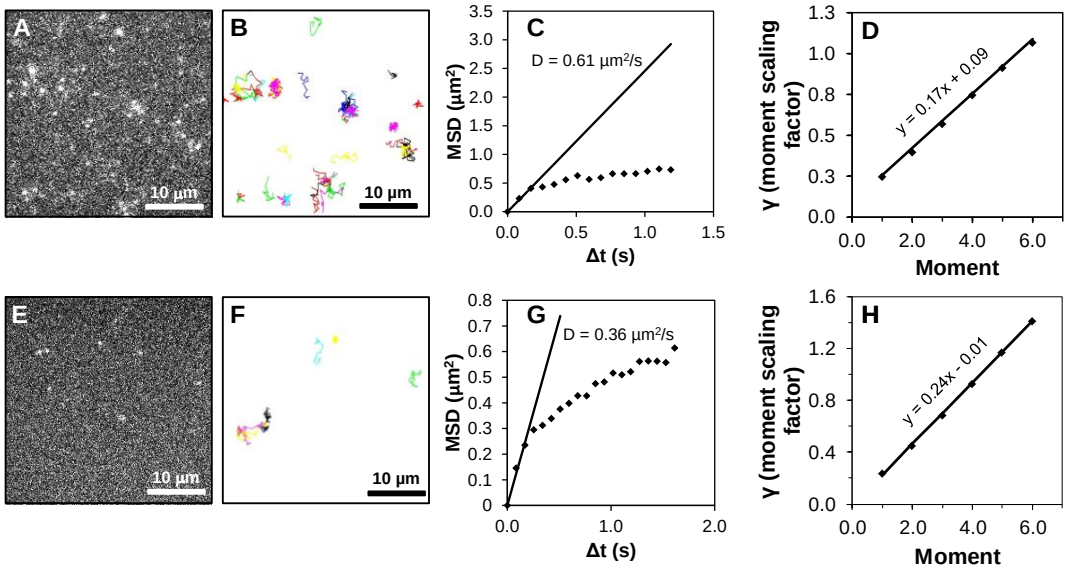

Figure 3.5. GPI-YFP fluorescent proteins tracked on bleb bilayer membrane and analyzed (A-D). A) First frame of fluorescent image of GPI-YFP bleb bilayer. B) Trajectories of GPI-YFP diffusion in the bleb bilayer (same region as A). C) Example trajectory mean squared displacement (MSD) analysis. The diffusion coefficient can be found from initial slope of the MSD. D) Plot of moment scaling factors determined in moment scaling spectrum analysis. The slope of this plot, β, indicates the type of particle motion for this trajectory is subdiffusive. Corresponding figures are shown for P2X2-Neon bleb bilayers in E-H.

By compiling the diffusion coefficients for collected trajectories, we can determine the ensemble diffusivity from fitting to a cumulative distribution function described by a gamma distribution (Eq. 3.5) where $k\theta$ represents the average diffusivity and $k\theta^2$ is the variance[75,218].

$$\frac{1}{\Gamma(k)}\gamma\left(k,\frac{\theta}{x}\right) \qquad \text{(Eq. 3.5)}$$

This can also be represented as the probability density function, which overlays the diffusion coefficient histogram well (Fig 3.6 and 3.7). Additionally, we determine the percentage of mobile particles from the total particles observed. With this analysis, we have measures comparable to the standard bilayer diffusivity method of fluorescence recovery after photobleaching (FRAP). To ensure our results for the bleb bilayers were reliable, we compared results of single molecule tracking analysis with FRAP results for a peripheral protein probe.

We compared the single molecule tracking results with ensemble FRAP measurements for diffusivity of fluorescent Alexa Fluor 594 Streptavidin (ThermoFisher) bound to biotin-X-DHPE (ThermoFisher) in our standard POPC-PEG5k cushioned bilayer. The use of these probes enabled tuning of bilayer concentration to both the low range for SPT and the high range required for FRAP. A FRAP experiment was performed using the POPC-PEG5k lipids doped with 0.2% biotin-X-DHPE. After bilayer formation, 1 μL of 2.5 x 10^{-5} mg/mL streptavidin-594 was added, allowed to bind for 10 minutes and then rinsed. The diffusivity reported from three FRAP experiments was 0.98 ± 0.15 $\mu m^2/s$, in the expected range for a probe of this type in a highly fluid bilayer. The mobile fraction was determined to be 0.96 ± 0.05.

Next, we generated a single particle tracking sample using POPC-PEG5k doped with 10^{-6}% biotin-X-DHPE. After bilayer formation, 30 μL of 0.1 mg/mL bovine serum albumin (BSA) was added to prevent nonspecific binding of streptavidin and rinsed after 10 minutes. Then, 1 μL of 2.5 x 10^{-5} mg/mL streptavidin-594 was added, allowed to bind for 10 minutes and rinsed. The diffusivity measured from single

particle tracking was 0.89 ± 0.30 $\mu m^2/s$, close to that of the FRAP results (Figure 3.6, A). To provide a second point of comparison to further compare these methods, we looked at using a lipid bilayer composition that would provide a lower diffusion coefficient. We used a mixture of 60% *N-palmitoyl-D-erythro-sphingosylphosphorylcholine* (PSM) and 40% ovine wool cholesterol (both from Avanti Lipids) that generates a liquid ordered phase and doped in 10-6 % biotin-X-DHPE. From the SPT experiments on the ordered phase bilayer, streptavidin diffused with an average diffusivity of 0.58 ± 0.27 $\mu m^2/s$ which is slower as expected for an ordered phase bilayer (Figure 3.6, B). Because the diffusion was determined from the initial slope of the MSD, these values represent the free microdiffusion of the tracers, and as such may not correspond with the macro measurement from FRAP[75,213].

Diffusional mode analysis shows that 43% of streptavidin trajectories in the disordered bilayer exhibited free diffusion with $0.4<\beta<0.6$, while only 15% of streptavidin trajectories in the ordered bilayer showed free diffusion. In both cases, the majority of trajectories were confined (Fig 3.6 C,D). The very high percentage of trajectories showing confined behavior in the ordered bilayer is expected because the increased lipid order and packing prevent free diffusion of membrane species. It is unclear why the disordered bilayer shows a significant degree of confinement in SPT tracking, but nearly full recovery in FRAP. We posit that it arises from the differences in the length and timescales of the experiments, whereby the SPT may be more sensitive to microdefects in the bilayer that hinder diffusion on the nanoscale length and millisecond time scale of these experiments.

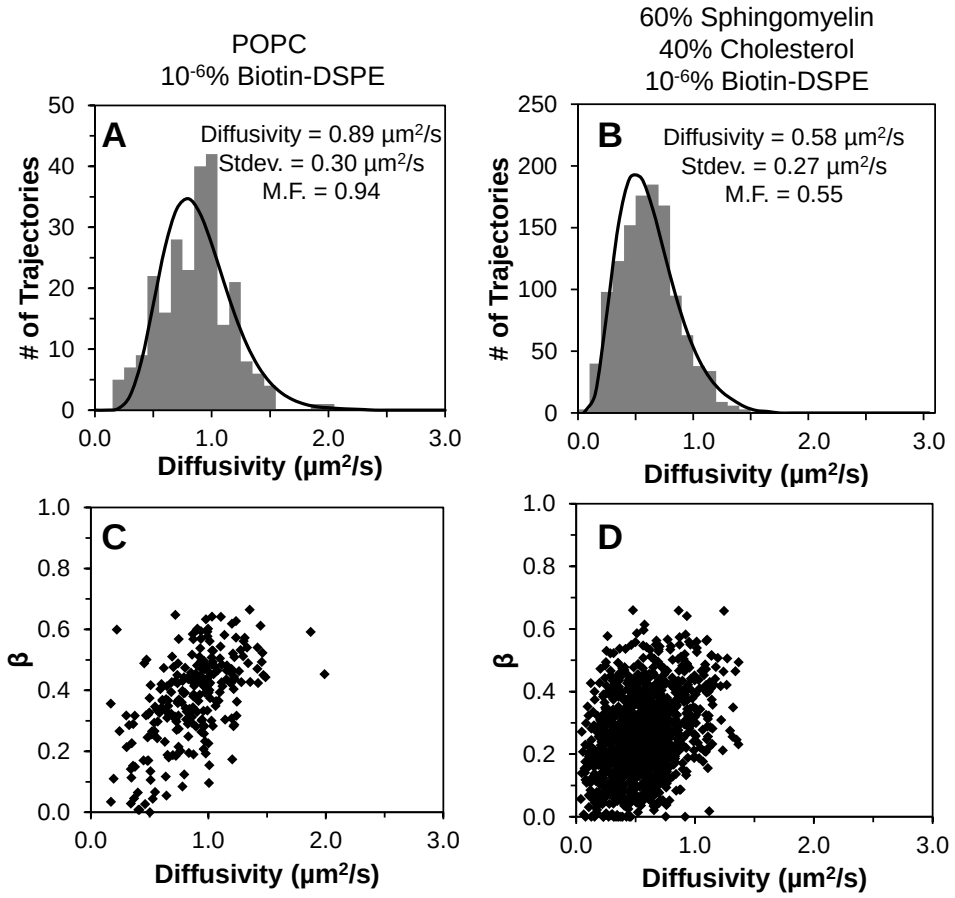

Figure 3.6. Diffusion coefficient histograms for Streptavidin-594 tracking experiments in disordered and ordered bilayers. Histograms are shown by gray bars and probability density function fits to a gamma distribution are shown with the black line A-B). Additionally, scatter plots for each trajectory show the individual β-parameters and diffusivities.

For bleb bilayer tracking, initial control experiments were used to track protein diffusion in uncushioned POPC bilayers. P2X2-Neon was completely immobile in an uncushioned POPC bilayer, while GPI-YFP was 96% mobile. Next, we carried out trajectory analysis for bleb bilayers with either GPI-YFP or P2X2-Neon to characterize the diffusion of these membrane proteins in cushioned POPC-PEG5k bleb bilayers. Figure 3.7 shows the histograms of diffusion coefficients for both proteins as well as plots of the corresponding mobility parameters. For both proteins, more than half were mobile, with GPI-YFP proteins at 90% mobility while P2X2-Neon was 53%

mobile, verifying the critical requirement of the PEG cushion for providing enough space for the P2X2-Neon extramembranous domains. GPI-YFP had an average diffusion coefficient of 0.75 $\mu m^2/s$ while P2X2-Neon was 0.51 $\mu m^2/s$.

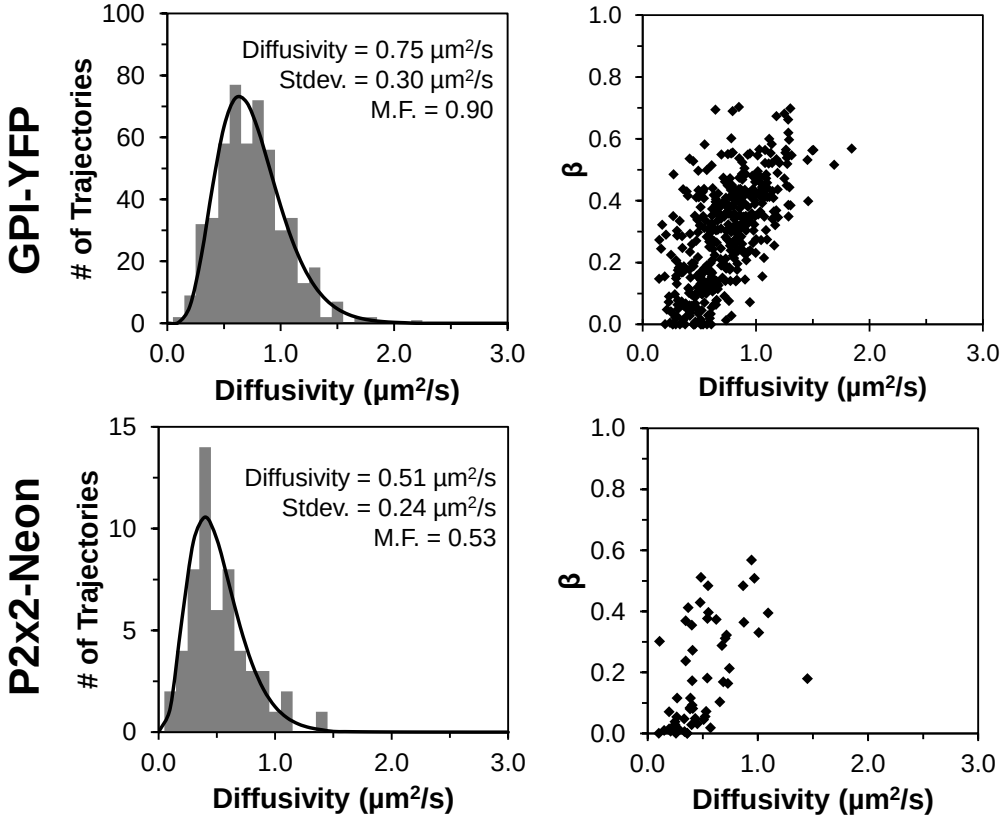

Figure 3.7. Diffusion coefficients of membrane proteins are shown for GPI-YFP and P2X2-Neon compiled from several tracking videos. Each distribution was fit to a gamma distribution from which average diffusivities and standard deviations were found (left). Mobile fractions were calculated as the fraction of trajectories meeting a mobility criterion described in the text. Plots of β vs. diffusivity quantify the type of motion associated with each trajectory (right).

According to the Saffman-Delbrück approximation, which has been upheld by recent literature on membrane protein diffusivity in black lipid membranes[219] and giant unilamellar vesicles[220], the diffusion coefficient scales inversely proportional to the logarithm of the membrane-embedded radius of the protein. As expected, the P2X2-Neon protein diffused slower than GPI-YFP because of its significant

transmembrane domains that increase its drag[221]. Particularly, the radius of GPI-YFP is approximately 0.4 nm while P2X2-Neon is 3.3 nm from the crystal structure of P2X4[208], so the predicted diffusivity ratio between GPI and P2X2 from Saffman-Delbrück (using approximate parameters from Ramadurai et al[220]) is about 1.46, matching very closely to the ratio of the diffusivities we found here of 1.47. It is important to note that diffusivity measurements vary with the system being used and components included in the membrane so absolute values may differ, but our results still fall within the expected range from 0.01 – 1 $\mu m^2/s$ based on similar measurements reported in literature[123,124,222].

In POPC-PEG5k supported lipid bilayers, we found R18 diffused at 0.41 ± 0.14 $\mu m^2/s$ via FRAP experiments. R18 is typically a slow diffusing probe with between 1/3 to 1/10 the diffusivity of other membrane lipid probes[223,224]. When cell material from blebs is present in the cushioned bilayer, R18 diffusion is reduced by about 25% to 0.30 ± 0.02 $\mu m^2/s$. For proteins in bleb bilayers, most β values fall in the range of anomalous subdiffusive behavior with 73% of GPI-YFP and 87% of P2X2-Neon trajectories having β values less than 0.4. Thus the additional material in the bilayer delivered during bleb rupture impacts diffusion of both protein and lipid probes. It is expected that the diffusion would be slowed and present confined behavior in a bleb bilayer compared with a purely artificial membrane because of the presence of a variety of membrane heterogeneities.

The spread in β values from the SPT experiments indicate that heterogeneities exist. These may result from unruptured vesicles; membrane heterogeneity (e.g., domains of differing compositions); and immobilized or cross-linked proteins. Each of

these factors influences the diffusion of species in the membrane. Unruptured vesicles prevent bilayer formation at their location, creating voids in the SLB. These voids reduce the total free area the probes have to diffuse around, thus leading to subdiffusive behavior. We believe that this effect is minor given the uniform spread of R18 dye in the bleb bilayer and the near full recovery in fluorescence following photobleaching as observed by florescence microscopy.

Membrane heterogeneity can arise if there are patches of plasma membrane not well mixed with the surrounding lipid bilayer, which could reduce diffusion due to different local viscosities. Alternatively, membrane heterogeneity could arise from the non-uniform distribution of PEG resulting in cushioned bilayer domains and uncushioned domains[131]. Both of these situations could explain the confined, subdiffusive protein diffusion we observe. However, because the GPI protein also shows a significant anomalous diffusive behavior with a very high mobile fraction, and they are located predominantly in the upper leaflet (details provided in later section), we believe that the more likely cause of the confinement is due to the heterogeneity of the plasma membrane itself. Studies of membrane protein diffusivity in cell membranes show that a large fraction of proteins, usually more than half, show confined motion[215], thus this critical feature of "real" cell membranes appears to be preserved in this platform, even though it is "diluted" with extra lipid material from the fusogenic liposomes.

Protein immobilization results when the extramembranous parts of the protein come into contact with the underlying support, as observed when non-PEGylated fusogenic vesicles are used to rupture blebs on the support. We note that the PEG

cushion that should result from the PEGylated fusogenic vesicle formulation used here is expected to be on the order of ~ 6 nm, based on deGennes' theory[129]. The neon green label of the P2X2 on the cytosolic side is about 4 nm long. On the other side of the membrane, the extramembranous P2X2 loop extends 7 nm. With protein oriented such that the neon green label is between the bilayer and substrate it is possible that some proteins are not fully fluidized and still able to interact with the glass surface; however, if the proteins are inverted in the bilayer, the much larger extracellular domain would contact the support and the P2X2 receptor would not be fluidized at all. While it is appealing to consider using higher molecular weight PEGs to accommodate larger proteins, we note that increasing the PEG length too much can reduce the fusogenicity of the vesicles and may also protrude past the protein and possibly hinder its interaction with extracellular species. To rule out protein inversion as a significant cause of immobilization, we conducted experiments to determine the orientation of proteins in the SLB derived from cell blebs (next section). We should point out that any immobile protein obstacles will act as barriers that hinder the free diffusion process as well as a give a hydrodynamic penalty, also leading to anomalous diffusion behavior we observe.

A final possibility to consider is that some of the proteins are cross-linked together by the blebbing chemicals. We also investigated this possibility and report our findings in a later section.

3.4.3 Orientation of membrane proteins in blebs and SLBs

Determining the orientation of membrane proteins in our system is useful in two ways. First, if there is little leaflet scrambling during the rupture process, one could

imagine designing experiments based on probing either the extracellular or cytosolic side of the plasma membrane, increasing the value of the this system as a cell membrane mimic. Second, this information can help us characterize the protein diffusion in the bilayer system and determine the extent to which extramembrane domain interaction with the support could be playing a role.

The vesicle rupture process is still not well understood. There are several theories on the mechanism of bilayer formation from lipid vesicles. Two important implications, the directionality and degree of lipid scrambling in the bilayer, are controversial. Because the rupture process is not known, it follows that the orientation of membrane proteins in the bleb SLB after rupture is also unknown. Here, we determine orientation in blebs and resulting bleb bilayers as a first step toward characterization of the blebbing process and the vesicle rupture mechanism. We expect the orientation of proteins in blebs to be the same as in the cell membrane because blebs arise as outward protrusions of the cell membrane, encapsulating cytosol in their lumen[117]. To verify this, we adsorbed blebs to glass slides prior to addition of enzymes to cleave accessible protein domains in a manner similar to the fluorescence protease protection assay described by Lorenz et al[225]. Protein domains on the outside of the blebs are accessible, while luminal domains are inaccessible to the enzymes. For GPI-YFP, Proteinase K was added which will cleave any accessible protein releasing the YFP from its GPI anchor. Since GPI-linked proteins are monotopic peripheral membrane proteins, GPI-YFP will only be cleaved by Proteinase K if it is on the outer leaflet of the bleb membrane. For P2X2-neon, we added thrombin, a specific protease that can cleave a thrombin cleavage site inserted between

P2X2 and the neon fusion protein at the N-terminus of the protein. In both of these cases, a signal drop reports on when proteins are cleaved as the fluorescent fusion proteins diffuse out of the TIRF field, and can be used to interpret protein orientation. To control for photobleaching effects, we performed side-by-side experiments without enzyme.

A significant drop in signal of 74% was observed for GPI-YFP blebs (99.9% confidence compared to control), but no significant change in signal was detected for P2X2-Neon blebs during this 40 minute assay (Fig. 3.8). This indicates that the GPI-YFP proteins are on the surface of the blebs. Since the GPI-YFP proteins are located on the outside of the cell membrane this means most of the proteins have the same orientation in the blebs. The thrombin site on the P2X2-Neon protein is inaccessible in the blebs, indicating it is in the lumen, matching its cytosolic location in cells. Bleb orientation indeed mimics orientation in the cell membrane for both of these proteins, as expected.

To determine the final orientation of proteins in our SLBs, we used the same enzymatic assays on bleb SLBs. In this case, the enzymes cannot access protein domains that are underneath the bilayer. GPI-YFP signal dropped for almost all particles at the first time point after addition of enzyme. The percent change of 95% was significantly different than a control without enzyme to 99.9% confidence. P2X2 signal did not change appreciably compared to control, although in both control and enzyme tests, a slow signal drop over the time course of the experiment was observed. This drop may be attributed to photobleaching, as a similar drop was observed in all control experiments.

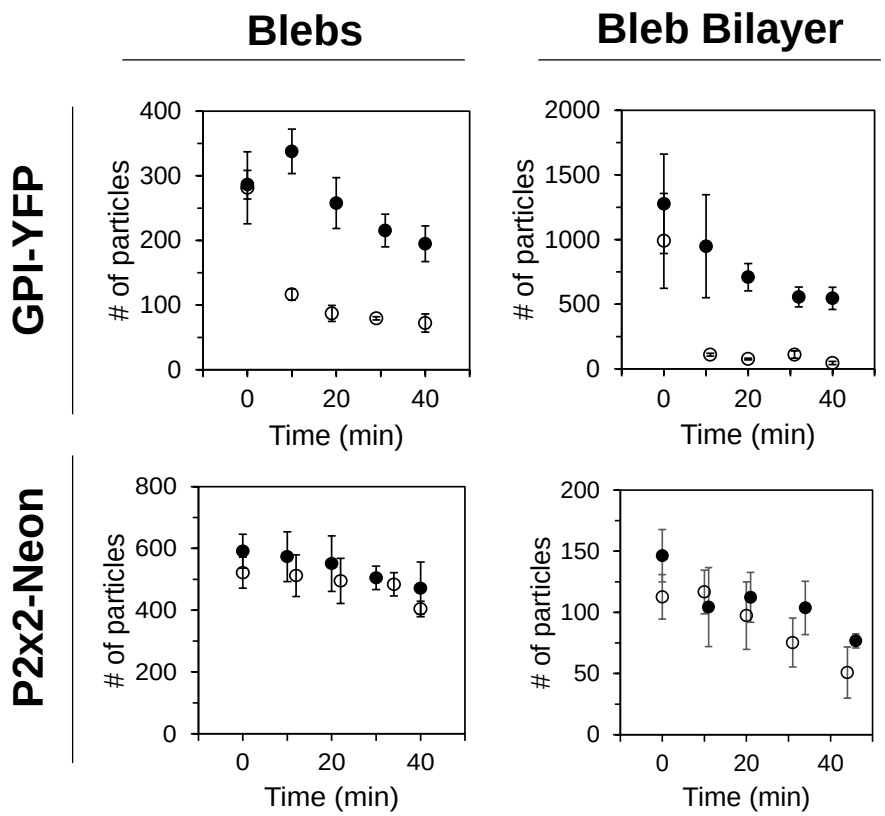

Figure 3.8. Determination of protein orientation through fluorescence enzyme accessibility assays. Solid circles indicate control experiments; empty circles indicate experiments with enzyme added. Bleb and bilayer orientation were determined for GPI-YFP and P2x2-Neon membrane proteins. The signal change in GPI-YFP shows a sharp drop after addition of proteinase K with percent change of about 74% for intact blebs and 95% for bilayer. P2X2-Neon signal after thrombin addition does not change significantly compared to control. GPI-YFP was accessible to enzyme in both blebs and bilayers, but the fluorescent N-terminus of P2X2-Neon was not. This indicates that GPI-YFP is predominantly located in the outer leaflet of the blebs and upper leaflet of the SLB, and P2X2-Neon is oriented with its termini extending from the inner leaflet of blebs and large extramembranous loop above the SLB.

Because the result for P2X2 was derived from a lack of significant change in particle counts after addition of thrombin, we performed an additional control to verify thrombin activity. Following the general procedure for scrambling proteoliposomes presented by Pace et al[202] we investigated thrombin activity on P2X2 proteins in bilayers created from scrambled blebs. In our experiments, P2X2-Neon containing blebs were mixed with POPC-0.5%PEG5K vesicles and then subjected to both tip

sonication using a Branson Sonifier 450 for 1 min at 30% level 3 and bath sonication for 1 hr. Bilayers were formed in wells using this solution. Next, thrombin was added to one well to cleave at the thrombin cleavage site between the P2X2 protein and the neon fusion protein. Images at 100x magnification were taken and particle counts at time 0 and 60 minutes were tallied. Figure 3.9 shows that in the presence of thrombin, the mixed bilayer dropped in particle count, thus proving that the thrombin is in fact capable of cleaving out P2X2 protein when the site is exposed to it.

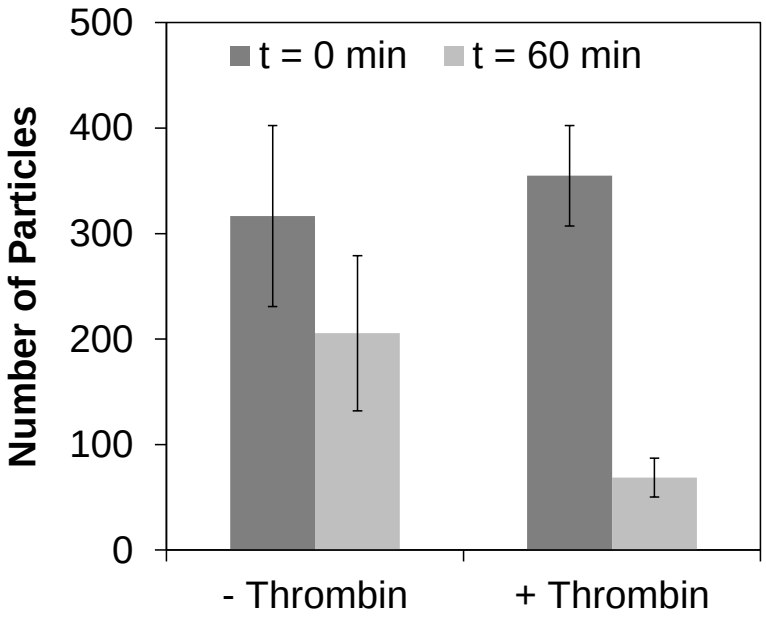

Figure 3.9. Comparison of particle counts without (-) and with (+) thrombin for scrambled P2X2 bilayers exposing inner side of the P2X2 to the bulk phase. After 60 minutes with thrombin, a significant number of particles were lost relative to the (-) case, which represents the amount of photobleaching. Error bars represent the standard deviation for 5 different bilayer locations.

For both GPI-YFP and P2X2-Neon, bleb bilayer orientation matches that of the cell and the blebs, i.e. the extracellular domains are accessible to the bulk and cytosolic domains are not. We conclude that blebs appear to rupture with the luminal

sides down towards the glass (see schematic in Fig. 1). This “parachute” mechanism may result in a small patch of the bleb inverting where it initially contacts the substrate, but we cannot resolve this with our methods. Literature shows that factors that support this mechanism include high surface potential, vesicle crowding and vesicle cargo which may play a role in our system. Interestingly, the bleb lumen may hold various soluble proteins as cargo which could adsorb to the surface underneath the bilayer during rupture. These adsorbed proteins could provide additional passivation of the surface and further improve the membrane protein mobility in an analogous manner to Diaz et al’s[125] BSA passivation layer approach. However, large proteins could also adversely affect the bilayer and may be a source of the anomalous diffusion behavior we observe.

As mentioned above, bilayer formation is an unclear process and while both of these membrane proteins demonstrated the same orientation after rupture, it may not be the case for all membrane proteins or for bleb lipids. To test the orientation of an endogenous membrane protein and confirm that the PEGylated bilayer does not inhibit binding of extracellular species to receptors on the bleb bilayer, we examined the ability of transferrin receptor to bind its antibody. Transferrin is natively expressed in the HeLa cell used here to form the blebs. A FITC-labeled monoclonal antibody against human transferrin receptor CD71 (clone MEM-75, ThermoFisher Scientific) was used. A blebbed SLB prepared with POPC-PEG5k lipids was made as previously described, along with a POPC-PEG5K bilayer (no blebs) as a control case. After blocking with 0.005 mg/ml bovine serum albumin (BSA) for 150 minutes to reduce non-specific adsorption, the samples were thoroughly rinsed with PBS. Next, 1 μl of

the antibody solution was added to each well and incubated for 20 minutes before thoroughly rinsing with PBS to remove unbound antibodies. Fluorescent images of the bilayer using a 100x objective were recorded and the fluorescent particles were counted from these images. These results, shown in Figure 3.10, clearly show that the antibody is able to bind its target in the blebbed SLB despite the presence of PEG. The control bilayer showed limited non-specific adsorption. Additionally, this result provides further support for the bleb bilayer orientation we concluded from the thrombin enzyme experiments because the antibody binds to the extracellular domains of transferrin receptor, though we could not quantify the extent using the antibody binding approach alone.

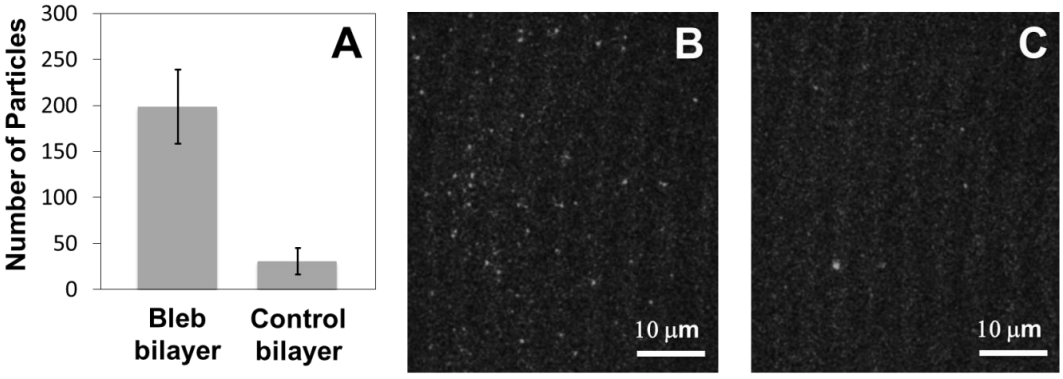

Figure 3.10. Binding of FITC-labeled anti-CD 71 antibody to blebbed SLB. The number of fluorescent particles, averaged over at least seven images, is shown in (a) for a blebbed SLB and a non-blebbed SLB. Representative images are shown for (b) a bleb SLB, and (c) a control SLB.

This data further supports the parachute mechanism. Importantly, this experiment also shows that the PEG cushion does not prevent binding of ligands to membrane proteins. Additional experiments are required to determine the orientation of other bleb constituents, particularly lipids, and the destination of luminal cargo molecules, to develop a more complete picture of the rupture process. However these studies are

not as straightforward to carry out and interpret due to experimental limitations, and thus are beyond the scope of this work.

3.4.4 Effect of chemically induced blebbing on protein mobility in SLBs

Production of cell membrane blebs using chemical induction is an established technique for harvesting and studying membrane proteins in vesicles[226–228]. However for their use in SLBs it is important to ensure the chemicals used for blebbing do not adversely affect the protein quality particularly in a sensitive application such as tracking mobility. Formaldehyde (FA) (at 4%) is a typical non-specific cross-linking reagent, and dithiothreitol (DTT) may reduce disulfides and palmitoylated cysteines, which may lead to differences in phase partitioning[69,87]. Additionally, chemical treatment has been found to alter the phase behavior and even compositions of bleb membranes[96]. Thus, to test the effect of chemical induction on bleb bilayer quality, we prepared YFP-GPI bleb bilayers using three different bleb preparation conditions: serum-starved (i.e. chemical-free) blebbing; standard chemical induction at 0.075% FA (2mM DTT, 25mM FA); and high chemical induction at 1.5% FA (40mM DTT, 500mM FA) (Table 3.1). The amount of formaldehyde at the high chemical induction case is still much less than the 4% used for a standard fixation protocol, but still may be enough to cause some localized crosslinking[229,230] and a commensurate reduction in protein mobility due to increased size.

Table 3.1. Comparison of GPI-YFP protein mobility and diffusivity in bleb bilayers for three different bleb induction processes: chemical-free blebbing, 25mM FA 2mM DTT chemical induction (0.075% FA), and 500mM FA 40mM DTT (1.5% FA) chemical induction from HeLa cells. Trajectories are grouped by diffusional modes as either: confined, quasi-free or convective.

		Confined (β < 0.4)		**Pseudonormal (0.4<β<0.6)**		**Convective (0.6<β)**	
Treatment	% Mobile	% of Trajectories	Diffusivity ($\mu m^2/s$)	% of Trajectories	Diffusivity ($\mu m^2/s$)	% of Trajectories	Diffusivity ($\mu m^2/s$)
GPI-YFP Serum Starved (0% FA)	72	84.7	0.54	14.0	0.73	1.3	1.02
GPI-YFP 25mM FA 2mM DTT (0.075% FA)	95	75.7	0.69	22.9	0.97	1.4	1.26
GPI-YFP 500mM FA 40mM DTT (1.5% FA)	70	83.5	0.55	16.1	0.80	0.4	1.34

The 0.075% FA condition resulted in a bleb bilayer with very high protein mobility at 95%. Interestingly, both the 0% and 1.5% FA conditions resulted in bilayers with protein mobility around 70%. In the 0.075% FA case, the highest percentage of quasi-freely diffusing proteins ($0.4 \leq \beta \leq 0.6$) was found at 23% vs. 14% and 16% for 0% FA and 1.5% FA blebs, respectively. The diffusion coefficient for GPI-YFP proteins in the pseudo-normal regime was found to be 0.97 $\mu m^2/s$ for the standard 0.075% FA chemically-induced blebs, slightly higher than that of the other two cases as well (0.73 $\mu m^2/s$ for chemical-free and 0.80 $\mu m^2/s$ for 1.5% FA). Similarly, the diffusivity of the confined proteins in the standard chemical case was highest at 0.69 $\mu m^2/s$ as compared to 0.54 $\mu m^2/s$ for chemical-free and 0.55 $\mu m^2/s$ for 1.5% FA chemical induction. In all cases, there was only a very small fraction (<2%) of proteins showing convective or directed motion, potentially reflective of capturing late rupturing blebs, bilayer reorganization or rare unruptured blebs rolling on the surface.

The mobility trend for the 1.5% FA case can be explained as a result of some crosslinking of membrane species causing diffusion barriers or even crosslinking of some YFP-GPI reporter proteins. For the chemical-free case, one plausible explanation for the lower mobile fraction and slightly lower diffusivity is the presence of more unruptured blebs. If the blebs do not fuse into the bilayer, then the proteins within them are immobilized, and the blebs themselves act as barriers to diffusion in the SLB. We hypothesize that blebs formed from serum starving may not be as fusogenic as chemically-induced blebs as a result of their formation process. It is possible that the mechanism of formation is different when not chemically induced, resulting in changes in bleb composition and size. Evidence to support that bleb formation could be different depending on the inducing method comes from light scattering measurements that show chemical-free blebs are smaller, with a peak size of about 125 nm, compared to about 200 nm for chemically-induced blebs (see next section). We note that while the mobile fractions from the chemical-free blebs are not as high as those from the standard chemically-induced blebs (0.075% FA); they are still high enough to deliver protein to bilayers when blebbing chemicals could adversely affect the experiment. In conclusion, using the 0.075% FA blebbing formulation does not appear to crosslink proteins or adversely affect membrane protein diffusivity in the final bleb bilayers. We would like to point out that alternative bleb preparations exist, e.g. *N*-ethyl maleimide (NEM), but examining them thoroughly is beyond the scope of this work. Future studies will report on these results.

3.4.5 Bleb size and concentration measurements

A ZetaSizerNano (Malvern) was used to measure particle sizes for undiluted samples of harvested blebs. Settings were chosen to maximize particles in focus with in-range signal intensities. Duplicate runs were performed on each sample and each sample showed similar results. The induced blebbing cases were about twice the concentration of the native samples (Figure 3.11). This factor may be partly attributed to variations in viability and cell density, but in all cases, cells were grown to similar confluency before inducing blebbing. Both conditions had two main peaks, one around 100 nm and a second around 200 nm. The 200 nm peak represented a larger portion of the bleb population in the induced case than it did in the native, chemical-free blebbing case. There seems to be more dispersity in size in the induced case, maybe indicating that the process has some variability in terms of how it acts on certain regions of the membrane or based on local chemical concentrations.

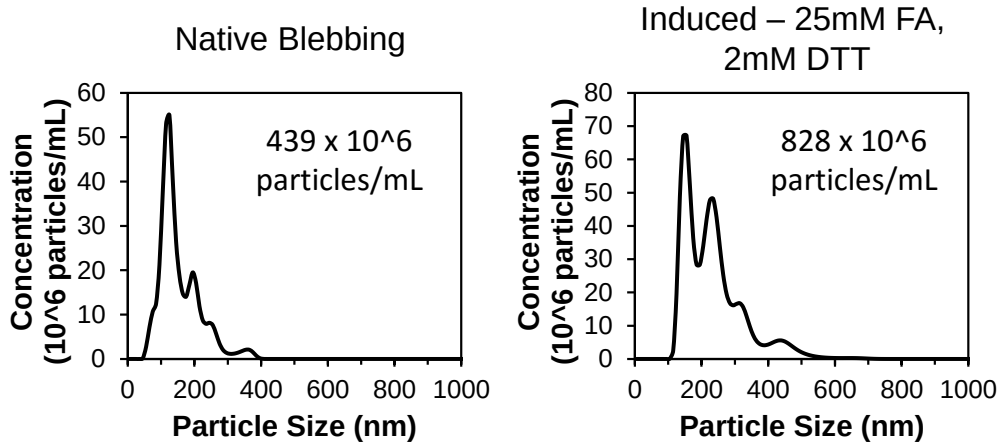

Figure 3.11. Particle size profiles for blebs generated using the native, chemical free blebbing (left) and chemically induced (right) methods. Total particle concentrations are given in insets.

3.4.6 Quartz crystal microbalance with dissipation (QCM-D) batch variability

To see how bleb surface coverage varies from batch to batch when using the same blebbing conditions, QCM-D was used to monitor bleb adsorption of three different batches. For each bleb batch, three (or more) independent experiments were performed on different days. Frequency and dissipation signals (Fig. 3.12) show that bleb surface coverage is reasonably similar across batches; this result suggests that bleb concentration across batches is fairly consistent.

To be sure that bleb adsorption kinetics are solution concentration dependent, we also performed QCM-D experiments using blebs with different dilutions. Fig 3.13 shows that the surface coverage is limited by solution concentration, and hence we can conclude that the reproducibility shown in Fig 3.12 is due to the uniformity in bleb concentration.

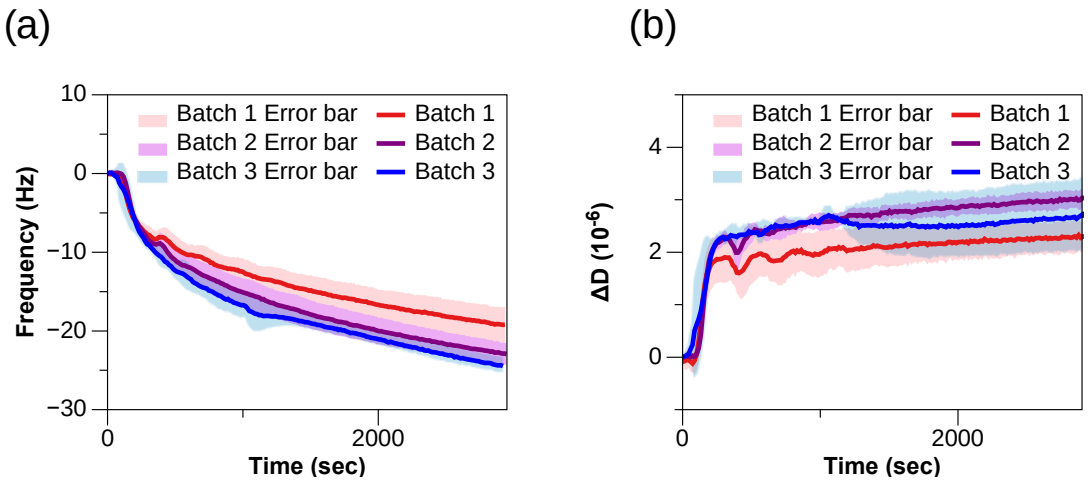

Figure 3.12. The (a) frequency and (b) dissipation signals showing the adsorption of three different batches of blebs. Each batch of blebs was used to perform three (or more) different independent experiments.

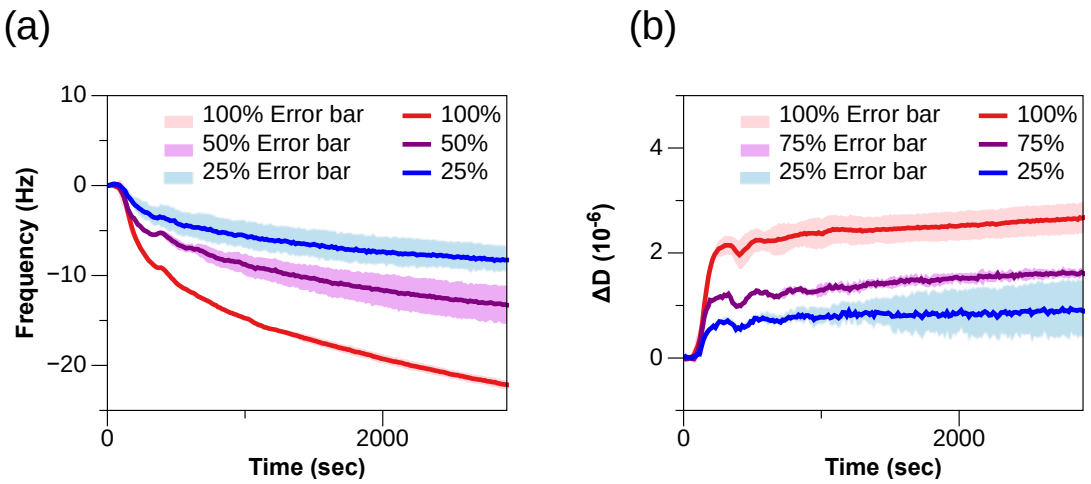

Figure 3.13. The (a) frequency and (b) dissipation signals showing the adsorption of bleb solution with different concentration. 100%: bleb solution without dilution; 50%: 50: 50 bleb solution to PBS in volume; 25%: 25: 75 bleb solution to PBS in volume. Each concentration of bleb solution was used to perform three (or more) different independent experiments.

3.5 CONCLUSION

The membrane protein platform described here using cell blebs to deliver species directly to a supported lipid bilayer is widely-applicable to the study of membrane proteins derived from various mammalian cell hosts, and to membrane spanning proteins as well as peripheral proteins. In this work, we addressed several of the chief concerns of membrane protein incorporation into SLBs – particularly, the immobilizing interactions of the extramembranous domains of the proteins with the support and maintaining protein orientation. Our use of PEGylated lipids in the rupture vesicles provided enough of a cushion to retain mobility for greater than 50% of the multi-pass transmembrane proteins tested. However, this particular cushion may not be universal for all proteins and we are currently testing modified cushions to further improve this technique. Tethered cushions may provide more even spacing at the cost of some additional bilayer resistance[218]. Including a passivation layer on the glass surface may also improve the mobile fraction by preventing irreversible binding of membrane proteins[125]. Many other cushioning options exist and deserve further study[121–124].

The techniques for single particle tracking and theory for membrane protein dynamics have seen much development recently. Until now, most of the work has been performed either on simplified model probes in artificial membranes or with difficult to interpret cell-based measurements of real membrane proteins. This platform enables a crossover of the two methods, bringing membrane proteins to the artificial membrane system and opening up a new avenue of study using planar characterization tools. To our knowledge, this is the first planar bilayer platform to

demonstrate mobility and proper orientation of a truly integral transmembrane protein of this size, derived directly from cell source without reconstitution.

The cushioned bleb bilayer provides a simple way to build more biological complexity into the supported lipid bilayer model membrane system and addresses the key challenge of membrane protein reconstitution. This promotes the use of the rich SLB and SPT toolset to answer important elusive questions about membrane proteins. While the focus of this work was to characterize the quality of the membrane protein platform by measuring diffusion and orientation of proteins, there are many studies in the directions of fundamental protein function and biosensing applications that could benefit from using this platform. For example, combining this technology with bilayer patterning and other surface assays, it may be possible to reveal information about membrane protein compartmentalization, interactions with lipid rafts and proteins, oligomeric state kinetics[231] and other stochastic level dynamic processes due to the capabilities of SPT methods. We foresee use of this platform as a backbone to enable modular on-chip assays for membrane proteins. For example, after bleb bilayer formation, proteins could be separated by charge[166], separated by lipid phase affinity[193], or screened for binding interactions with drug candidates[113].

3.6 SUPPORTING INFORMATION

The Supporting Information is available free of charge on the ACS Publications website at http://pubs.acs.org.

SUPPLEMENTAL VIDEO FILES

V1. TIRF image series showing rupture of GPI-YFP blebs during addition of POPC-PEG5k vesicles. Initially, GPI-YFP proteins are confined to the adsorbed blebs, some in large clusters, but as fusogenic lipid vesicles are added, it is clear that the proteins are able to spread out from blebs and diffuse laterally in the newly forming bilayer. This early-time diffusion shortly after addition of lipids is more hindered than the diffusion we report on after waiting for 30 min to allow complete bilayer formation. The field of view is 82 x 82 microns and playback is in real time. – "Adding POPCPEG5k to GPI-YFP on glass"

V2. TIRF image series showing rupture of P2X2-Neon blebs during addition of POPC-PEG5k vesicles. Initially, P2X2-Neon proteins are visible in isolated blebs that are adsorbed to the surface. As fusogenic lipid vesicles are added, diffusion out from these positions is apparent, indicating bleb rupture into the lipid bilayer. The field of view is 82 x 82 microns and playback is in real time. – "Adding POPCPEG5k to P2X2-Neon on glass"

V3. TIRF image series of P2X2-Neon proteins diffusing in the SLB formed from blebs and POPC-PEG5k vesicles. Colored tracks are superimposed on the image to highlight some of the particle trajectories determined by the tracking algorithm. The field of view is 82 x 82 microns and the playback is in real time. – P2X2-Neon Tracking in POPCPEG5k bilayer

3.7 ACKNOWLEDGEMENTS

This chapter has been submitted for publication in Langmuir. Co-authors include Chih-Yun Hsia, Rohit R. Singh, Huma Haider, Julia Kumpf, Toshimitsu Kawate, and Susan Daniel. The authors would like to thank Barbara Baird and David Holowka of Cornell University for providing the pYFP-GPI-N1 plasmid and related reference material. We thank the National Science Foundation (grant CBET-1149452) for supporting the work presented in this article. M.J.R. is a fellow in Flexible Electronics for Biological and Life Science Applications. This fellowship is supported by the IGERT Program of the NSF (DGE-0654112) administered by the Nanobiotechnology Center at Cornell.

CHAPTER 4

TWO-PHASE SUPPORTED LIPID BILAYER MIMIC OF MEMBRANE RAFTS VIA POLYMER STAMPING AND STENCILING

4.1 ABSTRACT

The supported lipid bilayer has been portrayed as a useful model of the cell membrane and many techniques have been demonstrated to illustrate its appeal. However, much of its potential has yet to be realized, particularly in the area of bilayer patterning. In this work, we generate complex, continuous bilayer patterns as a mimic for membrane heterogeneities or lipid rafts. Micropatterned polymer templates of two types are investigated for patterned bilayer formation: polymer blotting and polymer lift-off stenciling. We examine effectors of membrane domain stability including temperature and cholesterol content to investigate raft dynamics. The development of continuous membrane patterning as a model of lipid rafts expands the application of the SLB to an area with current appeal and brings with it a large toolset to help answer pressing questions about lipid raft function.

4.2 INTRODUCTION

Organization of the membrane is a means by which the cell orchestrates membrane function[31,36,159]. There is increasing evidence that the cell membrane has dynamic heterogeneous "raft" domains enriched in cholesterol, sphingolipids, and certain membrane proteins that phase separate from the surrounding phospholipid-rich membrane[29,30,32,194] Manipulating the dynamics of these domains and therefore species partitioning could control when and where species can interact and impact biological function. This is a unique post-translational regulation mechanism with the potential to be wide-reaching in membrane-mediated function.

Previous results from cell-based studies have shown factors like temperature, ligand induced crosslinking, and changes in the composition of the membrane (e.g. through cholesterol efflux) may control domain dynamics, however few studies exist which explicitly investigate these routes of control[35–37]. While these studies provide useful information, it is difficult to decouple effects and determine mechanistic information in live cells. Using a bilayer patterning technique, we can carefully test these hypotheses on a model lipid raft platform within our SLB.

The supported lipid bilayer platform is a convenient tool for *in vitro* study of the cell and cellular processes as evidenced by studies on virus fusion[191], cell adhesion[168], and immune reactions[232] among other examples. Lipid compositions can be chosen to cause spontaneous phase segregation into coexisting phases in the SLB[233], but this strategy results in random location of domains. Control over domain locations is helpful in key ways. First, it can be used as a design parameter. For example, being able to set and vary the domain size is valuable to look at domain stability to

determine the interplay of line tension and domain size. Second, labels are not necessarily required to pinpoint domain locations since they are controlled. Instead, labels can be saved for critical target species and domain locations can be inferred. Third, quantification of results is made much easier with predetermined domain locations. Simple geometries with regular spacing can be used to simplify calculations.

Control over domain locations and sizes enables design of a variety of experiments. For example, one design of a patterned two-phase supported lipid bilayer can be used to separate membrane species based on their phase affinity and direct them to specific locations within a chip[193]. More complex geometries, such as discrete domains within a larger continuous phase, would be useful in mimicking and studying lipid raft dynamics, but are impossible to form using the laminar flow patterning technique described in that work.

We seek to generate two-phase bilayers with continuity between phases to allow for partitioning behavior representative of rafts in cell membranes. Currently, most patterned bilayers in the literature have been developed as a microarray analogue for screening assays with vast libraries[146,151,154,113]. Arrays are made by corralling bilayers with various types of boundaries impenetrable to bilayer diffusion. Here we seek to adapt two different supported lipid bilayer patterning techniques – polymer blotting, and polymer lift-off – to our design goals for applications in the study of raft dynamics. After the standard patterning steps resulting in voids between bilayer patches, we propose a secondary backfill step for the second bilayer phase. Compositions of contacting regions are chosen to be in phase equilibrium to ensure stability of the patterned bilayer in the predetermined organization[145,193,234]. We

characterize the bilayer patterning methods and use the patterned bilayers to investigate partitioning and stability of lipid rafts under influence of biologically-relevant stimuli. In particular we will look at: 1) temperature changes; and 2) a mimic of sterol efflux using externally added cyclodextrin to sequester cholesterol.

4.3 EXPERIMENTAL SECTION

4.3.1 Materials

Lipids used to make bilayers were 1-palmitoyl-2-oleoyl-sn-glycero-3-phosphocholine (POPC), ovine wool cholesterol (Chol), 16:0 N-palmitoyl-D-erythro-sphingosylphosphorylcholine (PSM), and 1,2-dipalmitoyl-sn-glycero-3-phosphoethanolamine-N-[methoxy(polyethylene glycol)-5000] (PEG5000-PE), all purchased from Avanti Polar Lipids (Alabaster, AL). Two fluorescent lipids were used as phase markers. N-(4,4-difluoro-5,7-dimethyl-4-bora-3a,4a-diaza-s-indacene-3-propionyl)-1,2-dihexadecanoyl-sn-glycero-3-phosphoethanolamine, triethylammonium (BODIPY-FL-DHPE) was purchased from Invitrogen (Eugene, OR) and will be denoted as BODIPY-DHPE in this work. Bovine brain asialoganglioside-GM1 (Sigma, St. Louis, MO) was labeled with AlexaFluor 594 hydrazide (Invitrogen, Eugene, OR) as described previously[145] and will be denoted as Alexa 594-GM1. Texas Red 1,2-dihexadecanoyl-*sn*-glycero-3-phosphoethanolamine, triethylammonium (TR-DHPE) was used as a tracer lipid (Invitrogen, Eugene, OR). Glass coverslips (25 mm x 25 mm; No. 1.5) from VWR were used as solid supports for the bilayers. Polydimethylsiloxane (PDMS; Sylgard 184) polymer used to fabricate microfluidic devices was purchased from Robert McKeown Company (Branchburg, NJ). Methyl-β-cyclodextrin was purchased from Sigma (St. Louis, MO). All unspecified reagents were purchased from Sigma (St. Louis, MO).

4.3.2 Preparation of Lipid Vesicles for Formation of Supported Lipid Bilayers

Lipids dissolved in a methanol and chloroform solution were mixed together at the desired compositions and then dried under a vacuum desiccator to remove solvent for

3 hr. The dried lipid mixture was then reconstituted into vesicles at a concentration of 2 mg/ml in buffer composed of 5 mM phosphate buffered saline (PBS) with 150 mM NaCl at a pH of 7.4. LUVs were formed by extruding the reconstituted mixture 19 times through a 50 nm Whatman polycarbonate filter in an Avanti Mini-Extruder (Alabaster, AL). The vesicle solutions stored at 4°C and were diluted to 0.5 mg/mL before use. All vesicles were on the order of 100 nm in diameter after processing as determined by dynamic light scattering measurements (Zetasizer Nano, Malvern Instruments, Worcestershire, UK). For two-phase coexistence studies, compositions used were 70/20/10 molar ratio of POPC/PSM/Chol, denoted as *ld* disordered phase, and 60/40 molar ratio of PSM/Chol, denoted as *lo* ordered phase. Various preparations were made with tracer molecules, 1% Alexa 594-G_{M1}, 0.1% or 0.5% BODIPY-DHPE and/or 0.1% TR-DHPE added. In POPC + 0.5%PEG5000-PE experiments, octadecyl rhodamine (R18, Molecular Probes), a membrane-intercalating fluorophore, was doped into lipid vesicles, and unincorporated probe was removed using a G25 spin column (GE Healthcare, Buckinghamshire, UK) prior to use.

4.3.3 Polymer Stamp Preparation

Patterned silicon wafer masters were generated using photolithographic techniques at the Cornell Nanofabrication Facility. Briefly, wafers were spin-coated with SPR 220-7 photoresist and exposed using the ABM-Contact Aligner for 7.5 s. Wafers were developed using Microposit MIF 300 developing solution from Shipley (Marlboro, MA). Etching was performed using the Unaxis Deep Silicon Etcher to the desired depth. Wafers were cleaned and subjected to a hydrophobic coating of vapor deposited chlorotrimethylsiloxane prior to use to prevent sticking of polymer. Micropatterned

PDMS stamps with 10% crosslinker were created by pouring films of degassed PDMS mixture over master patterned silicon wafers and curing for 3 hr at 90°C. PDMS stamps were subjected to oxygen plasma cleaning at 700 microns for 60 s using a Harrick Plasma Cleaner (Model # PDC-32G, Ithaca, NY). Before use, stamps were cleaned with ethanol and flushed extensively with DI water and then dried under a stream of nitrogen.

4.3.4 Parylene Stencil Preparation

Parylene pattern generation procedure was modified from Ilic & Craighead[148]. Glass slides were used as substrates for the Parylene stencil production. Initially, 2g of Parylene C was deposited onto piranha cleaned cover glass (70% sulfuric acid, 30% hydrogen peroxide (50 wt%) for 10 min) using a PDS-2010 Labcoater 2 Parylene deposition system (Specialty Coating Systems, Indianapolis, IN) to generate an approximately 2 μm thick parylene layer. Parylene coated substrates were then subjected to the same photolithographic steps as described above for PDMS stamps except etching of Parylene was performed using a Plasma Therm 72 oxygen-based reactive ion etching to the desired depth. Resist was stripped with acetone and rinsed with IPA and DI water, then dried under nitrogen.

4.3.5 Contact Angle Measurement

Static contact angle measurements were used to characterize surface wettability. 20uL droplets of DI water were carefully placed on the test surface with a micrometer syringe (Gilmont Instruments, GS-1200) and images were recorded. At least three droplets were measured for each surface. Contact angles were measured using ImageJ (available free of charge from the NIH)[235].

4.3.6 Polymer Stamp Blot Patterning

Supported lipid bilayer patterning by polymer stamp blotting was performed as follows. The continuous phase bilayer was formed by incubation of lipid vesicles at 0.5 mg/mL with piranha cleaned cover glass substrates for at least 10 min, and then rinsed extensively with PBS buffer. In the case where the continuous phase bilayer is liquid ordered phase, the formation was performed on a hot plate set to 70°C with lipids preheated to 70°C. After bilayer formation and rinsing, blotting was performed using a small PDMS stamp (2 mm x 2 mm) affixed to a glass slide. The stamp was lowered to be in contact with the support and weighted with a desired weight. The stamp was left in contact for 7 min and then quickly removed from the sample. The bilayer was immediately rinsed with PBS to prevent any backfilling of the patterned regions. At this stage, the second phase was backfilled by incubating 0.5 mg/mL vesicles of the second composition for at least 10 min before extensive rinsing with PBS buffer.

4.3.7 Parylene Lift-Off Patterning

Supported bilayer patterning via parylene lift-off was performed as follows. Parylene patterning was either performed directly on the etched slide or the parylene stencil was transferred to a new slide. For transfer, parylene patterns were peeled from etched substrate with forceps and carefully placed on fresh piranha cleaned slides to avoid wrinkles or gaps between pattern and substrate. Slides were then baked for 1 hr at 85°C to facilitate stencil adhesion. In both cases, discontinuous phase was formed by incubating 0.5 mg/mL vesicles of desired composition on the parylene coated substrate for at least 10 min. Extensive rinsing with PBS was performed and parylene

pattern was removed with forceps followed by additional PBS rinsing. Next the continuous phase bilayer was added at 0.5 mg/mL for at least 10 min followed by extensive rinsing with PBS buffer.

4.3.8 Diffusivity Characterization by Fluorescence Recovery After Photobleaching (FRAP) Experiments

To measure the diffusion coefficient of species in the supported bilayer, a 20 μm diameter spot in the supported lipid bilayer was bleached with a 4.7 mW wavelength tunable Argon/Krypton laser (CVI Melles Griot, Model 643-AP-A01) for 200 ms at the appropriate wavelength for each fluorophore label. The recovery of the fluorescence intensity of the photobleached spot was recorded for 15 minutes. Each image was background subtracted and normalized. The recovery data was fit using a Bessel function following the method of Soumpasis[184]. The diffusion coefficient (*D*) was then calculated using the following equation: $D = w^2/4t_{1/2}$, where *w* is the width at half-maximum of the Gaussian profile of the focused beam.

4.3.9 Methyl-β-Cyclodextrin-Mediated Cholesterol Depletion

To probe bilayer phase segregation dynamics during cholesterol depletion, methyl-β-cyclodextrin (MβCD) was added to patterned bilayers. Patterned bilayers contained either BODIPY-DHPE, Alexa 594-GM1 or both to track phase locations. MβCD was added to the sample well up to 6.4 mM concentration and gently pipetted up-and-down to ensure complete mixing.

4.4 RESULTS AND DISCUSSION

The parylene lift-off and microcontact stamping methods are both promising for our purposes of creating a continuous patterned bilayer. The focus of this work is on

the generation of raft-mimicking bilayers which contain patches of raft-like l_o phase bilayer surrounded by a continuous l_d phase bilayer or vice-versa. In the microcontact stamping method, a master pattern is created with photolithography. From this master, molds are made using polydimethylsiloxane (PDMS) polymer. The l_o phase bilayer is formed on the entirety of the glass substrate via vesicle fusion and then portions are removed by blotting with the PDMS mold. The remaining voids can be backfilled with l_d phase bilayer (Fig. 4.1, left). Alternatively, parylene lift-off involves the patterning of parylene on a glass substrate using standard photolithography. The l_o phase bilayer is formed from vesicle fusion through the void spaces in the patterned parylene. The parylene layer is then carefully peeled off of the glass substrate leaving a lipid bilayer array with voids surrounding bilayer patches that can then be backfilled with l_d phase bilayer (Fig. 4.1, right).

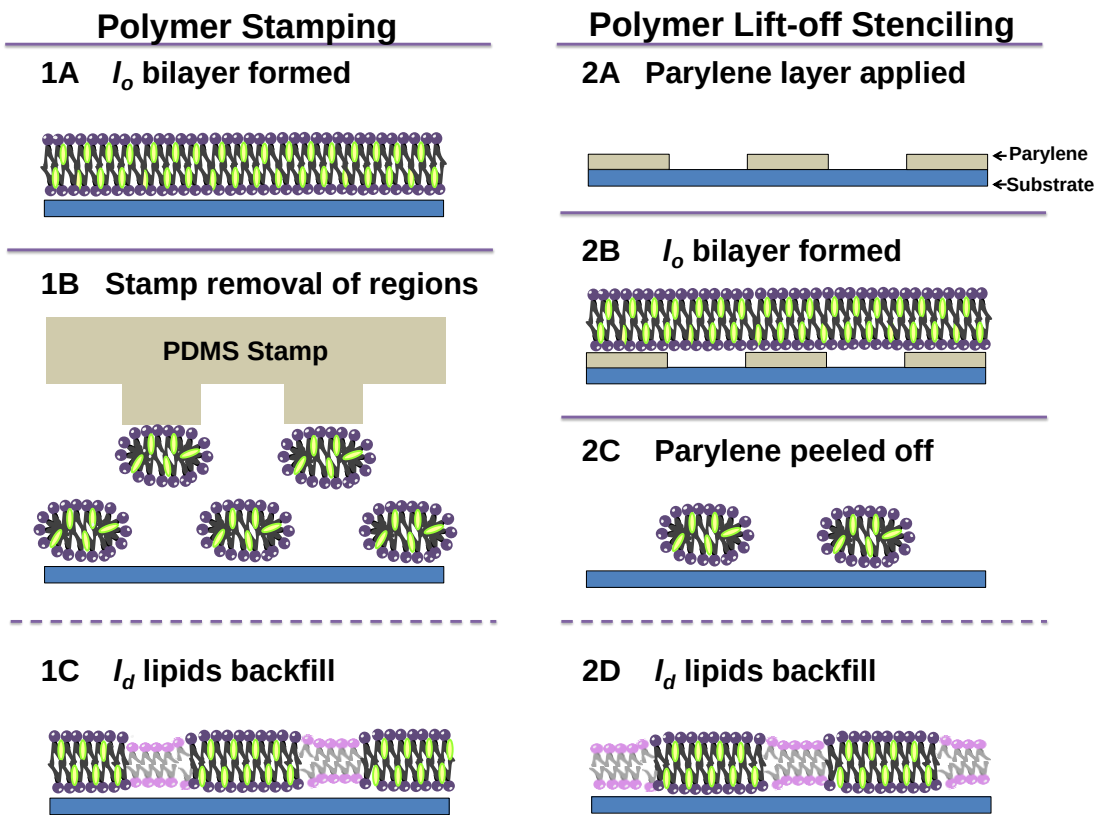

Figure 4.1. Bilayer patterning via polymer stamp blotting and polymer lift-off stenciling. Initially l_o phase bilayer is formed via vesicle fusion on the glass substrate (1A) or the parylene patterned substrate (2A, B). Patterned voids in the bilayer are generated by either polymer stamp contact and removal (1B) or lifting off parylene stencil (2C). These steps remove lipid bilayer from the substrate. The final step is addition of ld phase lipid bilayer via vesicle fusion (1C, 2D).

4.4.1 Polymer Blotting Characterization

First we characterized the removal process via stamp blotting. For these experiments, POPC bilayer was used. We designed stamps with heights of 3 μm to strike a balance between high enough features to allow adequate space for unpatterned bilayer to fit, while not so large that the posts distort under pressure, negatively impacting the pattern quality. The stamp feature height was not quantitatively studied or optimized. Stamps were weighted with glass slides and checked for balance.

Empirically, we found that applying the stamps at a pressure of ~3500 Pa for 7 minutes of contact time, results in high fidelity removal of bilayer in the patterned geometry. Pressure was calculated by dividing the force of the weight over the contact area of the stamp being sure to only account for contacting feature area in the calculation. We also determined that feature sizes down to 5 μm diameter circles could be reproduced well although square corners became appreciably rounded below 20 μm (Fig. 4.2).

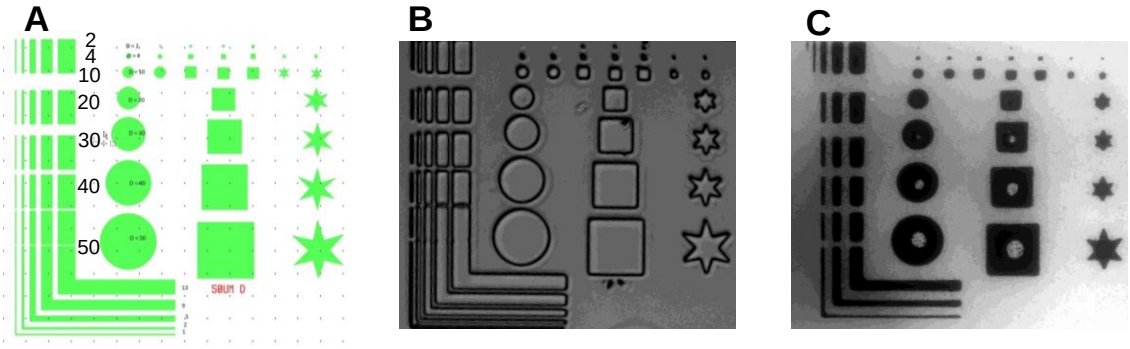

Figure 4.2. Characterization of feature size achievable with polymer blotting process. The pattern used had feature sizes from 50 μm down to 2 μm and a variety of shapes (A). A brightfield image of the polymer stamp reveals some loss of feature fidelity for more complex features below 20 μm (B). POPC + 0.1% TR-DHPE was used as the test bilayer. Stamp was applied at 3500 Pa for 7 min. The smallest features, less than 2 μm, did not transfer to the supported lipid bilayer (C). Some micron sized lipid droplets fell into larger patterned regions on stamp removal.

Next we examined the backfilling bilayer quality after blotting. As a reminder, the patterning application we seek differs from most literature applications[151,154] because it requires that lipids can be backfilled into the blotted-out regions. This means the surface quality after blotting is critical and any PDMS debris left behind or other fouling of the surface would be detrimental to the utility of this method. We tested backfill bilayer quality by first forming a bilayer of POPC doped with 0.1% TR-DHPE and blotting out the patterned regions. The patterned voids were then backfilled with

pure POPC. TR-DHPE lipids diffused laterally across these regions to make the fluorescence uniform, meaning that we were able to form a lipid bilayer in the blotted out regions, and it could fuse with the original bilayer (Fig. 4.3). The blotting process was repeated 4 times on the same bilayer region, and each time the bilayer was able to recover completely for all stamped regions aside from a few defects (not shown). Those that did not recover were probably subject to uneven pressure from the stamp irreversibly fouling the surface.

Intensity in the unstamped bilayer regions was found to be slightly higher after mixing, possibly due to some unruptured POPC + 0.1% TR-DHPE vesicles. We find that recovery occurs in 2 to 3 mins with a diffusion coefficient of 0.5 $\mu m^2/s$ which about half that of a typical POPC bilayer, assuming the mixing is diffusion limited because of the excess vesicle concentration used in backfill bilayer formation. However, there will be some effect of the rate of bilayer formation and healing, and in addition the surrounding fluorescence reservoir cannot be approximated as infinite, as is assumed in the standard calculation. Both of these reasons explain the underestimated diffusivity of mixing as compared to a preformed bilayer. Large regions of clean patterning were achieved in the central and evenly-weighted regions, but bilayer patterned by the edges of the stamp showed distorted patterning and incomplete recovery probably because of uneven force during the stamping process.

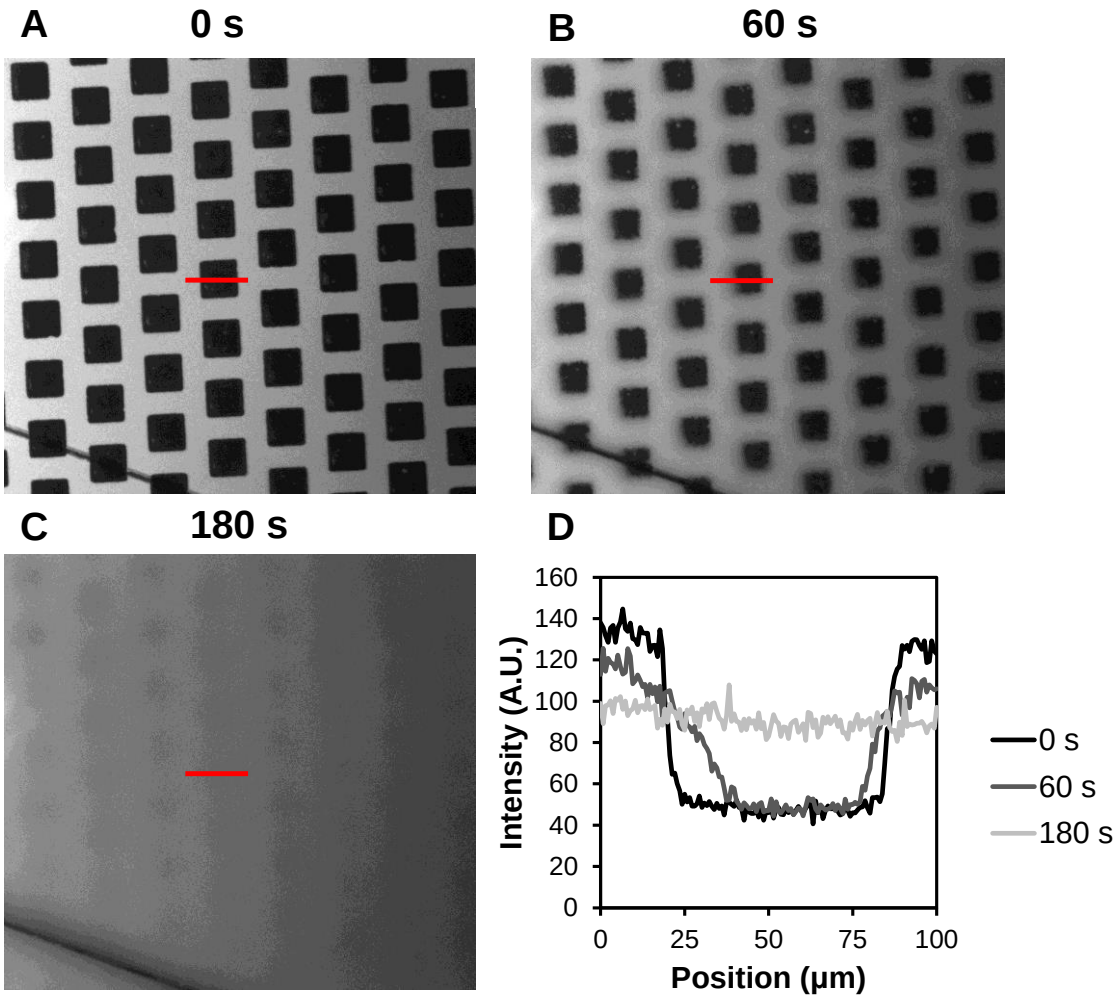

Figure 4.3. Demonstration of low-defect bilayer patterning by PDMS blotting method. POPC + 0.1% TR-DHPE bilayer blotted with patterned PDMS to remove array of 50 μm squares and backfilled with POPC (A). At t = 0 s POPC vesicles are added to the buffer above pre-patterned POPC + 0.1% TR-DHPE bilayer. As these vesicles spontaneously rupture in the voids, the TR-DHPE lipids begin to diffuse into the TR-free bilayer regions where new bilayer is forming (B). By 180 s the bilayer is nearly uniform again because the TR-DHPE lipids have had a chance to fully spread out, and the newly deposited bilayer has a low level of defects (C). A line scan across a patterned square shows the intensity recovery over time as mixing occurs (D).

The planned use of this pattern technique is in providing a model of lipid rafts in a supported lipid bilayer, perhaps including membrane proteins. Including membrane proteins in a supported lipid bilayer requires a cushioning strategy to prevent unwanted interaction between the protein and the substrate. We have shown that

PEGylated bilayers can be used to fluidize membrane proteins (Richards, M.J. et al., *In Review*). To this end, we have tested patterning of polyethylene glycol (PEG) functionalized lipid bilayers. In similar experiments to those shown above, POPC + 0.5% PEG5000-PE + R18 was used to form the first bilayer phase. After blotting with a polymer stamp, POPC + 0.5% PEG5000-PE was backfilled into the bilayer. Complete mixing occurred by 620 s (Fig. 4.4) similar to FRAP results for R18 bilayers.

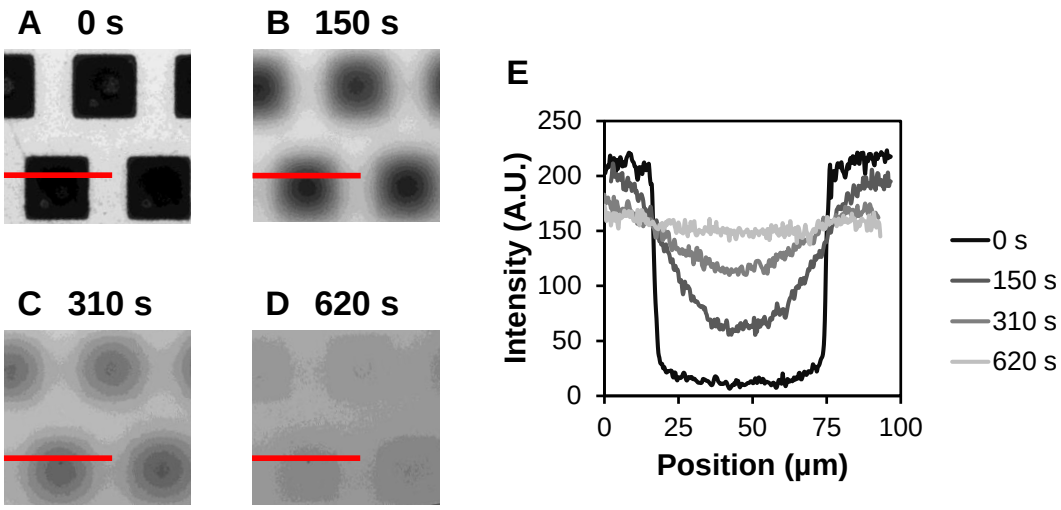

Figure 4.4. Bilayer quality and continuity demonstration for polymer blotting method with PEGylated lipid bilayer. POPC + 0.5% PEG5000-PE + R18 is patterned by polymer blotting. Backfilling is performed with POPC + 0.5% PEG5000-PE lipids at t = 0 (A). Shortly after addition, bilayer formation occurs in void locations as evidenced by spreading of R18 from initial locations (B, C). By 620 s after addition bilayer formation and mixing are complete (D). A line scan across a patterned square shows the intensity recovery over time as mixing occurs (E).

4.4.2 Parylene Stencil Characterization

Initial characterization studies on parylene stencils sought to evaluate the

patterning capability in terms of bilayer quality in stencil regions, bilayer removal fidelity and backfilled bilayer quality as described above for polymer blotting. These characteristics represent the key requirements for patterning a two-phase bilayer. To carry out these studies, a simple POPC lipid composition with 0.1% TR-DHPE was used.

Parylene stenciling was initially evaluated on the same glass substrate used to generate the patterned parylene as shown for patterning isolated domains[236]. In this case, termed etched substrate, the substrate with patterned polymer coating was subjected to a pre-use treatment with oxygen plasma in a Harrick Plasma Cleaner. Bilayer formation quality was poor within the stencil regions with a high amount of unruptured vesicles (Fig. 4.5). We determined that the bilayer quality may be impacted by surface fouling from the parylene coating and etching process. Another concern is that if the stencil is over-etched, there will be increased roughness and perhaps even a significant step height between the exposed and protected regions of the glass. This step height change in the substrate could affect diffusion of species in the bilayer at the boundary and continuity of bilayer at these points. To avoid this problem, parylene stencils were transplanted to freshly piranha cleaned glass coverslips using forceps and DI water to smooth out wrinkles. DI water was dried with nitrogen to ensure complete adhesion of the stencil to the surface and visual inspection was performed. Using this technique, both the initial and backfilled bilayers formed with high quality.

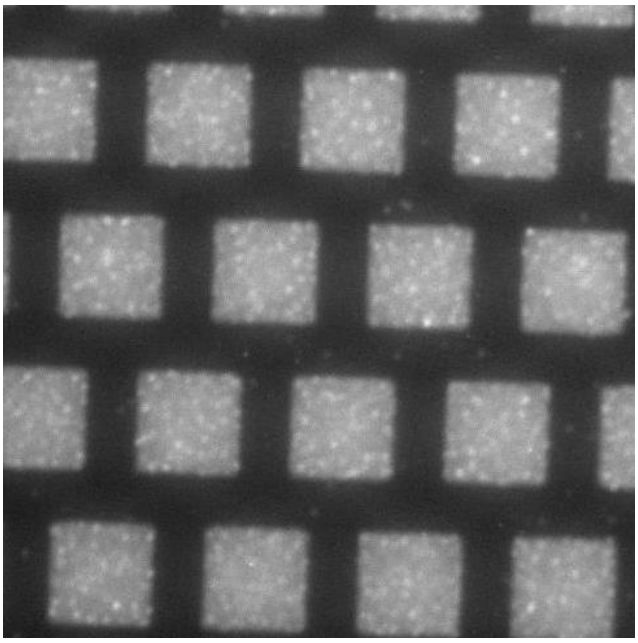

Figure 4.5. POPC + 0.1% TR-DHPE bilayers formed through parylene stencil using etched substrate with 50 μm x 50 μm squares. Bright spots and overall, non-uniformity indicate poor bilayer quality with a mixture of adsorbed unruptured vesicles on the surface.

To further investigate the cause of poor bilayer formation with etched substrates, the surface properties were characterized using contact angle measurements (Table 4.1). Traditional use of the vesicle fusion bilayer formation method relies on a very hydrophilic, wetting surface to for high quality bilayer formation. The surface is typically prepared with piranha cleaning and/or oxygen plasma treatment to make it amenable to bilayer formation. Slides treated with these methods are completely wetting, with immeasurable contact angles. In the etched substrate method, we found that regions of slides exposed during the parylene etch step had a contact angle of 63 ± 1°. This can be explained by increased roughness of the glass during etching or fouling from residual parylene. Regions of slides that were protected under parylene had more wetting contact angles of 37 ± 5°. However, we find that for the transplanted

parylene procedure, contact angles in both exposed and protected regions were both below 30° after removal of parylene, indicating that parylene residue or surface roughening is not a problem after transplantation.

Table 4.1. Contact angle measurements of etched substrate and transplanted substrate. Measurements were performed on exposed regions of the slide as well as regions that were initially protected by parylene.

Condition	Contact Angle	Standard Deviation
Etched Exposed	63	1
Etched Protected	37	5
Transplant Exposed	30	5
Transplant Protected	27	5

Backfilling was performed with unlabeled POPC lipids to evaluate the continuity of the patterned membrane between the initial and backfilled bilayers. The bilayer formation and mixing was monitored during addition of POPC and images were taken at several time points (Fig. 4.6). A rapid change was detected after addition of POPC backfill lipids indicated by a blurring of the edges of the POPC + 0.1% TR-DHPE domains. By 120 s, complete mixing of lipids had occurred between bilayer regions. Bilayer formation with minimal defects in both regions is confirmed as well as continuity between regions.

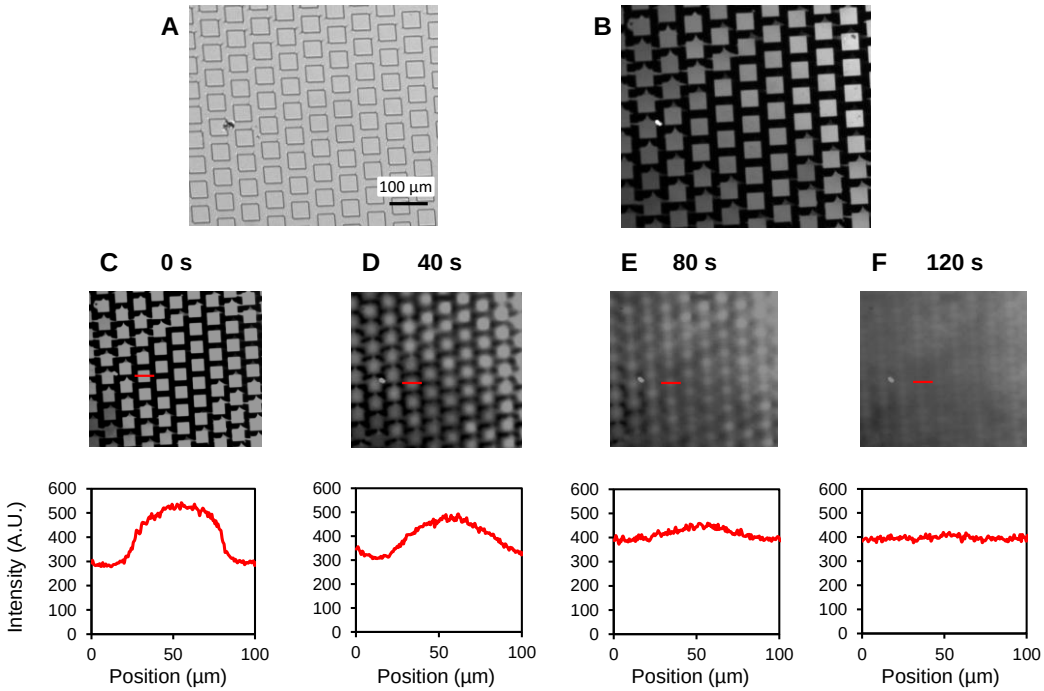

Figure 4.6. Bilayer quality and continuity demonstration for parylene stenciling transplant method. Parylene pattern is transplanted to a fresh piranha slide and inspected for wrinkles (A). POPC + 0.1% TR-DHPE is patterned through the parylene stencil and polymer is lifted off (B). Backfilling is performed with POPC lipids at t = 0 (C). Shortly after addition, bilayer formation occurs in void locations as evidenced by spreading of TR-DHPE from initial locations (D). By 80 s after addition bilayer formation and mixing are nearing completion (E). At 120 s, bilayer mixing is complete, with uniform bilayer fluorescence.

Some leaking underneath the polymer stencil was observed in the transplant case. The leaking issue can arise because of poor contact between the polymer stencil and glass substrate during the transplant process. For example, macro-scale wrinkles in the polymer translate into readily-apparent unpatterned bilayer streaks. There are also some smaller scale leaks around pattern boundaries which do not appear to be a result of poor transplant technique, but instead are a limitation of the method perhaps due to weak adhesion between the polymer and the glass.

4.4.3 Two-Phase Bilayer Patterning

We extended the pattern backfilling method to creating stable patterned bilayers by

introducing equilibrium liquid ordered (l_o) and liquid disordered (l_d) compositions. Stable phase patterning has been demonstrated before with DLPC and DPPC[158]. However, the compositions we use here for l_o phase; 60% cholesterol, 40% sphingomyelin and l_d phase; 70% POPC, 20% cholesterol, and 10% sphingomyelin are more physiologically relevant. Because of the more densely packed nature of the l_o bilayer phase, there are additional challenges associated with its use. It must be heated to above its transition temperature (around 65°C) when incubated with the substrate to form a bilayer. Because of this it must be the first phase incubated. If a two-phase l_o and l_d phase bilayer is heated to this temperature, destabilization is expected.

For the blot patterning technique, we expected potential difficulty in removing the l_o bilayer. Surprisingly, we found it was possible to remove ordered phase lipids with the same technique as disordered phase even after the lipids had cooled to room temperature. After backfilling and rinsing, phases were stable as indicated by the phase markers used – Alexa 594-G_{M1} for ordered phase and BODIPY-DHPE for disordered phase (Fig. 4.7). Bilayer recovery was observed after bleaching with a laser pulse in both phases. There were some defects in the initial l_o phase bilayer that were backfilled with the BODIPY-DHPE containing l_d phase as well as some incomplete removal via stamp blotting. The defects in the l_o phase may be a result of shrinking and cracking of the l_o bilayer when cooling to room temperature after formation at 70°C and might be avoided with a slower cooling process.

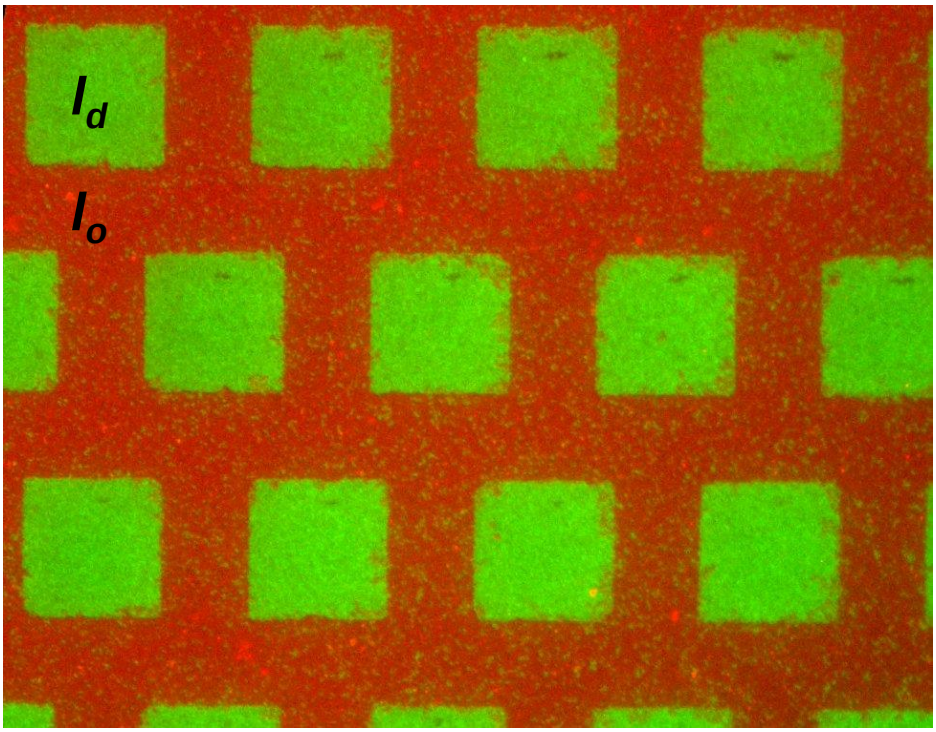

Figure 4.7. Blot patterning of two phase coexistent bilayers. l_o phase with Alexa 594-G_{M1} (red) was initially formed on the entire surface. A polymer stamp with an array of 50 μm x 50 μm square posts was used to blot away square sections of the bilayer. After removal, l_d phase with BODIPY-DHPE (green) was backfilled into the square voids.

To test for bilayer continuity between phases, a similar patterning experiment was performed. In this case the l_d phase marker probe BODIPY-DHPE was added as part of the l_o phase. In the stencil lift-off experiment (Fig. 4.8), after addition of the secondary l_d phase, continuity between phases is demonstrated by BODIPY-DHPE partitioning out of the l_o phase and into the newly formed l_d phase.

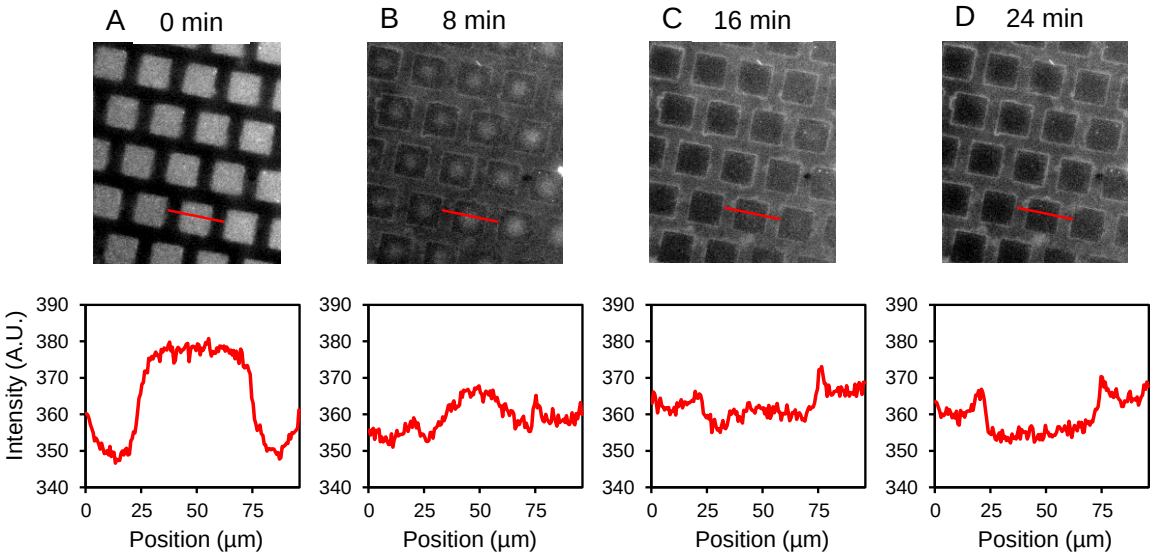

Figure 4.8. Transplant showing continuity and phase affinity partitioning by BODIPY-DHPE transfer from l_o to l_d phase. l_o phase with 0.1% BODIPY-DHPE formed within exposed 50 µm squares of polymer stencil. At t = 0 min, l_d phase vesicles were added (A). As l_d phase bilayer formed in the void region, BODIPY-DHPE began to partition out of the l_o squares and into the l_d continuous region (B). At 16 min it is possible to see the left side of the field of view has nearly completed partitioning while the right side has just started (C). At 24 min, partitioning of BODIPY-DHPE into the l_d phase is complete for the whole field of view.

Following successful patterning of multiphase bilayers, we decided to test our ability to impact the stability by heating the bilayer. Phases mix and lose distinct coexisting domains above a critical temperature. To demonstrate this, the two-phase bilayer patterned by blotting was exposed to "hot" buffer (~80 °C) by exchanging the bulk in the well (Fig. 4.9). We saw that BODIPY-DHPE moved from l_d to l_o phase becoming less strongly partitioned into the square, originally l_d, domains. Additionally, we observed small defects that formed predominantly along initial l_o/l_d phase boundaries, possibly due to the rapid temperature change. Determination of the exact miscibility point may be determined with a more sensitive temperature control mechanism.

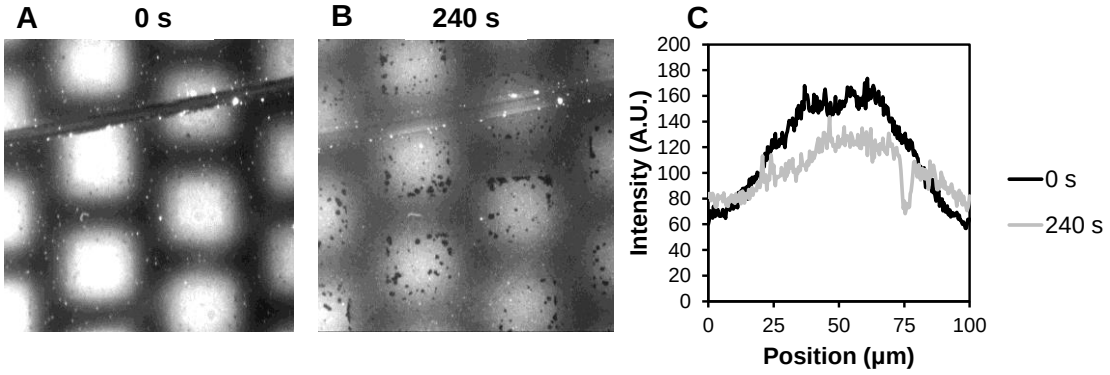

Figure 4.9. Polymer blotting applied to two phase coexistent l_o with l_d phase heated to 80°C. Initially, a liquid-ordered bilayer was blotted revealing square voids. These voids were subsequently backfilled with a liquid-disordered lipid composition doped with a 0.5% BODIPY-DHPE fluorescent marker by a vesicle fusion method (A). Because these two phase compositions are thermodynamically stable, they do not mix. Mixing of the membrane phases was be induced by increasing the temperature to 80°C via buffer exchange. At this point the two phases no longer show stable coexistence, thus mixing until the bilayer cooled (B). Intensity of line scans show some BODIPY-DHPE moves from central square region to outer region during heating (C).

We also tested use of methyl-β-cyclodextrin (MβCD), a cholesterol acceptor, as a means to trigger phase mixing (Fig. 4.10). Cholesterol efflux is a mechanism in the biological process of sperm capacitation that results in large scale changes to membrane organization[54]. This experiment was performed by first patterning a bilayer using the parylene stencil method with l_o phase bilayer in the 50 µm squares and l_d phase with Alexa 594-G_{M1} outside. Then MβCD was added to a concentration of 6.4 mM, removing cholesterol from the bilayer, changing the composition and affecting the equilibrium between the patterned phases. We observed an increase in intensity in the regions which were initially l_d phase. This could be attributed to a repartitioning of the small amount of Alexa 594-G_{M1} in l_o regions at the start to the l_d phase.

During this process, the membrane may redistribute species to maintain phase stability or even undergo phase transitions. With enough cholesterol removed (<10% remaining), we would expect a change from l_d and l_o phase coexistence to l_d and solid

ordered (s_o) phase coexistence[234], perhaps changing partitioning of components leading to increased concentration of Alexa 594-G_{M1} in the l_d phase. The details of the cholesterol removal are still unclear, but it is thought to depend on lipid phase and cholesterol concentration[237,238]. This patterned bilayer can be used to investigate these concepts further.

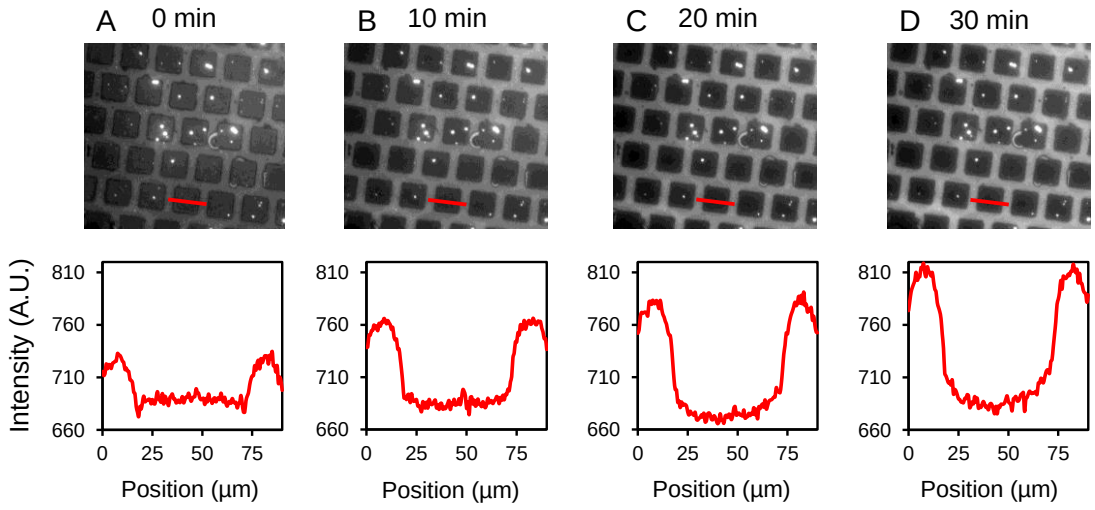

Figure 4.10. *lo* and *ld* phase bilayer patterned with parylene stenciling. Initially, *lo* phase is present in squares and *ld* phase with Alexa 594-G_{M1} in the surrounding bilayer (A). 6.4mM MβCD is added to the buffer and cholesterol is removed from the bilayer. Images are shown at 10 min (B), 20 min (C) and 30 min (D) time points. Repartitioning of Alexa 594-G_{M1} begins as the species moves from the inner regions into the surrounding fluid. After 30 minutes, the repartitioning reaches its equilibrium.

4.5 CONCLUSION

In this work we demonstrate two techniques for patterning continuous, two-phase lipid bilayers with backfilling after initial patterning. The patterned supported lipid bilayers have mobility similar to biological membranes, and show continuity between phases demonstrated with partitioning of lipid probes. In preliminary experiments, we

demonstrated an application of this mimic by testing two effectors of phase stability: temperature and cholesterol efflux by MβCD.

While both methods yielded acceptable results, there are some different challenges associated with each method. Removal with stenciling was typically better than stamping. Less material was left behind and edges down to small features were preserved in agreement with literature[236]. Polymer stenciling is a slightly more cumbersome technique than polymer blotting. Instead of making a reusable mold from which each reusable polymer stamp can be generated as in the blotting technique, each polymer stencil has to be patterned using photolithography. With both methods, the physical application of the polymer is the critical step: transplanting the polymer stencil to the fresh substrate and blotting the bilayer surface evenly to achieve clean removal are both delicate operations with high fail rates. Appropriate engineering solutions are useful in abetting this issue. For instance, we have designed a scaffold to lower and raise the polymer stamp during blotting that improves the evenness of our process over large surface areas.

We have developed a supported lipid bilayer (SLB) patterning method that allows us to design an array of model lipid "rafts" *in vitro* using biologically relevant membrane components. The periodic array of stable phases gives a reference point for assays such that they can be performed without the need for extra fluorescent labels. Additionally, having a controlled array of structures allows for the multiplexing of experiments with simultaneous events on a single SLB. One of the most useful applications of this platform is investigation of how raft stability is affected by different stimuli. This may lead to improved understanding of biological phenomena

as well as control strategies for model membrane devices including biosensors. At this stage, we have carried out preliminary proof-of-concept experiments to test mechanisms for controlling raft dynamics.

The patterned lipid bilayer described here, with continuous, phase stable domains, provides a useful model of lipid rafts in the cell membrane. A large library of characterization tools are available to the SLB system and can be used in combination with this patterned bilayer to further our knowledge of the way membrane heterogeneities, such as lipid rafts, can be modulated by external factors. One can envision expanding the complexity of this system by including membrane proteins, to better understand how they interact and are modified by lipid raft domains.

4.6 ACKNOWLEDGMENTS

We thank the National Science Foundation (grant CBET-1149452) for supporting the work presented in this article. M.J.R. is a fellow in Flexible Electronics for Biological and Life Science Applications. This fellowship is supported by the IGERT Program of the NSF (DGE-0654112) administered by the Nanobiotechnology Center at Cornell. The Cornell Nanofabrication Facility was used in this work under grant NSF funding grant ECCS-15420819.

CHAPTER 5

OUTLOOK

Several advancements to protein-lipid interaction studies including the development of novel tools and techniques for studying them are presented in this thesis. Artificial membranes – in particular, supported lipid bilayers – are a valuable platform for probing membrane protein interactions with lipids in a simplified but biologically relevant system. This work expands on the supported bilayer platform in aspects critical to extending its usefulness in studying membrane proteins and crucial lipid interactions by addressing key shortcomings of the platform: the lack of a native environment and difficulties and its preparation. Traditionally, methods by which membrane species are studied and separated did not include native cell membrane components and incorporation of membrane proteins into a supported lipid bilayer was a tedious process wherein non-native membrane-support interactions resulted in immobilization of target proteins. Our work has expanded the supported lipid bilayer's utility for studying a wide range of biological processes.

In Chapter 2, we developed a novel method of membrane species separation in a supported lipid bilayer. We extended the capability of patterning lipid bilayers to generating a two-phase lipid bilayer extraction channel. Using this channel, we demonstrated that membrane species could be convected through this separation medium, allowing for separation based on chemical affinity for the particular bilayer phase. This model gives insight into the phenomena by which proteins may

preferentially associate with different lipid environments in cell membrane. An appropriate mass transfer model was developed that can be used to predict the behavior of other separation targets and improve the design of the device. This work demonstrates the capabilities of the supported lipid bilayer as it relates to separation of membrane species in a native-like medium.

The second drawback we addressed resolved the two key problems with working with membrane proteins in supported lipid bilayers: 1) delivery of membrane proteins into the lipid bilayer and 2) preventing interaction of the membrane proteins with the underlying solid support. Traditionally, difficult and low yield purification and reconstitution methods that must be optimized for each protein are employed. We have developed a system that utilizes cell derived blebs as the carrier for membrane proteins and is described in Chapter 3. Any membrane proteins that can be expressed and collected in blebs can then be transferred onto the cushioned supported lipid bilayer for further analysis. This more universal approach will have a large impact on the field.

No detergents are involved at any step of the process, which eliminates a source of non-native interactions that could result in non-native folding of the membrane proteins. To provide cushioning between the bilayer and the solid support, a fraction of the lipids used in the rupture-assisting vesicles added to the blebs were PEGylated. The use of PEG had a two-fold positive effect. First, The PEGylated lipids improved the rupturing process, as is a known function of PEG[239], and second, it increased the distance between the bilayer and the substrate enough that transmembrane proteins could remain mobile.

In characterizing this platform, we showed that after the rupture process, properties of the cell membrane are retained in our cushioned bleb bilayer. For one, we found that the orientation of proteins is conserved; the bleb-derived bilayer is oriented such that the extracellular side of the membrane is exposed to the bulk. We also found that the mode of diffusion of membrane species mimics that of the cell membrane as well where subdiffusion is the prominent mode. While further study is warranted to investigate the diffusive behavior in more detail, we believe the subdiffusion is a result of the presence of small membrane domains among other factors. One of the biggest features of this technology is that it is convenient to use and can be combined into other standard SLB techniques. This new approach replaces the tedious purification and reconstitution steps previously required. At the same time, it opens up an immense set of possibilities in terms of the complexity that can be worked into the experiments by introduction of membrane proteins.

Future work in this area should be focused on two closely connected aspects: improvement and expansion of this technology. While there are aspects of the platform that are amenable to further development, there are also a variety of experiments that can be performed with what we have already developed. It is to be expected that some further applications will have their own technical challenges that will require some additional development of the platform and should be drivers for design.

Currently, there is interest in using this platform to learn more about membrane protein oligomerization. We have ongoing collaborations with the Kawate and Linder labs at Cornell University seeking to use this platform to characterize oligomerization

behavior of several types of transmembrane proteins. The benefit of this platform is that we can image the proteins in real-time in a native-like membrane which maintains critical lipid-protein interactions required for native oligomerization. We can also use this platform to probe potential effectors of oligomerization such as the lipid composition or presence of particular ligands. Investigating the effect of lipid composition on oligomerization is something that cannot be performed in cells. Other characterization assays could also be performed on this system with little further development including measuring differences in protein activity as a function of bilayer composition or measuring protein partitioning rate constants to better understand how lipid rafts can organize cell membranes. We plan to combine the bleb delivery system with the extraction channel device to sort membrane proteins based on their chemical affinities for raft-like phases. The design of the extraction channel could also be fine-tuned to further separate and concentrate a specific membrane protein target. It is our goal to develop this platform into a primary tool for all aspects of membrane protein characterization.

The most obvious opportunity for improvement of the current technology is in cushion design. Fortunately, there has been significant work in devising a variety of different types of cushioning strategies from polymer supports to floating bilayers tethered to the surface[135,240]. Many of these techniques have yet to be tested as fully as we are now capable of with the robust method of introducing membrane proteins to the SLB using the blebbing technique. An improvement to current cushioning strategies could be to tether the PEGylated bilayer to the substrate using a biotin-streptavidin linkage. This method not only ensures that the PEGylated lipids should

not be able to redistribute themselves unfavorably, but the streptavidin also acts as a passivating coating on the surface of the slide, preventing interaction between the membrane proteins and the glass. In some preliminary work, we have generated cushioned bleb bilayers with this technique and visualized translational motion of membrane proteins in the bilayer. The particular proteins we looked at, DHHC proteins showed increased mobility in the tethered PEG bilayer over our standard untethered cushioned bleb bilayers.

Other cushioning options exist that deserve investigation as they may prove to be more effective or could be designed to be better mimics of the cell. For example, cellulose, dextran or chitosan films can be coated onto glass slides prior to bilayer formation. These materials can mimic the native characteristics of an artificial extracellular matrix (ECM) or cytoskeleton. It might be possible to use actual components of the ECM or cytoskeleton when designing a cushion to provide even more biological relevance if probing those specific interactions are desirable. ECM extracts are available and could be tested for cushioning quality using our bleb bilayer platform. Individually, components like collagens, fibronectin, or glycans such as heparin sulfate or hyaluronic acid could be used to form a cushioning passivation layer. Particularly, hyaluronic acid is a strong candidate since it absorbs water to resist compression in load-bearing areas[241].

Key experiments should focus on characterization of the mobility of a spectrum of membrane proteins with different structural features, e.g. monotopic, transmembrane with short extramembranous extensions, and transmembrane with larger extensions using each cushion candidate. The function of each cushion can be evaluated from the

mobile fraction and diffusional mode information attainable with single particle methods. The ideal cushion can provide enough space to allow high mobile fractions for all types of transmembrane proteins and that the platform acts as a mimic of the cell membrane.

Additional characterization work is required for the process of forming the bleb bilayers as well. Currently, the amount of blebs used to form the bilayer is somewhat empirical. Each bleb preparation is slightly different as they rely on a different batch of cells with variable viability and density. Though we have measured bleb counts in several batches and found only about a four-fold difference between the highest and lowest concentrations, there are additional challenges to consistent bleb bilayer composition for certain cushion types. In preliminary work, we have noted that when incubating blebs on a passivated protein surface compared to bare glass, we find that after rinsing, many blebs desorb from samples coated with passivated protein. This is probably because in the bare glass experiments, some proteins were sticking to the glass, holding the blebs in place. The passivating layer prevents this interaction, but a negative side-affect is that blebs are more easily rinsed away before bilayer formation occurs. A new procedure will have to be developed to minimize loss during rinsing or avoid rinsing before bilayer formation, while maintaining the desired ratio of blebs to fusogenic lipid vesicles. This ratio would be a useful metric to guide PEGylated lipid concentration for obtaining a desired cushion length and gain a sense of the final bilayer composition. Some initial work to characterize this ratio has been performed using QCMD in our group and could be further extended to studying this particular mammalian bleb bilayer platform.

One further application we have started to pursue is looking into the interaction between membrane proteins and lipid domains. Of particular interest is the dynamics of domain formation. Different phase geometries are needed for this study that cannot be achieved with the laminar flow patterning techniques we used on the extraction channel, so we investigated developing other techniques to meet this need as discussed in Chapter 4. We showed that polymer mold blotting and polymer lift-off could be used to pattern phase stable bilayers, but in both cases there are some drawbacks limiting reliability that require more elegant engineering solutions. For polymer blotting, we find that defects are formed during the blotting process that prevent clean patch formation and sometimes prevent healing between domains. For polymer lift-off, the original region under the polymer is not amenable to backfilling for bilayer formation because of the surface quality. If the patterned polymer is transferred to a clean substrate before bilayer formation, bilayer can be backfilled in that region. However, we find that leaking underneath the polymer stencil is an issue that prevents consistent, high-quality pattern generation. Both methods are promising, but there are consistency issues that need to be addressed through further testing of methods and optimization of parameters such as: stamping pressure, pillar height, parylene thickness and bilayer formation time among others.

The type of bilayer patterns (isolated domains within a large continuous phase) we can achieve with stamping or stenciling allows us to look at how various external stimuli can affect domain stability. We showed that increasing temperature can cause disruption of domains and complete mixing as had been demonstrated for GPMV and GUV systems in the past as a result of going above the miscibility critical point.

Recognizing the potential of this simplified model for raft phases, we investigated the use of cyclodextrins on raft dynamics. The use of a particular cyclodextrin, methyl-β cyclodextrin (MβCD), to probe for raft-association, cholesterol effects and raft-mediated cellular processes is a common technique. MβCD binds and removes cholesterol from lipid bilayers and since the raft phase is enriched in cholesterol, it is believed to cause a disruption of rafts. However, there are questions surrounding the actual effect of cyclodextrin on the bilayer. It is known to act promiscuously at high concentration and can remove other membrane lipids as well as cholesterol[242]. Additionally, upon closer examination of the ternary phase diagram determined for POPC, cholesterol and sphingomyelin[234], seen as a representative mixture for cell membranes, it is unclear if removal of cholesterol would lead to formation of a single lipid phase. Removal of cholesterol from the system may result in coexisting disordered and gel-like phases, rather than a single lipid phase. Using this patterned bilayer platform to perform these types of studies, we can provide a valuable insight to the mechanisms behind lipid raft domain dynamics.

Lipid-protein interactions are only starting to become appreciated for their role in cell physiology. Part of the reason for this is that there have been very few methods to directly investigate them. Until now, most of the work has been performed either on simplified model probes in simple artificial membranes or with difficult to interpret cell-based measurements. The techniques described here: supported lipid bilayer patterning and generation of a cushioned bleb bilayer enable a bridging of two previously distinct methods, bringing more biological relevance in terms of bilayer heterogeneity and membrane proteins to the artificial membrane system. These

platforms have the capability to provide a framework for fundamental study of protein-lipid interaction as well as act as scaffolding for drug screening or other biosensor applications on a membrane mimic with a high level of biological complexity.

REFERENCES

(1) Overington, J. P.; Al-Lazikani, B.; Hopkins, A. L. How Many Drug Targets Are There? *Nat. Rev. Drug Discov.* **2006**, *5*, 993–996.

(2) Lundstrom, K. Structural Genomics on Membrane Proteins: Mini Review. *Comb Chem High Throughput Screen* **2004**, *7*, 431–439.

(3) Cooper, M. A. Optical Biosensors in Drug Discovery. *Nat. Rev. Drug Discov.* **2002**, *1*, 515–528.

(4) Amzel, L. M. Structure-Based Drug Design. *Curr. Opin. Biotechnol.* **1998**, *9*, 366–369.

(5) Seddon, A. M.; Curnow, P.; Booth, P. J. Membrane Proteins, Lipids and Detergents: Not Just a Soap Opera. *Biochim. Biophys. Acta* **2004**, *1666*, 105–117.

(6) George, S. R.; O'Dowd, B. F.; Lee, S. P. G-Protein-Coupled Receptor Oligomerization and Its Potential for Drug Discovery. *Nat. Rev. Drug Discov.* **2002**, *1*, 808–820.

(7) Verlinde, C.; Hol, W. Structure-Based Drug Design: Progress, Results and Challenges. *Structure* **1994**, 577–587.

(8) Congreve, M.; Marshall, F. The Impact of GPCR Structures on Pharmacology and Structure-Based Drug Design. *Br. J. Pharmacol.* **2010**, *159*, 986–996.

(9) Lee, A. G. How Lipids Affect the Activities of Integral Membrane Proteins. *Biochim. Biophys. Acta* **2004**, *1666*, 62–87.

(10) Schonenbach, N. S.; Hussain, S.; O'Malley, M. A. Structure and Function of G Protein-Coupled Receptor Oligomers: Implications for Drug Discovery. *Wiley Interdiscip. Rev. Nanomedicine Nanobiotechnology* **2014**, *7*, 408–427.

(11) Reimhult, E.; Kumar, K. Membrane Biosensor Platforms Using Nano- and Microporous Supports. *Trends in Biotechnology*, 2008, *26*, 82–89.

(12) Andersson, A.-S.; Glasmästar, K.; Sutherland, D.; Lidberg, U.; Kasemo, B. Cell Adhesion on Supported Lipid Bilayers. *J. Biomed. Mater. Res. A* **2003**, *64*, 622–629.

(13) Benamara, H.; Rihouey, C.; Jouenne, T.; Alexandre, S. Impact of the Biofilm Mode of Growth on the Inner Membrane Phospholipid Composition and Lipid Domains in Pseudomonas Aeruginosa. *Biochim. Biophys. Acta* **2011**, *1808*, 98–105.

(14) Lundstrom, K. Structural Genomics for Membrane Proteins. *Cell. Mol. Life Sci.* **2006**, *63*, 2597–2607.

(15) Bill, R. M.; Henderson, P. J. F.; Iwata, S.; Kunji, E. R. S.; Michel, H.; Neutze, R.; Newstead, S.; Poolman, B.; Tate, C. G.; Vogel, H. Overcoming Barriers to Membrane Protein Structure Determination. *Nat. Biotechnol.* **2011**, *29*, 335–

340.

(16) Wiener, M. A Pedestrian Guide to Membrane Protein Crystallization. *Methods* **2004**.

(17) Koutsopoulos, S.; Kaiser, L.; Eriksson, H. M.; Zhang, S. Designer Peptide Surfactants Stabilize Diverse Functional Membrane Proteins. *Chem. Soc. Rev.* **2012**, *41*, 1721–1728.

(18) Wu, C. C.; MacCoss, M. J.; Howell, K. E.; Yates, J. R. A Method for the Comprehensive Proteomic Analysis of Membrane Proteins. *Nat. Biotechnol.* **2003**, *21*, 532–538.

(19) Lundbæk, J. Lipid Bilayer Regulation of Membrane Protein Function: Gramicidin Channels as Molecular Force Probes. *J. R. Soc. Interface* **2010**, *7*, 373–395.

(20) Soubias, O.; Gawrisch, K. *Rhodopsin-Lipid Interactions Studied by NMR*; 1st ed.; Elsevier Inc., 2013; Vol. 522.

(21) Soubias, O.; Teague, W. E.; Hines, K. G.; Mitchell, D. C.; Gawrisch, K. Contribution of Membrane Elastic Energy to Rhodopsin Function. *Biophys. J.* **2010**, *99*, 817–824.

(22) Lee, A. G. Lipid-Protein Interactions in Biological Membranes: A Structural Perspective. *Biochim. Biophys. Acta - Biomembr.* **2003**, *1612*, 1–40.

(23) Contreras, F.-X.; Ernst, A. M.; Wieland, F. Specificity of Intramembrane Protein − Lipid Interactions Specificity of Intramembrane Protein – Lipid Interactions. *Cold Spring Harb. Perspect. Biol.* **2011**.

(24) Marius, P.; De Planque, M. R. R.; Williamson, P. T. F. Probing the Interaction of Lipids with the Non-Annular Binding Sites of the Potassium Channel KcsA by Magic-Angle Spinning NMR. *Biochim. Biophys. Acta - Biomembr.* **2012**, *1818*, 90–96.

(25) Gimpl, G.; Wiegand, V.; Burger, K.; Fahrenholz, F. Cholesterol and Steroid Hormones: Modulators of Oxytocin Receptor Function. *Prog. Brain Res.* **2002**, *139*, 43–55.

(26) Pucadyil, T. J.; Chattopadhyay, A. Cholesterol Modulates Ligand Binding and G-Protein Coupling to serotonin1A Receptors from Bovine Hippocampus. *Biochim. Biophys. Acta - Biomembr.* **2004**, *1663*, 188–200.

(27) Eroglu, C.; Brugger, B.; Wieland, F.; Sinning, I. Glutamate-Binding Affinity of Drosophila Metabotropic Glutamate Receptor Is Modulated by Association with Lipid Rafts. *Proc. Natl. Acad. Sci. U. S. A.* **2003**, *100*, 10219–10224.

(28) Beel, A. J.; Sakakura, M.; Barrett, P. J.; Sanders, C. R. Direct Binding of Cholesterol to the Amyloid Precursor Protein: An Important Interaction in Lipid-Alzheimer's Disease Relationships? *Biochim. Biophys. Acta - Mol. Cell Biol. Lipids* **2010**, *1801*, 975–982.

(29) Hancock, J. Lipid Rafts: Contentious Only from Simplistic Standpoints. *Nat.*

Rev. Mol. Cell Biol. **2006**, *7*, 5658–5659.

(30) Simons, K.; Toomre, D. Lipid Rafts and Signal Transduction. *Nat. Rev. Mol. Cell Biol.* **2000**, *1*, 31–41.

(31) Simons, K.; Ikonen, E. Functional Rafts in Cell Membranes. *Nature* **1997**, *387*, 569–572.

(32) Brown, D.; London, E. Functions of Lipid Rafts in Biological Membranes. *Annu. Rev. Cell Dev. Biol.* **1998**, *14*, 111–136.

(33) Perozo, E.; Kloda, A.; Cortes, D. M.; Martinac, B. Physical Principles Underlying the Transduction of Bilayer Deformation Forces during Mechanosensitive Channel Gating. *Nat. Struct. Biol.* **2002**, *9*, 696–703.

(34) Milovanovic, D.; Honigmann, A.; Koike, S.; Göttfert, F.; Pähler, G.; Junius, M.; Müllar, S.; Diederichsen, U.; Janshoff, A.; Grubmüller, H.; et al. Hydrophobic Mismatch Sorts SNARE Proteins into Distinct Membrane Domains. *Nat. Commun.* **2015**, *7*, 5984.

(35) Harder, T.; Engelhardt, K. R. Membrane Domains in Lymphocytes - from Lipid Rafts to Protein Scaffolds. *Traffic* **2004**, *5*, 265–275.

(36) Matkó, J.; Szöllősi, J. Regulatory Aspects of Membrane Microdomain (raft) Dynamics in Live Cells. *Membr. Microdomain Signal.* **2005**, 15–46.

(37) Blitterswijk, W. Van; Luit, A. Van Der. Ceramide: Second Messenger or Modulator of Membrane Structure and Dynamics? *Biochem. J* **2003**, *211*, 199–211.

(38) Lentz, B. R.; Barrow, D. A.; Hoechli, M. Cholesterol-Phosphatidylcholine Interactions in Multilamellar Vesicles. *Biochemistry* **1980**, *19*, 1943–1954.

(39) Ipsen, J. H.; Karlström, G.; Mouritsen, O. G.; Wennerström, H.; Zuckermann, M. J. Phase Equilibria in the Phosphatidylcholine-Cholesterol System. *Biochim. Biophys. Acta* **1987**, *905*, 162–172.

(40) Lingwood, D.; Simons, K. Lipid Rafts as a Membrane-Organizing Principle. *Science* **2010**, *327*, 46–50.

(41) Brown, D. A.; Rose, J. K. Sorting of GPI-Anchored Proteins to Glycolipid-Enriched Membrane Subdomains during Transport to the Apical Cell Surface. *Cell* **1992**, *68*, 533–544.

(42) Harder, T.; Scheiffele, P.; Verkade, P.; Simons, K. Lipid Domain Structure of the Plasma Membrane Revealed by Patching of Membrane Components. *J. Cell Biol.* **1998**, *141*, 929–942.

(43) Fujiwara, T.; Ritchie, K.; Murakoshi, H.; Jacobson, K.; Kusumi, A. Phospholipids Undergo Hop Diffusion in Compartmentalized Cell Membrane. *J. Cell Biol.* **2002**, *157*, 1071–1081.

(44) Kusumi, A.; Koyama-Honda, I.; Suzuki, K. Molecular Dynamics and Interactions for Creation of Stimulation-Induced Stabilized Rafts from Small Unstable Steady-State Rafts. *Traffic* **2004**, *5*, 213–230.

(45) Gidwani, A.; Holowka, D.; Baird, B. Fluorescence Anisotropy Measurements of Lipid Order in Plasma Membranes and Lipid Rafts from RBL-2H3 Mast Cells. *Biochemistry* **2001**, *40*, 12422–12429.

(46) Ge, M.; Gidwani, A.; Brown, H. A.; Holowka, D.; Baird, B.; Freed, J. H. Ordered and Disordered Phases Coexist in Plasma Membrane Vesicles of RBL-2H3 Mast Cells. An ESR Study. *Biophys. J.* **2003**, *85*, 1278–1288.

(47) Richter, M.; Hedegaard, M.; Deckert-Gaudig, T.; Lampen, P.; Deckert, V. Laterally Resolved and Direct Spectroscopic Evidence of Nanometer-Sized Lipid and Protein Domains on a Single Cell. *Small* **2011**, *7*, 209–214.

(48) Henriques, R.; Mhlanga, M. M. PALM and STORM: What Hides beyond the Rayleigh Limit? *Biotechnol. J.* **2009**, *4*, 846–857.

(49) Owen, D. M.; Magenau, A.; Williamson, D.; Gaus, K. The Lipid Raft Hypothesis Revisited - New Insights on Raft Composition and Function from Super-Resolution Fluorescence Microscopy. *BioEssays* **2012**, *34*, 739–747.

(50) Owen, D. M.; Rentero, C.; Rossy, J.; Magenau, A.; Williamson, D.; Rodriguez, M.; Gaus, K. PALM Imaging and Cluster Analysis of Protein Heterogeneity at the Cell Surface. *J. Biophotonics* **2010**, *3*, 446–454.

(51) Wu, J.; Gao, J.; Qi, M.; Wang, J.; Cai, M.; Liu, S.; Hao, X.; Jiang, J.; Wang, H. High-Efficiency Localization of Na(+)-K(+) ATPases on the Cytoplasmic Side by Direct Stochastic Optical Reconstruction Microscopy. *Nanoscale* **2013**, *5*, 11582–11586.

(52) Mueller, V.; Ringemann, C.; Honigmann, A.; Schwarzmann, G.; Medda, R.; Leutenegger, M.; Polyakova, S.; Belov, V. N.; Hell, S. W.; Eggeling, C. STED Nanoscopy Reveals Molecular Details of Cholesterol- and Cytoskeleton-Modulated Lipid Interactions in Living Cells. *Biophys. J.* **2011**, *101*, 1651–1660.

(53) Kellner, R. R.; Baier, C. J.; Willig, K. I.; Hell, S. W.; Barrantes, F. J. Nanoscale Organization of Nicotinic Acetylcholine Receptors Revealed by Stimulated Emission Depletion Microscopy. *Neuroscience* **2007**, *144*, 135–143.

(54) Selvaraj, V.; Buttke, D. E.; Asano, A.; McElwee, J. L.; Wolff, C. A.; Nelson, J. L.; Klaus, A. V; Hunnicutt, G. R.; Travis, A. J. GM1 Dynamics as a Marker for Membrane Changes Associated with the Process of Capacitation in Murine and Bovine Spermatozoa. *J. Androl.* **2007**, *28*, 588–599.

(55) Paulick, M.; Bertozzi, C. The Glycosylphosphatidylinositol Anchor: A Complex Membrane-Anchoring Structure for Proteins. *Biochemistry* **2008**, *47*, 6991–7000.

(56) Asano, A.; Nelson, J. L.; Zhang, S.; Travis, A. J. Characterization of the Proteomes Associating with Three Distinct Membrane Raft Sub-Types in Murine Sperm. *Proteomics* **2010**, *10*, 3494–3505.

(57) Legler, D.; Doucey, M.; Schneider, P. Differential Insertion of GPI-Anchored GFPs into Lipid Rafts of Live Cells. *FASEB J.* **2005**, *20*, 1–20.

(58) Gupta, N.; DeFranco, A. Visualizing Lipid Raft Dynamics and Early Signaling Events during Antigen Receptor-Mediated B-Lymphocyte Activation. *Mol. Biol. Cell* **2003**, *14*, 432–444.

(59) Chiantia, S.; Kahya, N.; Ries, J.; Schwille, P. Effects of Ceramide on Liquid-Ordered Domains Investigated by Simultaneous AFM and FCS. *Biophys. J.* **2006**, *90*, 4500–4508.

(60) Lin, W.-C.; Blanchette, C. D.; Ratto, T. V; Longo, M. L. Lipid Domains in Supported Lipid Bilayer for Atomic Force Microscopy. *Methods Mol. Biol.* **2007**, *400*, 503–513.

(61) Ratto, T.; Longo, M. Obstructed Diffusion in Phase-Separated Supported Lipid Bilayers: A Combined Atomic Force Microscopy and Fluorescence Recovery after Photobleaching. *Biophys. J.* **2002**, *83*, 3380–3392.

(62) Dietrich, C.; Bagatolli, L.; Volovyk, Z. Lipid Rafts Reconstituted in Model Membranes. *Biophys. J.* **2001**, *80*, 1417–1428.

(63) Stottrup, B. L.; Veatch, S. L.; Keller, S. L. Nonequilibrium Behavior in Supported Lipid Membranes Containing Cholesterol. *Biophys. J.* **2004**, *86*, 2942–2950.

(64) Dietrich, C.; Volovyk, Z. N.; Levi, M.; Thompson, N. L.; Jacobson, K. Partitioning of Thy-1, GM1, and Cross-Linked Phospholipid Analogs into Lipid Rafts Reconstituted in Supported Model Membrane Monolayers. *Proc. Natl. Acad. Sci. U. S. A.* **2001**, *98*, 10642–10647.

(65) Lichtenberg, D.; Goñi, F. M.; Heerklotz, H. Detergent-Resistant Membranes Should Not Be Identified with Membrane Rafts. *Trends Biochem. Sci.* **2005**, *30*, 430–436.

(66) Kusumi, A.; Suzuki, K. Toward Understanding the Dynamics of Membrane-Raft-Based Molecular Interactions. *Biochim. Biophys. Acta - Mol. Cell Res.* **2005**, *1746*, 234–251.

(67) Selvaraj, V.; Asano, A.; Buttke, D. E.; McElwee, J. L.; Nelson, J. L.; Wolff, C. A.; Merdiushev, T.; Fornés, M. W.; Cohen, A. W.; Lisanti, M. P.; et al. Segregation of Micron-Scale Membrane Sub-Domains in Live Murine Sperm. *J. Cell. Physiol.* **2006**, *206*, 636–646.

(68) Foster, L. J.; Chan, Q. W. T. Lipid Raft Proteomics: More than Just Detergent-Resistant Membranes. *Subcell. Biochem.* **2007**, *43*, 35–47.

(69) Levental, I.; Lingwood, D.; Grzybek, M.; Coskun, U.; Simons, K. Palmitoylation Regulates Raft Affinity for the Majority of Integral Raft Proteins. *Proc. Natl. Acad. Sci. U. S. A.* **2010**, *107*, 22050–22054.

(70) Diaz-Rohrer, B. B.; Levental, K. R.; Simons, K.; Levental, I. Membrane Raft Association Is a Determinant of Plasma Membrane Localization. *Proc. Natl. Acad. Sci. U. S. A.* **2014**, *111*, 8500–8505.

(71) Kabouridis, P. S.; Janzen, J.; Magee, A. L.; Ley, S. C. Cholesterol Depletion Disrupts Lipid Rafts and Modulates the Activity of Multiple Signaling

Pathways in T Lymphocytes. *Eur. J. Immunol.* **2000**, *30*, 954–963.

(72) Hao, M.; Mukherjee, S.; Maxfield, F. R. Cholesterol Depletion Induces Large Scale Domain Segregation in Living Cell Membranes. *Proc. Natl. Acad. Sci. U. S. A.* **2001**, *98*, 13072–13077.

(73) Zidovetzki, R.; Levitan, I. Use of Cyclodextrins to Manipulate Plasma Membrane Cholesterol Content: Evidence, Misconceptions and Control Strategies. *Biochim. Biophys. Acta - Biomembr.* **2007**, *1768*, 1311–1324.

(74) Asano, S.; Kitatani, K.; Taniguchi, M.; Hashimoto, M.; Zama, K.; Mitsutake, S.; Igarashi, Y.; Takeya, H.; Kigawa, J.; Hayashi, A.; et al. Regulation of Cell Migration by Sphingomyelin Synthases: Sphingomyelin in Lipid Rafts Decreases Responsiveness to Signaling by the CXCL12/CXCR4 Pathway. *Mol. Cell. Biol.* **2012**, *32*, 3242–3252.

(75) Sonnleitner, A.; Schütz, G. J.; Schmidt, T. Free Brownian Motion of Individual Lipid Molecules in Biomembranes. *Biophys. J.* **1999**, *77*, 2638–2642.

(76) Head, B. P.; Patel, H. H.; Insel, P. A. Interaction of Membrane/lipid Rafts with the Cytoskeleton: Impact on Signaling and Function: Membrane/lipid Rafts, Mediators of Cytoskeletal Arrangement and Cell Signaling. *Biochim. Biophys. Acta - Biomembr.* **2014**, *1838*, 532–545.

(77) Levitan, I.; Gooch, K. J. Lipid Rafts in Membrane-Cytoskeleton Interactions and Control of Cellular Biomechanics: Actions of oxLDL. *Antioxid. Redox Signal.* **2007**, *9*, 1519–1534.

(78) Kok, J. W.; Klappe, K.; Hummel, I. The Role of the Actin Cytoskeleton and Lipid Rafts in the Localization and Function of the ABCC1 Transporter. *Adv. Biol.* **2014**, *2014*, DOI: 10.1155/2014/105898.

(79) Ritchie, K.; Iino, R.; Fujiwara, T.; Murase, K.; Kusumi, A. The Fence and Picket Structure of the Plasma Membrane of Live Cells as Revealed by Single Molecule Techniques (Review). *Mol. Membr. Biol.* **2003**, *20*, 13–18.

(80) Iino, R.; Koyama, I.; Kusumi, A. Single Molecule Imaging of Green Fluorescent Proteins in Living Cells: E-Cadherin Forms Oligomers on the Free Cell Surface. *Biophys. J.* **2001**, *80*, 2667–2677.

(81) Weigel, A. V.; Simon, B.; Tamkun, M. M.; Krapf, D. Ergodic and Nonergodic Processes Coexist in the Plasma Membrane as Observed by Single-Molecule Tracking. *Proc. Natl. Acad. Sci. U. S. A.* **2011**, *108*, 6438–6443.

(82) Türkcan, S.; Richly, M. U.; Alexandrou, A.; Masson, J. B. Probing Membrane Protein Interactions with Their Lipid Raft Environment Using Single-Molecule Tracking and Bayesian Inference Analysis. *PLoS One* **2013**, *8*, e53073.

(83) Douglass, A. D.; Vale, R. D. Single-Molecule Microscopy Reveals Plasma Membrane Microdomains Created by Protein-Protein Networks That Exclude or Trap Signaling Molecules in T Cells. *Cell* **2005**, *121*, 937–950.

(84) Magenau, A.; Owen, D. M.; Yamamoto, Y.; Tran, J.; Kwiatek, J. M.; Parton, R. G.; Gaus, K. Discreet and Distinct Clustering of Five Model Membrane

Proteins Revealed by Single Molecule Localization Microscopy. *Mol Membr Biol* **2015**, 1–8.

(85) Popot, J.-L. Amphipols, Nanodiscs, and Fluorinated Surfactants: Three Nonconventional Approaches to Studying Membrane Proteins in Aqueous Solutions. *Annu. Rev. Biochem.* **2010**, *79*, 737–775.

(86) Merkle, D.; Kahya, N.; Schwille, P. Reconstitution and Anchoring of Cytoskeleton inside Giant Unilamellar Vesicles. *Chembiochem* **2008**, *9*, 2673–2681.

(87) Sezgin, E.; Kaiser, H.-J.; Baumgart, T.; Schwille, P.; Simons, K.; Levental, I. Elucidating Membrane Structure and Protein Behavior Using Giant Plasma Membrane Vesicles. *Nature protocols*, 2012, *7*, 1042–1051.

(88) Baumgart, T.; Hammond, A. T.; Sengupta, P.; Hess, S. T.; Holowka, D. A.; Baird, B. A.; Webb, W. W. Large-Scale Fluid / Fluid Phase Separation of Proteins and Lipids in Giant Plasma Membrane Vesicles. *Proc. Natl. Acad. Sci. U. S. A.* **2007**, *104*, 3165–3170.

(89) Sezgin, E.; Levental, I.; Grzybek, M.; Schwarzmann, G.; Mueller, V.; Honigmann, A.; Belov, V. N.; Eggeling, C.; Coskun, Ü.; Simons, K.; et al. Partitioning, Diffusion, and Ligand Binding of Raft Lipid Analogs in Model and Cellular Plasma Membranes. *Biochim. Biophys. Acta - Biomembr.* **2012**, *1818*, 1777–1784.

(90) Veatch, S. L.; Keller, S. L. Separation of Liquid Phases in Giant Vesicles of Ternary Mixtures of Phospholipids and Cholesterol. *Biophys. J.* **2003**, *85*, 3074–3083.

(91) Veatch, S. L.; Keller, S. L. Miscibility Phase Diagrams of Giant Vesicles Containing Sphingomyelin. *Phys. Rev. Lett.* **2005**, *94*, 3–6.

(92) Štefl, M.; Šachl, R.; Humpolíčková, J.; Cebecauer, M.; MacHáň, R.; Kolářová, M.; Johansson, L. B. Å.; Hof, M. Dynamics and Size of Cross-Linking-Induced Lipid Nanodomains in Model Membranes. *Biophys. J.* **2012**, *102*, 2104–2113.

(93) Keyes, T.; Gaul, V.; Lopez, S.; Moran, N.; Lentz, B.; Forster, R. The Lateral Diffusion and Fibrinogen Induced Clustering of Platelet Integrin αIIbβ3 Reconstituted into Physiologically Mimetic GUVs. *Integr. Biol.* **2015**, *7*, 402–411.

(94) Hammond, A. T.; Heberle, F. A.; Baumgart, T.; Holowka, D.; Baird, B.; Feigenson, G. W. Crosslinking a Lipid Raft Component Triggers Liquid Ordered-Liquid Disordered Phase Separation in Model Plasma Membranes. *Proc. Natl. Acad. Sci. U. S. A.* **2005**, *102*, 6320–6325.

(95) Veatch, S. L.; Cicuta, P.; Sengupta, P.; Honerkamp-Smith, A.; Holowka, D.; Baird, B. Critical Fluctuations in Plasma Membrane Vesicles. *ACS Chem. Biol.* **2008**, *3*, 287–293.

(96) Levental, I.; Grzybek, M.; Simons, K. Raft Domains of Variable Properties and Compositions in Plasma Membrane Vesicles. *Proc. Natl. Acad. Sci. U. S. A.*

2011, *108*, 11411–11416.

(97) Girard, P.; Pécréaux, J.; Lenoir, G.; Falson, P.; Rigaud, J.-L.; Bassereau, P. A New Method for the Reconstitution of Membrane Proteins into Giant Unilamellar Vesicles. *Biophys. J.* **2004**, *87*, 419–429.

(98) Rigaud, J.; Lévy, D. Reconstitution of Membrane Proteins into Liposomes. *Methods Enzymol.* **2003**, *372*, 65–86.

(99) Kreir, M.; Farre, C.; Beckler, M.; George, M.; Fertig, N. Rapid Screening of Membrane Protein Activity: Electrophysiological Analysis of OmpF Reconstituted in Proteoliposomes. *Lab Chip* **2008**, *8*, 587–595.

(100) Aimon, S.; Manzi, J.; Schmidt, D.; Larrosa, J. A. P.; Bassereau, P.; Toombes, G. E. S. Functional Reconstitution of a Voltage-Gated Potassium Channel in Giant Unilamellar Vesicles. *PLoS One* **2011**, *6*, e25529.

(101) Garten, M.; Aimon, S.; Bassereau, P.; Toombes, G. E. S. Reconstitution of a Transmembrane Protein, the Voltage-Gated Ion Channel, KvAP, into Giant Unilamellar Vesicles for Microscopy and Patch Clamp Studies. *J. Vis. Exp.* **2015**, *95*, e52281.

(102) Kalvodova, L.; Kahya, N.; Schwille, P.; Ehehalt, R.; Verkade, P.; Drechsel, D.; Simons, K. Lipids as Modulators of Proteolytic Activity of BACE: Involvement of Cholesterol, Glycosphingolipids, and Anionic Phospholipids in Vitro. *J. Biol. Chem.* **2005**, *280*, 36815–36823.

(103) Cordy, J. M.; Hussain, I.; Dingwall, C.; Hooper, N. M.; Turner, A. J. Exclusively Targeting Beta-Secretase to Lipid Rafts by GPI-Anchor Addition up-Regulates Beta-Site Processing of the Amyloid Precursor Protein. *Proc. Natl. Acad. Sci. U. S. A.* **2003**, *100*, 11735–11740.

(104) Sesana, S.; Re, F.; Bulbarelli, A.; Salerno, D.; Cazzaniga, E.; Masserini, M. Membrane Features and Activity of GPI-Anchored Enzymes: Alkaline Phosphatase Reconstituted in Model Membranes. *Biochemistry* **2008**, *47*, 5433–5440.

(105) Saslowsky, D. E.; Lawrence, J.; Ren, X.; Brown, D. a.; Henderson, R. M.; Michael Edwardson, J. Placental Alkaline Phosphatase Is Efficiently Targeted to Rafts in Supported Lipid Bilayers. *J. Biol. Chem.* **2002**, *277*, 26966–26970.

(106) Diaz, O.; Mébarek-Azzam, S.; Benzaria, A.; Dubois, M.; Lagarde, M.; Némoz, G.; Prigent, A.-F. Disruption of Lipid Rafts Stimulates Phospholipase D Activity in Human Lymphocytes: Implication in the Regulation of Immune Function. *J. Immunol.* **2005**, *175*, 8077–8086.

(107) Richter, R.; Bérat, R.; Brisson, A. Formation of Solid-Supported Lipid Bilayers: An Integrated View. *Langmuir* **2006**, *22*, 3497–3505.

(108) Tamm, L.; McConnell, H. Supported Phospholipid Bilayers. *Biophys. J.* **1985**, *47*, 105–113.

(109) Watts, T.; Gaub, H.; McConnell, H. T-Cell-Mediated Association of Peptide Antigen and Major Histocompatibility Complex Protein Detected by Energy

Transfer in an Evanescent Wave-Field. *Nature* **1986**, *320*, 179–181.

(110) Chiantia, S.; Ries, J.; Kahya, N.; Schwille, P. Combined AFM and Two-Focus SFCS Study of Raft-Exhibiting Model Membranes. *Chemphyschem* **2006**, *7*, 2409–2418.

(111) Cho, N.-J.; Frank, C. W.; Kasemo, B.; Höök, F. Quartz Crystal Microbalance with Dissipation Monitoring of Supported Lipid Bilayers on Various Substrates. *Nat. Protoc.* **2010**, *5*, 1096–1106.

(112) Terrettaz, S.; Stora, T.; Duschl, C.; Vogel, H. Protein Binding to Supported Lipid Membranes: Investigation of the Cholera Toxin-Ganglioside Interaction by Simultaneous Impedance Spectroscopy and Surface Plasmon Resonance. *Langmuir* **1993**, *9*, 1361–1369.

(113) Castellana, E. T.; Cremer, P. S. Solid Supported Lipid Bilayers: From Biophysical Studies to Sensor Design. *Surf. Sci. Rep.* **2006**, *61*, 429–444.

(114) Simonsson, L.; Gunnarsson, A.; Wallin, P.; Jönsson, P.; Höök, F. Continuous Lipid Bilayers Derived from Cell Membranes for Spatial Molecular Manipulation. *J. Am. Chem. Soc.* **2011**, *133*, 14027–14032.

(115) Schwoch, G.; Passow, H. Preparation and Properties of Human Erythrocyte Ghosts. *Mol. Cell. Biochem.* **1973**, *2*, 197–218.

(116) Tanaka, M.; Kaufmann, S. Orientation Selective Immobilization of Human Erythrocyte Membranes on Ultrathin Cellulose Films. *Phys. Chem. Chem. Phys.* **2001**, *3*, 4091–4095.

(117) Dogterom, M.; Koenderink, G. Cell-Membrane Mechanics: Vesicles in and Tubes Out. *Nat. Mater.* **2011**, *10*, 561–562.

(118) Holowka, D.; Baird, B. Structural Studies on the Membrane-Bound Immunoglobulin E-Receptor Complex. 1. Characterization of Large Plasma Membrane Vesicles from Rat Basophilic Leukemia. *Biochemistry* **1983**, 3466–3474.

(119) König, B.; Krueger, S.; Orts, W.; Majkrzak, C. Neutron Reflectivity and Atomic Force Microscopy Studies of a Lipid Bilayer in Water Adsorbed to the Surface of a Silicon Single Crystal. *Langmuir* **1996**, 1343–1350.

(120) Nam, H.-J.; Han, S. K.; Bowie, J. U.; Kim, S. Rampant Exchange of the Structure and Function of Extramembrane Domains between Membrane and Water Soluble Proteins. *PLoS Comput. Biol.* **2013**, *9*, e1002997.

(121) Martinez, K. L. K.; Meyer, B. B. H.; Hovius, R.; Lundstrom, K.; Vogel, H. Ligand Binding to G Protein-Coupled Receptors in Tethered Cell Membranes. *Langmuir* **2003**, *19*, 10925–10929.

(122) McCabe, I.; Forstner, M. Polymer Supported Lipid Bilayers. *Open J. Biophys.* **2013**, *3*, 59–69.

(123) Wagner, M. L.; Tamm, L. K. Tethered Polymer-Supported Planar Lipid Bilayers for Reconstitution of Integral Membrane Proteins: Silane-

Polyethyleneglycol-Lipid as a Cushion and Covalent Linker. *Biophys. J.* **2000**, *79*, 1400–1414.

(124) Goennenwein, S.; Tanaka, M.; Hu, B. Functional Incorporation of Integrins into Solid Supported Membranes on Ultrathin Films of Cellulose: Impact on Adhesion. *Biophys. J.* **2003**, *85*, 646–655.

(125) Diaz, A. J.; Albertorio, F.; Daniel, S.; Cremer, P. S. Double Cushions Preserve Transmembrane Protein Mobility in Supported Bilayer Systems. *Langmuir* **2008**, *24*, 6820–6826.

(126) Kaufmann, S.; Papastavrou, G.; Kumar, K.; Textor, M.; Reimhult, E. A Detailed Investigation of the Formation Kinetics and Layer Structure of Poly(ethylene Glycol) Tether Supported Lipid Bilayers. *Soft Matter* **2009**, *5*, 2804.

(127) Ye, Q.; Konradi, R.; Textor, M.; Reimhult, E. Liposomes Tethered to Omega-Functional PEG Brushes and Induced Formation of PEG Brush Supported Planar Lipid Bilayers. *Langmuir* **2009**, *25*, 13534–13539.

(128) Kaufmann, S.; Borisov, O.; Textor, M.; Reimhult, E. Mechanical Properties of Mushroom and Brush Poly(ethylene Glycol)-Phospholipid Membranes. *Soft Matter* **2011**, *7*, 9267.

(129) de Gennes, P. G. *Scaling Concepts in Polymer Physics*; Cornell University Press, 1979.

(130) Kenworthy, A. K.; Hristova, K.; Needham, D.; McIntosh, T. J. Range and Magnitude of the Steric Pressure between Bilayers Containing Phospholipids with Covalently Attached Poly(ethylene Glycol). *Biophys. J.* **1995**, *68*, 1921–1936.

(131) Watkins, E. B.; El-Khouri, R. J.; Miller, C. E.; Seaby, B. G.; Majewski, J.; Marques, C. M.; Kuhl, T. L. Structure and Thermodynamics of Lipid Bilayers on Polyethylene Glycol Cushions: Fact and Fiction of PEG Cushioned Membranes. *Langmuir* **2011**, *27*, 13618–13628.

(132) Klibanov, A. L.; Maruyama, K.; Beckerleg, A. M.; Torchilin, V. P.; Huang, L. Activity of Amphipathic Poly(ethylene Glycol) 5000 to Prolong the Circulation Time of Liposomes Depends on the Liposome Size and Is Unfavorable for Immunoliposome Binding to Target. *Biochim. Biophys. Acta* **1991**, *1062*, 142–148.

(133) Burridge, K. A.; Figa, M. A.; Wong, J. Y. Patterning Adjacent Supported Lipid Bilayers of Desired Composition to Investigate Receptor-Ligand Binding under Shear Flow. *Langmuir* **2004**, *20*, 10252–10259.

(134) Renner, L.; Pompe, T.; Lemaitre, R.; Drechsel, D.; Werner, C. Controlled Enhancement of Transmembrane Enzyme Activity in Polymer Cushioned Supported Bilayer Membranes. *Soft Matter* **2010**, *6*, 5382.

(135) Sackmann, E.; Tanaka, M. Supported Membranes on Soft Polymer Cushions: Fabrication, Characterization and Applications. *Trends Biotechnol.* **2000**, *22*,

58–64.

(136) Poudel, K. R.; Keller, D. J.; Brozik, J. A. Single Particle Tracking Reveals Corralling of a Transmembrane Protein in a Double-Cushioned Lipid Bilayer Assembly. *Langmuir* **2011**, *27*, 320–327.

(137) Reimhult, E.; Kasemo, B.; Höök, F. Rupture Pathway of Phosphatidylcholine Liposomes on Silicon Dioxide. *Int. J. Mol. Sci.* **2009**, *10*, 1683–1696.

(138) Contino, P.; Hasselbacher, C.; Ross, J.; Nemerson, Y. Use of an Oriented Transmembrane Protein to Probe the Assembly of a Supported Phospholipid Bilayer. *Biophys. J.* **1994**, *67*, 1113–1116.

(139) Jass, J.; Tjärnhage, T.; Puu, G. From Liposomes to Supported, Planar Bilayer Structures on Hydrophilic and Hydrophobic Surfaces: An Atomic Force Microscopy Study. *Biophys. J.* **2000**, *79*, 3153–3163.

(140) Fuhrmans, M.; Müller, M. Mechanisms of Vesicle Spreading on Surfaces: Coarse-Grained Simulations. *Langmuir* **2013**, *29*, 4335–4349.

(141) Salafsky, J.; Groves, J.; Boxer, S. Architecture and Function of Membrane Proteins in Planar Supported Bilayers: A Study with Photosynthetic Reaction Centers. *Biochemistry* **1996**, *2960*, 14773–14781.

(142) Orth, R.; Wu, M.; Holowka, D.; Craighead, H.; Baird, B. Mast Cell Activation on Patterned Lipid Bilayers of Subcellular Dimensions. *Langmuir* **2003**, 1599–1605.

(143) Dustin, M. L.; Bromley, S. K.; Kan, Z.; Peterson, D. A.; Unanue, E. R. Antigen Receptor Engagement Delivers a Stop Signal to Migrating T Lymphocytes. *Proc. Natl. Acad. Sci. USA* **1997**, *94*, 3909–3913.

(144) Majd, S.; Mayer, M. Hydrogel Stamping of Arrays of Supported Lipid Bilayers with Various Lipid Compositions for the Screening of Drug-Membrane and Protein-Membrane Interactions. *Angew. Chem. Int. Ed. Engl.* **2005**, *44*, 6697–6700.

(145) Chao, L.; Daniel, S. Measuring the Partitioning Kinetics of Membrane Biomolecules Using Patterned Two-Phase Coexistant Lipid Bilayers. *J. Am. Chem. Soc.* **2011**, *133*, 15635–15643.

(146) Kung, L. A.; Kam, L.; Hovis, J. S.; Boxer, S. G. Patterning Hybrid Surfaces of Proteins and Supported Lipid Bilayers. *Langmuir* **2000**, *16*, 6773–6776.

(147) Boxer, S. Molecular Transport and Organization in Supported Lipid Membranes. *Curr. Opin. Chem. Biol.* **2000**, *4*, 704–709.

(148) Ilic, B.; Craighead, H. Topographical Patterning of Chemically Sensitive Biological Materials Using a Polymer-Based Dry Lift off. *Biomed. Microdevices* **2000**, *2:4*, 317–322.

(149) Moran-Mirabal, J. M.; Edel, J. B.; Meyer, G. D.; Throckmorton, D.; Singh, A. K.; Craighead, H. G. Micrometer-Sized Supported Lipid Bilayer Arrays for Bacterial Toxin Binding Studies through Total Internal Reflection Fluorescence

Microscopy. *Biophys. J.* **2005**, *89*, 296–305.

(150) Yee, C. K.; Amweg, M. L.; Parikh, A. N. Membrane Photolithography: Direct Micropatterning and Manipulation of Fluid Phospholipid Membranes in the Aqueous Phase Using Deep-UV Light. *Adv. Mater.* **2004**, *16*, 1184–1189.

(151) Kam, L.; Boxer, S. G. Formation of Supported Lipid Bilayer Composition Arrays by Controlled Mixing and Surface Capture. *J. Am. Chem. Soc.* **2000**, *122*, 12901–12902.

(152) Kraft, M. L.; Fishel, S. F.; Marxer, C. G.; Weber, P. K.; Hutcheon, I. D.; Boxer, S. G. Quantitative Analysis of Supported Membrane Composition Using the NanoSIMS. *Appl. Surf. Sci.* **2006**, *252*, 6950–6956.

(153) Groves, J. T.; Ulman, N.; Boxer, S. G. Micropatterning Fluid Lipid Bilayers on Solid Supports. *Science* **1997**, *275*, 651–653.

(154) Hovis, J. S.; Boxer, S. G. Patterning Barriers to Lateral Diffusion in Supported Lipid Bilayer Membranes by Blotting and Stamping. *Langmuir* **2000**, *16*, 894–897.

(155) Cremer, P. S.; Boxer, S. G. Formation and Spreading of Lipid Bilayers on Planar Glass Supports. *J. Phys. Chem. B* **1999**, *103*, 2554–2559.

(156) Spycher, P. R.; Hall, H.; Vogel, V.; Reimhult, E. Patterning of Supported Lipid Bilayers and Proteins Using Material Selective Nitrodopamine-mPEG. *Biomater. Sci.* **2015**, *3*, 94–102.

(157) Roder, F.; Birkholz, O.; Beutel, O.; Paterok, D.; Piehler, J. Spatial Organization of Lipid Phases in Micropatterned Polymer-Supported Membranes. *J. Am. Chem. Soc.* **2013**, *135*, 1189–1192.

(158) Jung, S.-Y.; Holden, M. A.; Cremer, P. S.; Collier, C. P. Two-Component Membrane Lithography via Lipid Backfilling. *Chemphyschem* **2005**, *6*, 423–426.

(159) Hsia, C.; Richards, M. J.; Daniel, S. A Review of Traditional and Emerging Methods to Characterize Lipid-Protein Interactions in Biological Membranes. *Anal. Methods* **2015**, *7*, 7076–7094.

(160) Loll, P. J. Membrane Protein Structural Biology: The High Throughput Challenge. *J. Struct. Biol.* **2003**, *142*, 144–153.

(161) Sachs, J. N.; Engelman, D. M. Introduction to the Membrane Protein Reviews: The Interplay of Structure, Dynamics, and Environment in Membrane Protein Function. *Annu. Rev. Biochem.* **2006**, *75*, 707–712.

(162) Sprenger, R. R.; Horrevoets, A. J. G. The Ins and Outs of Lipid Domain Proteomics. *Proteomics*, 2007, *7*, 2895–2903.

(163) Zheng, Y. Z.; Foster, L. J. Biochemical and Proteomic Approaches for the Study of Membrane Microdomains. *Journal of Proteomics*, 2009, *72*, 12–22.

(164) Joshi, M. K.; Dracheva, S.; Mukhopadhyay, A. K.; Bose, S.; Hendler, R. W. Importance of Specific Native Lipids in Controlling the Photocycle of

Bacteriorhodopsin. *Biochemistry* **1998**, *37*, 14463–14470.

(165) Carlson, R. O.; Masco, D.; Brooker, G.; Spiegel, S. Endogenous Ganglioside GM1 Modulates L-Type Calcium Channel Activity in N18 Neuroblastoma Cells. *J. Neurosci.* **1994**, *14*, 2272–2281.

(166) Daniel, S.; Diaz, A.; Martinez, K.; Bench, B.; Albertorio, F.; Cremer, P. Separation of Membrane-Bound Compounds by Solid-Supported Bilayer Electrophoresis. *J. Am. Chem. Soc.* **2007**, *129*, 8072–8073.

(167) Weng, K. C.; Kanter, J. L.; Robinson, W. H.; Frank, C. W. Fluid Supported Lipid Bilayers Containing Monosialoganglioside GM1: A QCM-D and FRAP Study. *Colloids Surfaces B Biointerfaces* **2006**, *50*, 76–84.

(168) Groves, J. T.; Dustin, M. L. Supported Planar Bilayers in Studies on Immune Cell Adhesion and Communication. *Journal of Immunological Methods*, 2003, *278*, 19–32.

(169) Sumino, A.; Dewa, T.; Kondo, M.; Morii, T.; Hashimoto, H.; Gardiner, A. T.; Cogdell, R. J.; Nango, M. Selective Assembly of Photosynthetic Antenna Proteins into a Domain-Structured Lipid Bilayer for the Construction of Artificial Photosynthetic Antenna Systems: Structural Analysis of the Assembly Using Surface Plasmon Resonance and Atomic Force Microscopy. *Langmuir* **2011**, *27*, 1092–1099.

(170) Burns, A. R.; Frankel, D. J.; Buranda, T. Local Mobility in Lipid Domains of Supported Bilayers Characterized by Atomic Force Microscopy and Fluorescence Correlation Spectroscopy. *Biophys. J.* **2005**, *89*, 1081–1093.

(171) Shreve, A. P.; Howland, M. C.; Sapuri-Butti, A. R.; Allen, T. W.; Parikh, A. N. Evidence for Leaflet-Dependent Redistribution of Charged Molecules in Fluid Supported Phospholipid Bilayers. *Langmuir* **2008**, *24*, 13250–13253.

(172) Richter, R. P.; Brisson, A. R. Following the Formation of Supported Lipid Bilayers on Mica: A Study Combining AFM, QCM-D, and Ellipsometry. *Biophys. J.* **2005**, *88*, 3422–3433.

(173) Tokumasu, F.; Jin, A. J.; Feigenson, G. W.; Dvorak, J. A. Nanoscopic Lipid Domain Dynamics Revealed by Atomic Force Microscopy. *Biophys. J.* **2003**, *84*, 2609–2618.

(174) Cheetham, M. R.; Bramble, J. P.; McMillan, D. G. G.; Krzeminski, L.; Han, X.; Johnson, B. R. G.; Bushby, R. J.; Olmsted, P. D.; Jeuken, L. J. C.; Marritt, S. J.; et al. Concentrating Membrane Proteins Using Asymmetric Traps and AC Electric Fields. *J. Am. Chem. Soc.* **2011**, *133*, 6521–6524.

(175) Cremer, P. S.; Groves, J. T.; Kung, L. A.; Boxer, S. G. Writing and Erasing Barriers to Lateral Mobility into Fluid Phospholipid Bilayers. *Langmuir* **1999**, *15*, 3893–3896.

(176) Stelzle, M.; Miehlich, R.; Sackmann, E. Two-Dimensional Microelectrophoresis in Supported Lipid Bilayers. *Biophys. J.* **1992**, *63*, 1346–1354.

(177) van Oudenaarden, A.; Boxer, S. G. Brownian Ratchets: Molecular Separations in Lipid Bilayers Supported on Patterned Arrays. *Science* **1999**, *285*, 1046–1048.

(178) Nabika, H.; Takimoto, B.; Murakoshi, K. Molecular Separation in the Lipid Bilayer Medium: Electrophoretic and Self-Spreading Approaches. *Analytical and Bioanalytical Chemistry*, 2008, *391*, 2497–2506.

(179) Jönsson, P.; Beech, J. P.; Tegenfeldt, J. O.; Höök, F. Shear-Driven Motion of Supported Lipid Bilayers in Microfluidic Channels. *J. Am. Chem. Soc.* **2009**, *131*, 5294–5297.

(180) Jönsson, P.; Gunnarsson, A.; Höök, F. Accumulation and Separation of Membrane-Bound Proteins Using Hydrodynamic Forces. *Anal. Chem.* **2011**, *83*, 604–611.

(181) Veatch, S. L.; Gawrisch, K.; Keller, S. L. Closed-Loop Miscibility Gap and Quantitative Tie-Lines in Ternary Membranes Containing Diphytanoyl PC. *Biophys. J.* **2006**, *90*, 4428–4436.

(182) Veatch, S. L.; Polozov, I. V; Gawrisch, K.; Keller, S. L. Liquid Domains in Vesicles Investigated by NMR and Fluorescence Microscopy. *Biophys. J.* **2004**, *86*, 2910–2922.

(183) Ionova, I. V.; Livshits, V. A.; Marsh, D. Phase Diagram of Ternary Cholesterol/palmitoylsphingomyelin/ Palmitoyloleoyl-Phosphatidylcholine Mixtures: Spin-Label EPR Study of Lipid-Raft Formation. *Biophys. J.* **2012**, *102*, 1856–1865.

(184) Soumpasis, D. M. Theoretical Analysis of Fluorescence Photobleaching Recovery Experiments. *Biophys. J.* **1983**, *41*, 95–97.

(185) Jönsson, P.; Höök, F. Effects of Surface Pressure and Internal Friction on the Dynamics of Shear-Driven Supported Lipid Bilayers. *Langmuir* **2011**, *27*, 1430–1439.

(186) Granéli, A.; Rydström, J.; Kasemo, B.; Höök, F. Formation of Supported Lipid Bilayer Membranes on SiO2 from Proteoliposomes Containing Transmembrane Proteins. *Langmuir* **2003**, 842–850.

(187) Axelrod, D.; Koppel, D. E.; Schlessinger, J.; Elson, E.; Webb, W. W. Mobility Measurement by Analysis of Fluorescence Photobleaching Recovery Kinetics. *Biophys. J.* **1976**, *16*, 1055–1069.

(188) Jonsson, P.; Beech, J. P.; Tegenfeldt, J. O.; Hook, F. Mechanical Behavior of a Supported Lipid Bilayer under External Shear Forces. *Langmuir* **2009**, *25*, 6279–6286.

(189) Merkel, R.; Sackmann, E.; Evans, E. Molecular Friction and Epitactic Coupling between Monolayers in Supported Bilayers. *Journal de Physique*, 1989, *50*, 1535–1555.

(190) Tanaka, M.; Rossetti, F. F.; Kaufmann, S. Native Supported Membranes: Creation of Two-Dimensional Cell Membranes on Polymer Supports (Review).

Biointerphases **2008**, *3*, FA12.

(191) Costello, D. A.; Millet, J. K.; Hsia, C.-Y.; Whittaker, G. R.; Daniel, S. Single Particle Assay of Coronavirus Membrane Fusion with Proteinaceous Receptor-Embedded Supported Bilayers. *Biomaterials* **2013**, *34*, 7895–7904.

(192) Wong, W.; Schlichter, L. C. Differential Recruitment of Kv1.4 and Kv4.2 to Lipid Rafts by PSD-95. *J. Biol. Chem.* **2004**, *279*, 444–452.

(193) Chao, L.; Richards, M. J.; Hsia, C.-Y.; Daniel, S. Two-Dimensional Continuous Extraction in Multiphase Lipid Bilayers to Separate, Enrich, and Sort Membrane-Bound Species. *Anal. Chem.* **2013**, *85*, 6696–6702.

(194) Lingwood, D.; Simons, K. Lipid Rafts as a Membrane-Organizing Principle. *Science* **2010**, *327*, 46–50.

(195) Chan, Y.-H. M.; Boxer, S. G. Model Membrane Systems and Their Applications. *Curr. Opin. Chem. Biol.* **2007**, *11*, 581–587.

(196) Ziemba, B. P.; Falke, J. J. Lateral Diffusion of Peripheral Membrane Proteins on Supported Lipid Bilayers Is Controlled by the Additive Frictional Drags of (1) Bound Lipids and (2) Protein Domains Penetrating into the Bilayer Hydrocarbon Core. *Chem. Phys. Lipids* **2013**, *172-173*, 67–77.

(197) Tan, S.; Tan, H. T.; Chung, M. C. M. Membrane Proteins and Membrane Proteomics. *Proteomics* **2008**, *8*, 3924–3932.

(198) Cordwell, S. J.; Thingholm, T. E. Technologies for Plasma Membrane Proteomics. *Proteomics* **2010**, *10*, 611–627.

(199) Simeonov, P.; Werner, S.; Haupt, C.; Tanabe, M.; Bacia, K. Membrane Protein Reconstitution into Liposomes Guided by Dual-Color Fluorescence Cross-Correlation Spectroscopy. *Biophys. Chem.* **2013**, *184*, 37–43.

(200) Helenius, A. R. I.; Simons, K. A. I. Solubilization of Membranes by Detergents. *Biochim. Biophys. Acta* **1975**, *415*, 29–79.

(201) Erb, E. M.; Engel, J. Reconstitution of Functional Integrin into Phospholipid Vesicles and Planar Lipid Bilayers. *Methods Mol. Biol.* **2000**, *139*, 71–82.

(202) Pace, H. P.; Simonsson Nyström, L.; Gunnarsson, A.; Eck, E.; Monson, C. F.; Geschwindner, S.; Snijder, A.; Höök, F. Preserved Transmembrane Protein Mobility in Polymer-Supported Lipid Bilayers Derived from Cell Membranes. *Anal. Chem.* **2015**, DOI: 10.1021/acs.analchem.5b01449.

(203) Costello, D. A.; Hsia, C.-Y.; Millet, J. K.; Porri, T.; Daniel, S. Membrane Fusion-Competent Virus-like Proteoliposomes and Proteinaceous Supported Bilayers Made Directly from Cell Plasma Membranes. *Langmuir* **2013**, *29*, 6409–6419.

(204) Sharom, F. J.; Lehto, M. T. Glycosylphosphatidylinositol-Anchored Proteins: Structure, Function, and Cleavage by Phosphatidylinositol-Specific Phospholipase C. *Biochem. Cell Biol.* **2002**, *80*, 535–549.

(205) Li, M.; Bharadwaj, U.; Zhang, R.; Zhang, S.; Mu, H.; Fisher, W. E.; Brunicardi,

F. C.; Chen, C.; Yao, Q. Mesothelin Is a Malignant Factor and Therapeutic Vaccine Target for Pancreatic Cancer. *Mol. Cancer Ther.* **2008**, *7*, 286–296.

(206) Khakh, B. S.; North, R. A. P2X Receptors as Cell-Surface ATP Sensors in Health and Disease. *Nature* **2006**, *442*, 527–532.

(207) North, R. A. Molecular Physiology of P2X Receptors. *Physiol. Rev.* **2002**, *82*, 1013–1067.

(208) Kawate, T.; Michel, J. C.; Birdsong, W. T.; Gouaux, E. Crystal Structure of the ATP-Gated P2X(4) Ion Channel in the Closed State. *Nature* **2009**, *460*, 592–598.

(209) Marsh, D.; Bartucci, R.; Sportelli, L. Lipid Membranes with Grafted Polymers: Physicochemical Aspects. *Biochim. Biophys. Acta - Biomembr.* **2003**, *1615*, 33–59.

(210) Smith, M. B.; Karatekin, E.; Gohlke, A.; Mizuno, H.; Watanabe, N.; Vavylonis, D. Interactive, Computer-Assisted Tracking of Speckle Trajectories in Fluorescence Microscopy: Application to Actin Polymerization and Membrane Fusion. *Biophys. J.* **2011**, *101*, 1794–1804.

(211) Poudel, K. R.; Jones, J. P.; Brozik, J. A. A Guide to Tracking Single Transmembrane Proteins in Supported Lipid Bilayers. **2013**, *974*, 233–252.

(212) Vrljic, M.; Nishimura, S. Y.; Moerner, W. E. Single-Molecule Tracking. *Methods Mol. Biol.* **2007**, *398*, 193–219.

(213) Saxton, M. Single-Particle Tracking: The Distribution of Diffusion Coefficients. *Biophys. J.* **1997**, *72*.

(214) Ferrari, R.; Manfroi, A. J.; Young, W. R. Strongly and Weakly Self-Similar Diffusion. *Phys. D Nonlinear Phenom.* **2001**, *154*, 111–137.

(215) Kusumi, A.; Sako, Y.; Yamamoto, M. Confined Lateral Diffusion of Membrane Receptors as Studied by Single Particle Tracking (nanovid Microscopy). Effects of Calcium-Induced Differentiation in Cultured Epithelial Cells. *Biophys. J.* **1993**, *65*, 2021–2040.

(216) Smith, P. R.; Morrison, I. E.; Wilson, K. M.; Fernández, N.; Cherry, R. J. Anomalous Diffusion of Major Histocompatibility Complex Class I Molecules on HeLa Cells Determined by Single Particle Tracking. *Biophys. J.* **1999**, *76*, 3331–3344.

(217) Sbalzarini, I. F.; Koumoutsakos, P. Feature Point Tracking and Trajectory Analysis for Video Imaging in Cell Biology. *J. Struct. Biol.* **2005**, *151*, 182–195.

(218) Deverall, M. A.; Gindl, E.; Sinner, E.-K.; Besir, H.; Ruehe, J.; Saxton, M. J.; Naumann, C. A. Membrane Lateral Mobility Obstructed by Polymer-Tethered Lipids Studied at the Single Molecule Level. *Biophys. J.* **2005**, *88*, 1875–1886.

(219) Weiß, K.; Neef, A.; Van, Q.; Kramer, S.; Gregor, I.; Enderlein, J. Quantifying the Diffusion of Membrane Proteins and Peptides in Black Lipid Membranes

with 2-Focus Fluorescence Correlation Spectroscopy. *Biophys. J.* **2013**, *105*, 455–462.

(220) Ramadurai, S.; Holt, A.; Krasnikov, V.; van den Bogaart, G.; Killian, J. A.; Poolman, B. Lateral Diffusion of Membrane Proteins. *J Am Chem Soc* **2009**, *131*, 12650–12656.

(221) Zhang, F.; Crise, B.; Su, B.; Hou, Y.; Rose, J. K.; Bothwell, A.; Jacobson, K. Lateral Diffusion of Membrane-Spanning and Glycosylphosphatidylinositol-Linked Proteins: Toward Establishing Rules Governing the Lateral Mobility of Membrane Proteins. *J. Cell Biol.* **1991**, *115*, 75–84.

(222) Türkcan, S.; Richly, M. U.; Alexandrou, A.; Masson, J. B. Probing Membrane Protein Interactions with Their Lipid Raft Environment Using Single-Molecule Tracking and Bayesian Inference Analysis. *PLoS One* **2013**, *8*.

(223) Foley, M.; MacGregor, a N.; Kusel, J. R.; Garland, P. B.; Downie, T.; Moore, I. The Lateral Diffusion of Lipid Probes in the Surface Membrane of Schistosoma Mansoni. *J. Cell Biol.* **1986**, *103*, 807–818.

(224) Wang, T.; Smith, E. a.; Chapman, E. R.; Weisshaar, J. C. Lipid Mixing and Content Release in Single-Vesicle, SNARE-Driven Fusion Assay with 1–5 Ms Resolution. *Biophys. J.* **2009**, *96*, 4122–4131.

(225) Lorenz, H.; Hailey, D. W.; Wunder, C.; Lippincott-Schwartz, J. The Fluorescence Protease Protection (FPP) Assay to Determine Protein Localization and Membrane Topology. *Nat. Protoc.* **2006**, *1*, 276–279.

(226) Al-Nedawi, K.; Meehan, B.; Micallef, J.; Lhotak, V.; May, L.; Guha, A.; Rak, J. Intercellular Transfer of the Oncogenic Receptor EGFRvIII by Microvesicles Derived from Tumour Cells. *Nat. Cell Biol.* **2008**, *10*, 619–624.

(227) Antonyak, M. A.; Li, B.; Boroughs, L. K.; Johnson, J. L.; Druso, J. E.; Bryant, K. L.; Holowka, D. A.; Cerione, R. A. Cancer Cell-Derived Microvesicles Induce Transformation by Transferring Tissue Transglutaminase and Fibronectin to Recipient Cells. *Proc Natl Acad Sci U S A* **2011**, *108*, 4852–4857.

(228) Sengupta, P.; Baird, B.; Holowka, D. Lipid Rafts, Fluid/fluid Phase Separation, and Their Relevance to Plasma Membrane Structure and Function. *Semin. Cell Dev. Biol.* **2007**, *18*, 583–590.

(229) Weerasekera, R.; She, Y. M.; Markham, K. A.; Bai, Y.; Opalka, N.; Orlicky, S.; Sichert, F.; Kislinger, T.; Schmitt-Ulms, G. Interactome and Interface Protocol (2IP): A Novel Strategy for High Sensitivity Topology Mapping of Protein Complexes. *Proteomics* **2007**, *7*, 3835–3852.

(230) Vasilescu, J.; Guo, X.; Kast, J. Identification of Protein-Protein Interactions Using in Vivo Cross-Linking and Mass Spectrometry. *Proteomics* **2004**, *4*, 3845–3854.

(231) Zijlstra, N.; Blum, C.; Segers-Nolten, I. M. J.; Claessens, M. M. A. E.; Subramaniam, V. Molecular Composition of Sub-Stoichiometrically Labeled

Alpha-Synuclein Oligomers Determined by Single-Molecule Photobleaching. *Angew. Chemie - Int. Ed.* **2012**, *51*, 8821–8824.

(232) Pautot, S.; Lee, H.; Isacoff, E. Y.; Groves, J. T. Neuronal Synapse Interaction Reconstituted between Live Cells and Supported Lipid Bilayers. *Nat. Chem. Biol.* **2005**, *1*, 283–289.

(233) Crane, J. M.; Tamm, L. K. Role of Cholesterol in the Formation and Nature of Lipid Rafts in Planar and Spherical Model Membranes. *Biophys. J.* **2004**, *86*, 2965–2979.

(234) Veatch, S. L.; Keller, S. L. Miscibility Phase Diagrams of Giant Vesicles Containing Sphingomyelin. *Phys. Rev. Lett.* **2005**, *94*, 3–6.

(235) Schneider, C. A; Rasband, W. S.; Eliceiri, K. W. NIH Image to ImageJ: 25 Years of Image Analysis. *Nat. Methods* **2012**, *9*, 671–675.

(236) Orth, R. N.; Kameoka, J.; Zipfel, W. R.; Ilic, B.; Webb, W. W.; Clark, T. G.; Craighead, H. G. Creating Biological Membranes on the Micron Scale: Forming Patterned Lipid Bilayers Using a Polymer Lift-off Technique. *Biophys. J.* **2003**, *85*, 3066–3073.

(237) Beseničar, M. P.; Bavdek, A.; Kladnik, A.; Maček, P.; Anderluh, G. Kinetics of Cholesterol Extraction from Lipid Membranes by Methyl-β-Cyclodextrin-A Surface Plasmon Resonance Approach. *Biochim. Biophys. Acta - Biomembr.* **2008**, *1778*, 175–184.

(238) Sanchez, S. A.; Gunther, G.; Tricerri, M. A.; Gratton, E. Methyl-Beta-Cyclodextrins Preferentially Remove Cholesterol from the Liquid Disordered Phase in Giant Unilamellar Vesicles. *J. Membr. Biol.* **2011**, *241*, 1–10.

(239) Massenburg, D.; Lentz, B. R. Poly(Ethylene Glycol)-Induced Fusion and Rupture of Dipalmitoylphosphatidylcholine Large, Unilamellar Extruded Vesicles. **1993**, *32*, 9172–9180.

(240) Sengupta, K.; Schilling, J.; Marx, S.; Fischer, M.; Bacher, A.; Sackmann, E. Mimicking Tissue Surfaces by Supported Membrane Coupled Ultrathin Layer of Hyaluronic Acid. *Langmuir* **2003**, *19*, 1775–1781.

(241) Subramaniam, A. B.; Guidotti, G.; Manoharan, V. N.; Stone, H. a. Glycans Pattern the Phase Behaviour of Lipid Membranes. *Nat. Mater.* **2013**, *12*, 128–133.

(242) Zidovetzki, R.; Levitan, I. Use of Cyclodextrins to Manipulate Plasma Membrane Cholesterol Content: Evidence, Misconceptions and Control Strategies. *Biochim. Biophys. Acta - Biomembr.* **2007**, *1768*, 1311–1324.